Fabrication of Advanced Photocatalytic TiO_2 Coatings by Plasma Spraying Technique

Fuxing YE

December, 2003

Fabrication of Advanced Photocatalytic TiO_2 Coatings by Plasma Spraying Technique

Fuxing YE

(叶 福兴)

Department of Manufacturing Science
Graduate School of Engineering
Osaka University

December, 2003

Acknowledgments

I would like to express my great esteem and sincere appreciation to Prof. A. Ohmori for his guidance, encouragement and financial support throughout my PhD works in Osaka University without which this dissertation would not have been possible.

I am deeply grateful to Prof. S. Kuwabata and Prof. K. Nakata in Osaka University, for providing valuable discussion and insightful comments on this dissertation.

I would especially like to thank Prof. C.-J. Li in Xi'an Jiaotong University for his kind support, encouragement and extremely helpful suggestions. I am also particularly indebted to emeritus Prof. Y. Arata in Osaka University, who gave extraordinary support and discussion to this study.

I wish to acknowledge the staffs beginning with research associate, Mr. M. Maeda at Joining and Welding Research Institute in Osaka University for their extremely helpful comments and advices to my research. I would also like to thank the technicians, Mr. T. Horinouchi, Mr. R. Nagayama, Mr. K. Tomoto, Mr. E. Tanaka, Mr. M. Mizutani and Mr. M. Kamai at Joining and Welding Research Institute in Osaka University for their technical assistances and sincere advices.

Special thanks to all researchers and students in Ohmori Lab. in these three years. Their kindness and friendship made my study and foreign life enjoyable and happy.

Last but not least, I would like to express my grateful to my wife for her support and encouragement. I must also acknowledge my gratitude to my family for their love and support.

Table of Contents

CHAPTER 1

General Introduction

1.1. Background

In the 1980's, the UN set up the World Commission on Environment and Development, also called the Brundtland Commission [1~4]. They produced *"Our Common Future"*, otherwise known as the Brundtland Report. It defined sustainable development as development which;

"meets the needs of present generations without compromising the ability of future generations to meet their own needs"

To purify the polluted environment and avoid further pollution, heterogeneous photocatalysis has attracted great attention in recent years. Photocatalytic phenomenon was discovered by A. Fujishima and K. Honda in 1972 in Japan when they succeeded in splitting water using illuminated TiO_2 electrode [5]. From the first energy crisis of the 1970s, tremendous amount of research has been carried out in the two closely fields of semiconductor photo-electrochemistry and photocatalysis to provide fundamental insights and practical applications [6~10].

Heterogeneous photocatalysis is a discipline that includes a large variety of reactions, such as mild or total oxidations, dehydrogenation, hydrogen transfer, metal deposition, water detoxification, gaseous pollutant removal, etc. The latter two points can be considered as one of the new "advanced oxidation technologies" (AOT) for air and water purification treatment [11]. Various commercialized facilities have been developed especially in Europe, where renewable energy source is strongly emphasized. The solar photocatalytic degradation of pollutants in the compound parabolic concentrator photoreactor has been successfully applied at Plataforma Solar de Almeria Spain on the degradation of hazardous toxic compounds in water, such as phenol, atrazine, chlorinated solvents, imidacloprid, pirimicarb, acrinathrin, lindane and so on. **Fig.1.1** shows partial views of solar photochemistry compound parabolic concentrators facilities for photocatalysis installed at Hidrocen factory (Spain) and of photoelectrochemical reactors in operation [12~14]. In the reactors, powder photocatalysts are mainly applied.

The basic principles of heterogeneous photocatalysis can be summarized shortly as follows [15]. A semiconductor is characterized by an electronic band structure in

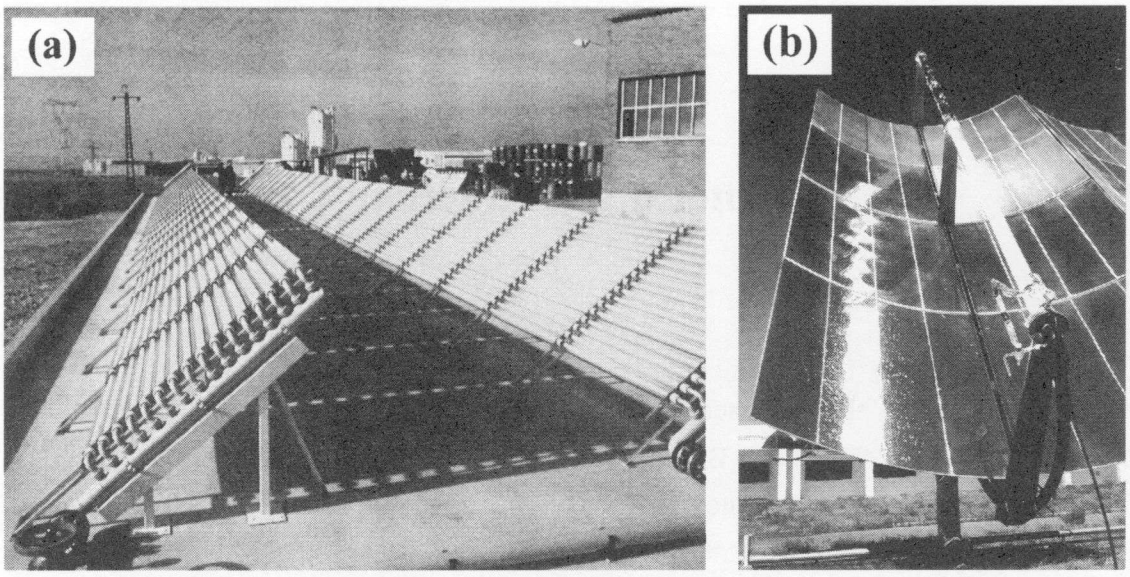

Fig.1.1. Partial views of solar photochemistry compound parabolic concentrators facilities for photocatalysis installed at Hidrocen factory (Arganda del Rey, Madfid, Spain) (a) and of photoelectrochemical reactors in operation (b). (Powder photocatalysts are mainly applied, Courtesy of S. Malato).

which the highest occupied energy band, call valence band (vb), and the lowest empty band, call conduction band (cb), are separated by a band gap, i.e. a region forbidden energies in a perfect crystal. When a semiconductor catalyst is illuminated with photons, whose energy is equal to or greater than the band-gap energy (E_{BG}), an electron from the valence band is initiated to the conduction band with simultaneous generation of a hole (h^+) in the valence band as illustrated in **Fig.1.2** [16]. The e^- and h^+ can recombine on the surface or in the bulk of the photocatalyst (particle or membrane) in a few nanoseconds (and the energy dissipated as heat) or can be trapped in surface states where they can react with donor (D) or accepter (A) species adsorbed or close to the surface of photocatalyst. Moreover, the e^- reacts with O_2 and h^+ reacts with H_2O, and consequently produce super-oxygen($\cdot O_2^-$) and OH radials($\cdot OH$) (Equations (1.1) and (1.2)), respectively. Thereby, subsequent anodic and cathodic redox reactions can be promoted. The difference with conventional catalysis is the mode of activation of the catalyst in which the thermal activation is replaced by a photonic activation.

$$O_2 + e^- \rightarrow \cdot O_2^- \tag{1.1}$$

$$H_2O + h^+ \rightarrow \cdot OH + H^+ \tag{1.2}$$

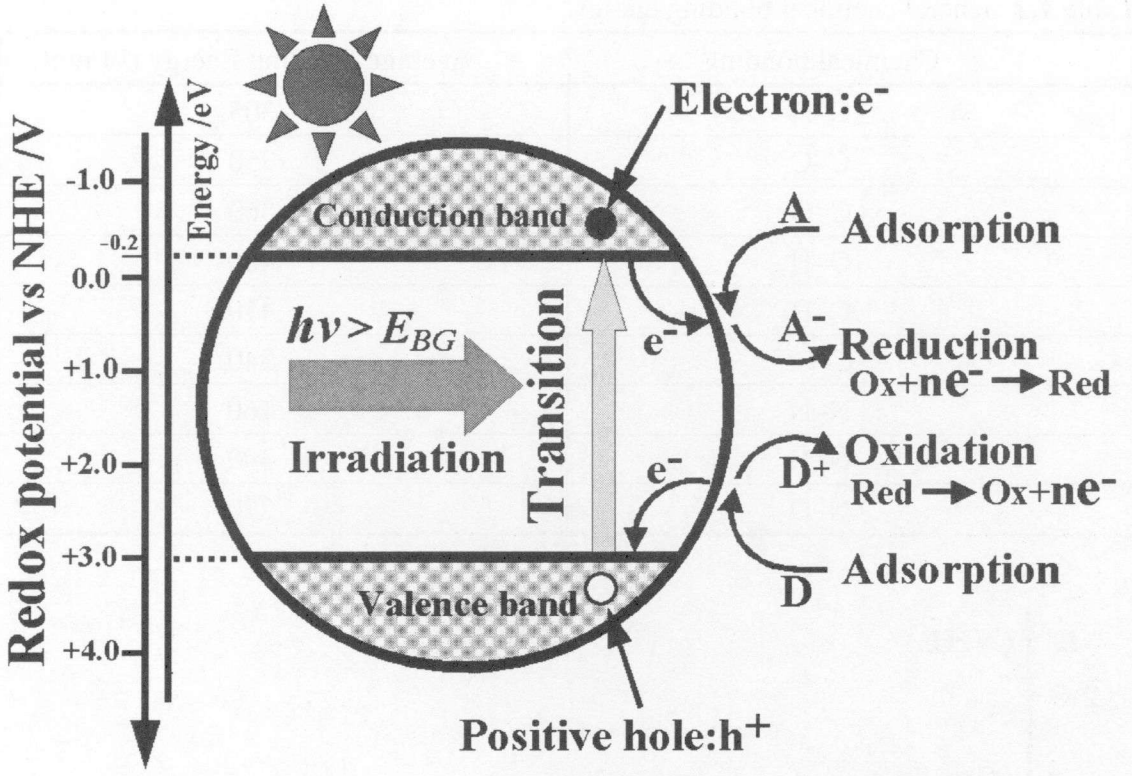

Fig.1.2. Energy band diagram of a spherical titanium dioxide particle and the basic principles of heterogeneous photocatalysis.

The oxidation potential of hydroxyl radical is 2.80V [16], which is higher than that of the general oxidizers as given in **Table 1.1**. The hydroxyl radical energy is 501kJ/mol, which is higher than the general bonding energy, such as C-C, N-H, C-O etc. as summarized in **Table 1.2**. Therefore, almost all kinds of organic substances can be oxidized by photocatalyst to simple species (H_2O, CO_2, etc).

Table 1.1 Oxidation potential of hydroxyl radical and general oxidizers.

Oxidizer	Oxidation potential (V)	Relative oxidation potential (V)
.OH	2.80	2.05
O	2.42	1.78
O_3	2.07	1.52
H_2O_2	1.77	1.30
HClO	1.49	1.10
Cl	1.36	1.00

Table 1.2 General chemical bonding energy.

Chemical bonding	Average Bonding Energy (kJ/mol)
C–N	305
C–C	350
C–O	360
O–H	460
C–H	410
C–Cl	340
N–N	160
N–H	390
N–O	220

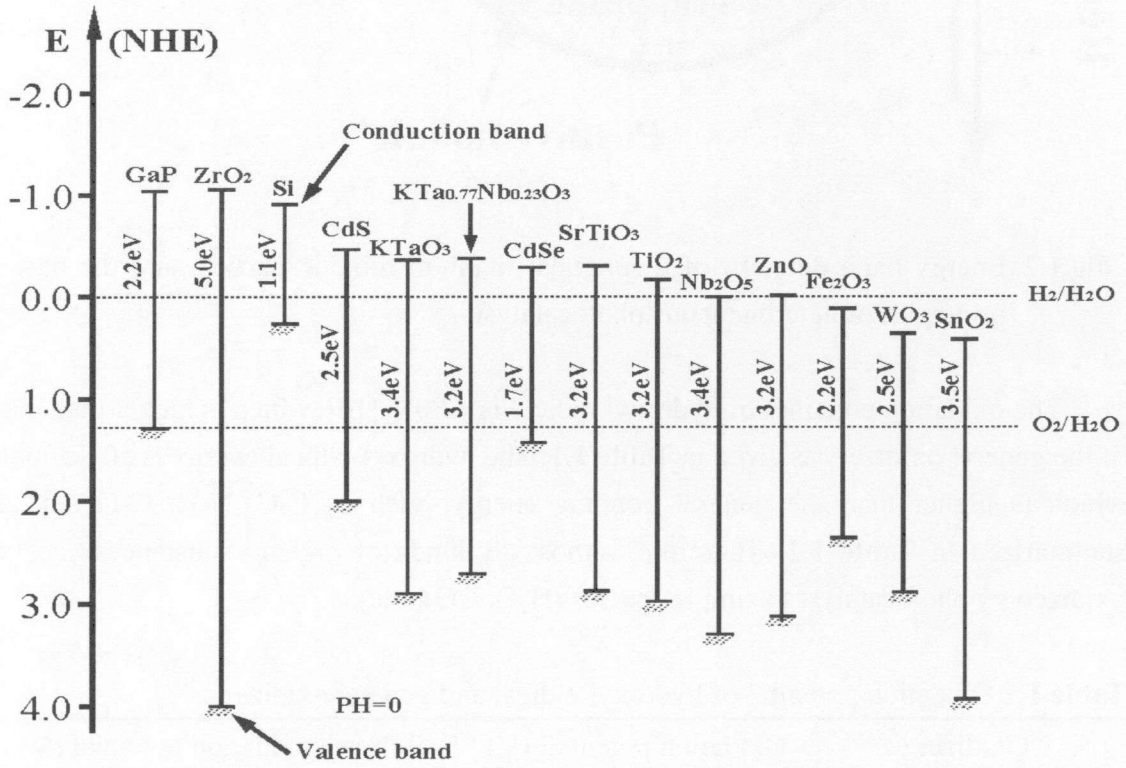

Fig.1.3. Band edge positions of various semiconductors in contact with aqueous electrolyte at pH 0.

Figure 1.3 illustrates the energy diagram of some general semiconductors [17, 18]. Among all the oxide semiconductors that have been reported, TiO_2 is an excellent photocatalyst due to its optical and electronic properties, chemical stability, non-toxicity and low cost, and can break down most kinds of refractory organic pollutants and

inorganic waste substances, including detergents, dyes, pesticides, herbicides, Cr^{3+}, $HgCl_2$ and CH_3HgCl under ultraviolet irradiation [19~22].

Titanium dioxide crystallized in three major different structures [23~26]: rutile (tetragonal), anatase (tetragonal) and brookite (rhombohedrical). Other structures exist as well, for example, cotunnite TiO_2 has been synthesized at high pressure and is one of the hardest polycrystalline materials known. However, only rutile and anatase play any role in the applications of TiO_2 and are of any interest as they have been studied with surface science techniques. Their unit cells [27] are shown in **Fig.1.4**. In both structures, each Ti^{4+} ion is surrounded by an octahedron of six O^{2-} ions. The octahedron in rutile is not regular, showing a slight orthorhombic distortion. The octahedron in anatase is significantly distorted so that its symmetry is lower than orthorhombic. The Ti-Ti distances in anatase are greater (3.79 and 3.04 Å vs. 3.57 and 2.96Å in rutile) whereas the Ti-O distances are shorter than in rutile (1.934 and 1.980 Å in anatase vs. 1.949 and 1.980 Å in rutile). In the rutile structure each octahedron is in contact with ten neighbor octahedrons (two sharing edge oxygen pairs and eight sharing corner oxygen atoms), while in the anatase structure each octahedron is in contact with eight neighbors (four sharing an edge and four sharing a corner). These differences in lattice structures cause different mass density and electronic band structure between the two crystal forms of TiO_2 as given in **Table 1.3**.

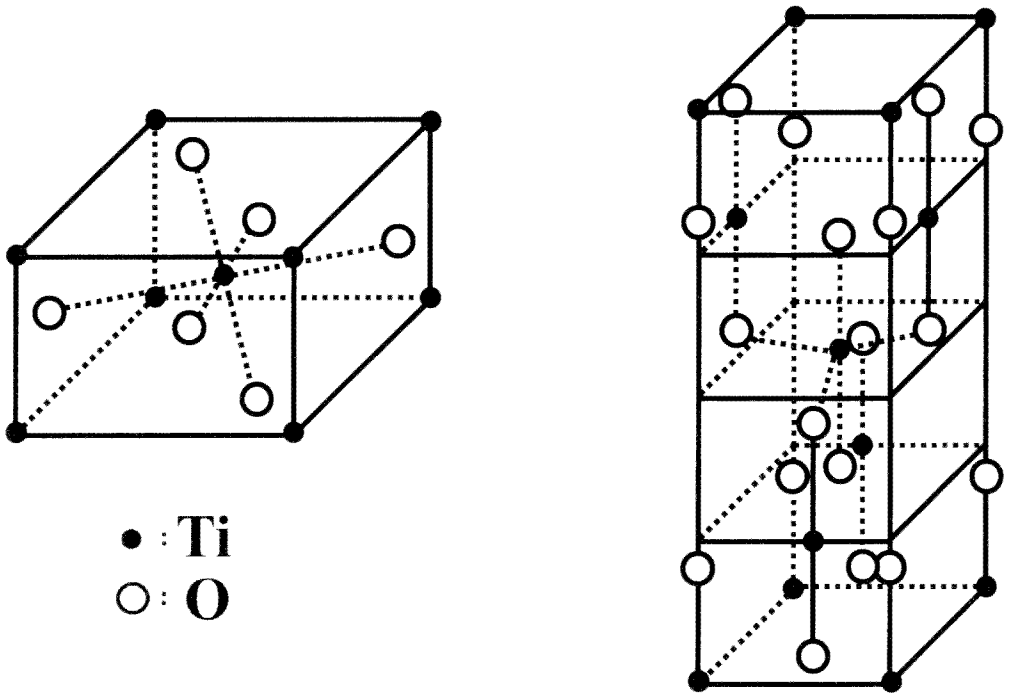

Fig.1.4. Crystal structures of rutile TiO_2 (a) and anatase TiO_2 (b).

Table 1.3 Properties of rutile and anatase TiO_2.

	Rutile TiO_2	Anatase TiO_2
Crystal system	Tetragonal	Tetragonal
Space group data	$D_{4h}^{14} - P4_2/mnm$	$D_{4h}^{19} - I4_1/amd$
Lattice constant a	4.593 Å	3.784 Å
Lattice constant b	2.959 Å	9.515 Å
Density	4.250 g/cm^3	3.894 g/cm^3
Melting point	2131 K	Meta-stable
Thermal expansion ($\times 10^{-6}$)	7.14	10.2

The melting point of rutile TiO_2 is 2131K, and the anatase TiO_2 is metal-stable, which will transform to rutile TiO_2 at elevated temperature. As a photocatalyst, anatase TiO_2 shows higher photocatalytic activity.

The photo efficiency can be reduced by the electron-hole recombination, which corresponds to the degradation of the photoelectric energy into heat.

$$e_{cb}^- + h_{vb}^+ \rightarrow N + E \qquad (1.3)$$

where N is the neutral center and E is the energy released in the form of light or of heat. To improve the photocatalytic efficiency of TiO_2, it is of great importance to inhibit the recombination of the photo-generated electrons and holes. To separate the photo-generated charges spatially, one approach is to apply composite films or powders such as TiO_2/WO_3, TiO_2/Nb_2O_5 [28~30], etc.

Moreover, it has been also realized that the forbidden energy gap of anatase TiO_2 (about 3.2eV) means that the electron can only be excited from the valence to the conduction band by the high power UV light irradiation with a wavelength less than 387nm. As shown in **Fig.1.5**, only the ultraviolet fraction (3-5%) of the solar irradiation is active in the photo-excitation processes using pure anatase TiO_2. This limits the application of sunlight as an energy source for the photocatalysis. Recently, there have many methods to extend the spectral response of semiconductor into visible region, such as ion implantation [31], doping with N [32], and using binary metal oxides [28~30].

Generally, the photocatalytic performance increases with the increasing of specific surface. Therefore, micro-powders are often applied as photocatalysts because the specific surface area is larger than that of membrane. But in practical application, micro-powder is very difficult to reclaim after photocatalytic reaction. In order to avoid this kind of technical problem, a number of methods have been used to form TiO_2 films, including wet chemical processing (e.g.: sol-gel, screen printing), vapor processing techniques (e.g.: CVD, PVD) and thermal oxidation of Ti [33].

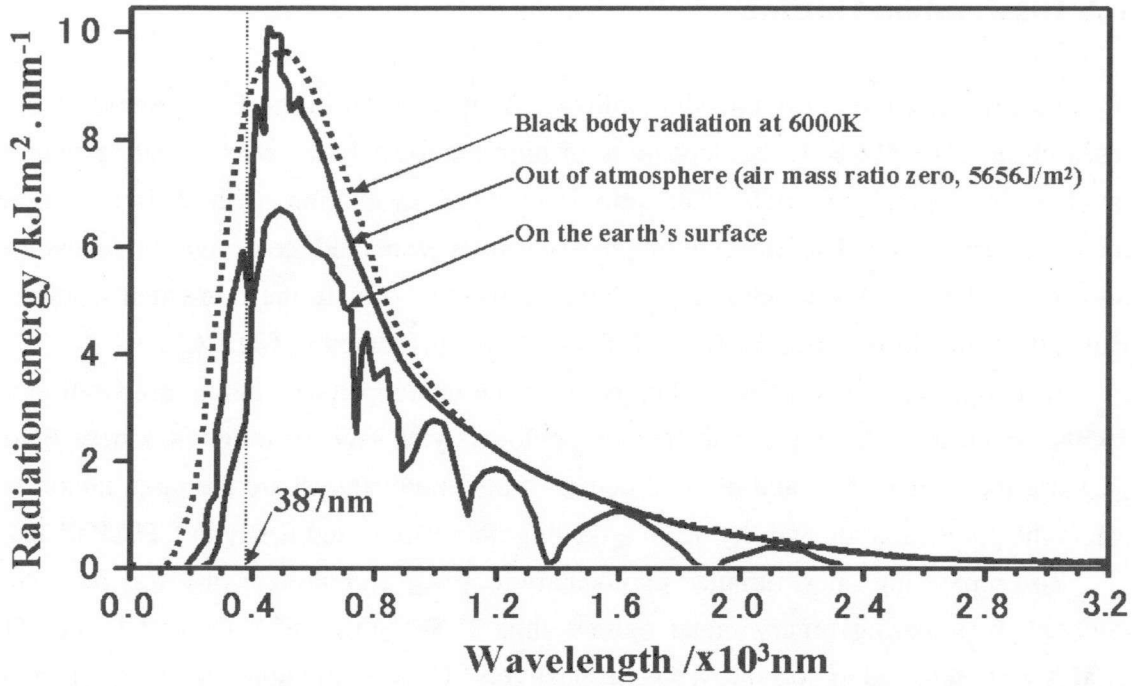

Fig.1.5. Solar energy density distribution at each wavelength.

The coating formation speed and bonding strength are very low and it is difficult to produce large surface coatings by chemical processes such as sol-gel and CVD. However, plasma spraying technique is an economical and versatile fabrication process to produce large surface coatings with almost unlimited types of materials. The coatings thickness, texture and bonding strength can be controlled easily through spraying parameters, powders and substrate state, etc [34]. A plasma sprayed deposit is formed by a stream of molten (or half-molten) droplets impacting on the substrate followed by flattening, rapid solidifying and cooling process. The individual molten (or half-molten) droplets spread to thin lamellae, the stacking of which constitutes the deposit. Therefore, it is easy to deposit composite coatings by plasma spraying technique if the feedstock powders are composite materials. The composite substances may also react with each other and then produce new compounds in plasma spraying processes.

Therefore, the present work was originally motivated to deposit high performance photocatalytic activity coatings based on the TiO_2 material on stainless steel (JIS SUS304) by plasma spraying technique, and to understand the influence of Al_2O_3, Y_2O_3 and Fe_3O_4 particles on the microstructure, phase composition and photocatalytic activity of TiO_2 coatings. To investigate the $FeTiO_3$ substance on the photocatalytic activity of TiO_2 coatings, composite TiO_2-$FeTiO_3$ coatings were prepared and analyzed. Finally, the photoelectrochemical characteristics of TiO_2 and TiO_2-Fe_3O_4 electrodes were examined.

1.2. Dissertation Outline

This dissertation is organized as follows. As mentioned in the Background of this research in **CHAPTER 1**, the deposition of high photocatalytic activity coating, which involves in original materials, fabrication technique, evaluation method, is becoming increasing important. Therefore, in this thesis, efforts were made to design the feedstock powders, to apply plasma spraying technique, and to evaluate the fabricated coatings. Block diagrams illustrating the flow of this study are presented in **Fig.1.6**.

Although plasma spraying technique has been developed for coating preparation in 1950s, application for the fabrication of photocatalytic TiO_2 coatings is a new field. Because the composition and microstructure of the photocatalyst are the main factors to affect the photocatalytic activity of TiO_2 coating, there are stated firstly in **CHAPTER 2.**

To prepare high performance photocatalytic TiO_2, a great deal of effort has been devoted in preparing binary metal oxides, thus $10\%Al_2O_3$, $10\%Y_2O_3$ and $10\%Fe_3O_4$ oxides were selected to add into TiO_2, respectively. Their evaluation results are given in **CHAPTER 3.**

Base on the research results in CHAPTER 3, the Fe_3O_4 content influence on the photocatalytic activity of TiO_2 coating was discussed in **CHAPTER 4** to clarify the original reasons of the good photocatalytic activity of TiO_2-$10\%Fe_3O_4$ coating. Because the photo absorbance character of photocatalyst is a key parameter to influence the photocatalytic activity, it was also given in it. Two-steps electron transfer model was proposed.

Next, in **CHAPTER 5**, to clarify the influence of $FeTiO_3$ substance on the photocatalytic activity of TiO_2 coatings, the TiO_2-$FeTiO_3$ powders were designed, and the composition and photocatalytic activity of TiO_2-$FeTiO_3$ coatings were investigated and discussed.

Because the fundamental principle of photocatalysis is the same as that of photoelectrochemistry, which originates from electron-hole pair generation and efficient separation, the photoelectrochemical characteristics of TiO_2 and TiO_2-$10\%Fe_3O_4$ electrodes were studied. A plasma sprayed deposit is formed by the stacking of lamellae (splats). The typical TiO_2-Fe_3O_4 splat was examined to explain the different photoelectrochemical phenomena between TiO_2 and TiO_2-$10\%Fe_3O_4$ electrode. Based on the above research results, a p-n junction formation model was proposed and confirmed. These research results are summarized in **CHAPTER 6.**

Finally, principle conclusions of this thesis are summarized in **CHAPTER 7.**

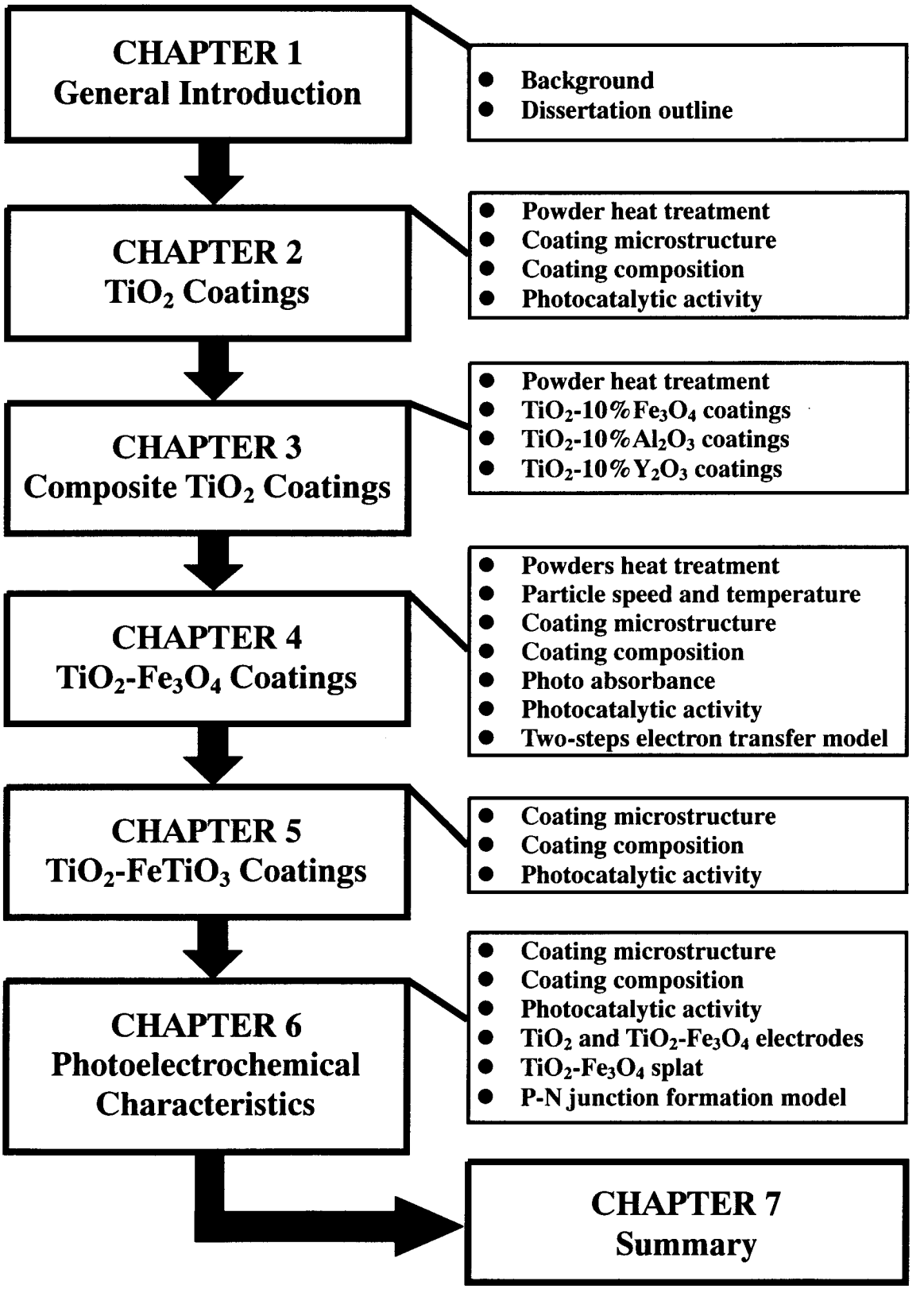

Fig.1.6. Block diagrams illustrating the flow of this study.

References

[1] http://www.un.org/esa/sustdev/about_us/aboutus.htm.

[2] A. Valentin and J. H. Spangenberg, A guide to community sustainability indicators, *Environmental Impact Assessment Review, Vol. 20(3) (2000) 381-392.*

[3] K. Dahle, Toward governance for future generations: How do we change course?, *Futures, Vol. 30(4) (1998) 277-292.*

[4] Y. M. Svirezhev and A. Svirejeva-Hopkins, Sustainable biosphere: critical overview of basic concept of sustainability, *Ecological Modelling, Vol. 106(1) (1998) 47-61.*

[5] A. Fujishima and K. Honda, Electrochemical photolysis of water at a semiconductor electrode, *Nature, Vol. 238(5358) (1972) 37-38.*

[6] H. Tributsch and L. Pohlmann, Synergetic molecular approaches towards artificial and photosynthetic water photoelectrolysis, *Journal of Electroanalytical Chemistry, Vol. 396 (1995) 53-61.*

[7] A. Fujishima, T.N. Rao and D.A. Tryk, Titanium dioxide photocatalysis, *Journal of Photochemistry and Photobiology C: Photobiology Reviews, Vol. 1(1) (2000) 1-21.*

[8] A. Mills and S. L. Hunte, An overview of semiconductor photocatalysis, *Journal of Photochemistry and Photobiology A: Chemistry, Vol. 108 (1997) 1-35.*

[9] K. Pirkanniemi and M. Sillanpaa, Heterogeneous water phase catalysis as an environmental application: a review, *Chemosphere, Vol. 48 (2002) 1047-1060.*

[10] J. Zhao and X. D. Yang, Photocatalytic oxidation for indoor air purification: a literature review, *Building and Environment, Vol. 38 (2003) 645-654.*

[11] J. M. Herrmann, Heterogeneous photocatalysis: fundamentals and applications to the removal of various types of aqueous pollutants, *Catalysis Today, Vol. 53 (1999) 115-129.*

[12] S. Malato, J. Blanco, A. Vidal, and C. Richter, Photocatalysis with solar energy at a pilot-plant scale: an overview, *Applied Catalysis B: Environmental, Vol. 37 (2002) 1-15.*

[13] P. Fernandez-Ibanez, S. Malato, and O. Enea, Photoelectrochemical reactors for the solar decontamination of water, *Catalysis Today, Vol. 54 (1999) 329-339.*

[14] D. Robert and S. Malato, Solar photocatalysis: a clean process for water detoxification, *The Science of the Total Environment, Vol. 291 (2002) 85-97.*

[15] M. Litter, Heterogeneous photocatalysis transition metal ions in photocatalytic systems, *Applied Catalysis B: Environmental, Vol. 23 (1999) 89-114.*

[16] M. R. Hoffmann, S. T. Martin, W. Y. Choi, and D. W. Bahnemann, Environmental applications of semiconductor photocatalysis, *Chemical Reviews, Vol. 95 (1995) 69-96.*

[17] M. Grätzel, Photoelectrochemical cells, *Nature, Vol. 414 (2001) 338-344.*

[18] A. Hagfeldt and M. Grätzel, Light-induced redox reactions in nanocrystalline systems, *Chemical Reviews, Vol. 95 (1995) 49-68.*

[19] A. Mills and J. Wang, Photobleaching of methylene blue sensitised by TiO_2: an ambiguous system? *Journal of Photochemistry and Photobiology A: Chemistry, Vol. 127(1-3) (1999) 123-134.*

[20] K. Tennakone and U.S. Ketipearachchi, Photocatalytic method for removal of mercury from contaminated water, *Applied Catalysis B: Environmental, Vol. 5(4) (1995) 343-349.*

[21] F. Zhang, J. Zhao, T. Shen, H. Hidaka, E. Pelizzetti, and N. Serpone, TiO_2-assisted photodegradation of dye pollutants. II. Adsorption and degradation kinetics of eosin in TiO_2 dispersions under visible light irradiation, *Applied Catalysis B: Environmental, Vol. 15(1-2) (1998) 147-156.*

[22] A. Sclafani and J. Herrmann, Influence of metallic silver and of platinum-silver bimetallic deposits on the photocatalytic activity of titania (anatase and rutile) in organic and aqueous media, *Journal of Photochemistry and Photobiology A: Chemistry, Vol. 113(2) (1998) 181-188.*

[23] U. Diebold, The surface science of titanium dioxide, *Surface Science Reports, Vol. 48 (2003) 53-229.*

[24] A. P. Rivera, K. Tanaka, and T. Hisanaga, Photocatalytic degradation of pollutant over TiO_2 in different crystal structures, *Applied Catalysis B: Environmental, Vol. 3(1) (1993) 37-44.*

[25] Y. Hu, H. -L. Tsai, and C. -L. Huang, Phase transformation of precipitated TiO_2 nanoparticles, *Materials Science and Engineering A, Vol.344(1-2) (2003) 209-214.*

[26] A. K. Sharma, R. K. Thareja, U. Willer, and W. Schade, Phase transformation in room temperature pulsed laser deposited TiO_2 thin films, *Applied Surface Science, Vol. 206(1-4) (2003) 137-148.*

[27] A. L. Linsebigler, G. Q. Lu, and J. T. Yates Jr., Photocatalysis on TiO_2 surfaces: principles, mechanisms, and selected results, *Chemical Reviews, Vol. 95 (1995) 735-758.*

[28] V. Keller, P. Bernhardt, and F. Garin, Photocatalytic oxidation of butyl acetate in vapor phase on TiO_2, Pt/TiO_2 and WO_3/TiO_2 catalysts, *Journal of Catalysis, Vol. 215(1) (2003) 129-138.*

[29] V. Iliev, D. Tomova, L. Bilyarska, L. Prahov, and L. Petrov, Phthalocyanine modified TiO_2 or WO_3-catalysts for photooxidation of sulfide and thiosulfate ions upon irradiation with visible light, *Journal of Photochemistry and Photobiology A: Chemistry, Vol. 159(3) (2003) 281-287.*

[30] H. Cui, K. Dwight, S. Soled, and A. Wold, Surface Acidity and Photocatalytic Activity of Nb_2O_5/TiO_2 Photocatalysts, *Journal of Solid State Chemistry, Vol. 115(1) (1995) 187-191.*

[31] H. Yamashita, M. Harada, J. Misaka, M. Takeuchi, K. Ikeue, and M. Anpo, Degradation of propanol diluted in water under visible light irradiation using metal ion-implanted titanium dioxide photocatalysts, *Journal of Photochemistry and Photobiology A: Chemistry, Vol. 148(1-3) (2002) 257-261.*

[32] R. Asahi, T. Morikawa, T. Ohwaki, K. Aoki, and Y. Taga, Visible-light photocatalysis in nitrogen-doped titanium oxides, *Science, Vol. 293 (2001) 269-271.*

[33] F. X. Ye and A. Ohmori, The photocatalytic activity and photo-absorption of plasma sprayed TiO_2-Fe_3O_4 binary oxide coatings, *Surface and Coatings Technology, Vol. 160(1) (2002) 62-67* (and references in it).

[34] R. Wang and C. H. Henager Jr., Arc-plasma-sprayed rutile anodes for photo-electrolysis of water, *Journal of the Electrochemical Society, Vol. 126(1) (1979) 83-85.*

CHAPTER 2

Evaluation of Plasma Sprayed TiO_2 Coatings

2.1. Introduction

Although thermal spray was invented by Swiss scientist Max Ulrich Schoop in 1910's, it was not extended until the 1950's when the expansion of the aerospace industry started to take a lead in industry technology and the development of plasma spray [1].

A plasma sprayed deposit is formed by a stream of molten (or half-molten) droplets impacting on the substrate followed by flattening, rapid solidifying and cooling process. The individual molten (or half-molten) droplets spread to thin lamellae, the stacking of which constitutes the deposit [2].

Nowadays, thermal spraying techniques have been widely applied for the production of metal and ceramic coatings on metals or the other kinds of surfaces. The applications of titanium dioxide coatings can be divided into two broad categories: as protection coatings using the rutile phase TiO_2 [3, 4] and as functional layers generally using the anatase phase TiO_2 [5, 6].

With regard to the functional layers of TiO_2, ever since the early work on photoelectrochemical reactions at TiO_2 semiconductor electrodes was reported in 1972[7], applications to environmental cleanup have been one of the most active areas in heterogeneous photocatalysis. This is inspired by the application of TiO_2-based photocatalysts for the total destruction of organic compounds in polluted air and wastewaters. Among the several semiconductor materials tested for photocatalysis, TiO_2 has proved to be the promising one due to its strong oxidizing power under UV illumination and its chemical stability [8~12].

Although extensive researches were focused on the preparation of high performance photocatalytic TiO_2 materials by chemical technique, there have not promising method to fix the photocatalytic TiO_2 powder on a kind of substrate to recycle it with high commercial interest. Furthermore, most of the supported TiO_2 is commonly reported to be less photoactive than the corresponding TiO_2 particle [13~15]. Moreover, the fabrication of photocatalytic TiO_2 coatings by thermal spraying technique can not be found except in our research group and related researchers with us until now. Therefore, the general features of plasma sprayed TiO_2 coating using anatase TiO_2

feedstock powder were studied and presented here firstly as fundamental knowledge.

In this chapter, the phase composition, microstructure and photocatalytic activity of plasma sprayed TiO_2 coatings were characterized and discussed in detail. The anatase-rutile phase transformation temperature of TiO_2 feedstock powder was investigated by electric furnace heat treatment method.

2.2. Materials and Experimental Procedures

2.2.1 Feedstock Powder and Substrate

The variation of catalytic activity with particle size is associated with an increase in the specific area and the corresponding increase of available active sites. If the size of the feedstock powder is smaller than 10μm, it is difficult to deposit coatings by thermal spraying for the low speed of the particles. So to satisfy these two demands, polyvinyl alcohol was used as a binder to agglomerate TiO_2 particles with average diameter of 0.2μm to powders with average diameter of about 30μm, which can be applied for thermal spraying. Because the photocatalytic activity of anatase titanium dioxide is better than of rutile, anatase TiO_2 was used as feedstock powder and the average size of the TiO_2 powder was 33.7μm. The size distribution of TiO_2 powder is given in **Table 2.1**. The x-ray diffraction result, morphologies of the TiO_2 powder are shown in **Fig.2.1** and **Fig.2.2**, respectively. The anatase-rutile transformation of primary anatase TiO_2 particles did not occur in the agglomeration process. Primary particle kept its original state. The substrate was stainless steel (JIS SUS304), which was washed by acetone and sandblasted before thermal spray.

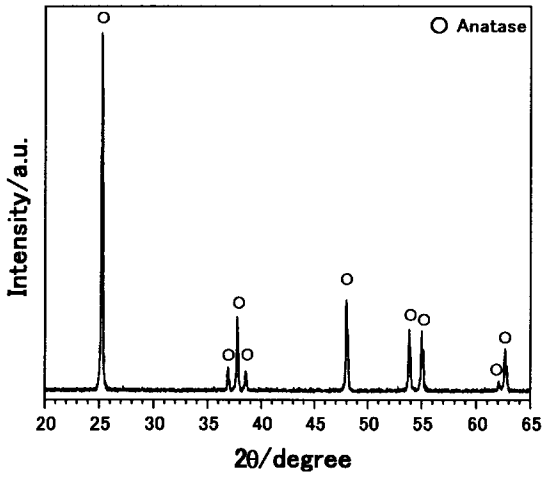

Fig.2.1. X-ray diffraction pattern of TiO_2 feedstock powder.

Table 2.1 Size distribution of TiO_2 feedstock powder.

Size (μm)	53	45	38	32	30	20	10	-10
Mass(%)	0.0	6.2	30.2	19.4	4.9	24.6	9.8	4.9

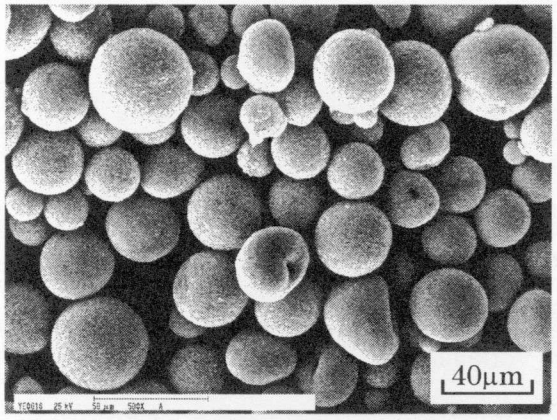

(a)

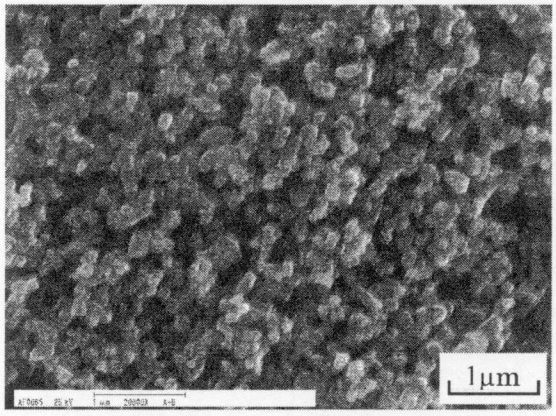

(b)

Fig.2.2. Morphologies of TiO_2 feedstock powder. (a) Low magnification, (b) High magnification.

2.2.2. Plasma Spraying Equipment

The plasma spraying system was commercial spraying equipment, which was Plasmadyne-Mach1 manufactured by Plasmadyne Company. The gun is schematically illustrated in **Fig.2.3**. The gun's unique design accepts internal or external powder injection. Because internal injection provides optimum energy transfer and particle velocity, internal injection with a powder port angle of 30° was chosen in this research. Argon was used as a primary plasma gas and helium was used as the secondary gas. Because the photocatalytic activity of anatase TiO_2 is better than that of rutile TiO_2 as

mentioned in Chapter 1, it is very important to inhibit the phase transformation of anatase TiO_2 in the heating process of plasma spraying. According to the research results of spray distance on the overall properties of TiO_2 coating, the spray distance was set as 70mm.The thermal spraying parameters are given in **Table 2.2**.

Table 2.2 Plasma spraying parameters.

Argon gas pressure (MPa)	0.42
Argon gas flow (slpm)	58
Helium gas pressure (MPa)	0.21
Helium gas flow (slpm)	9
Arc current (A)	400, 600, 800
Arc voltage (V)	28~30
Spraying distance (mm)	70

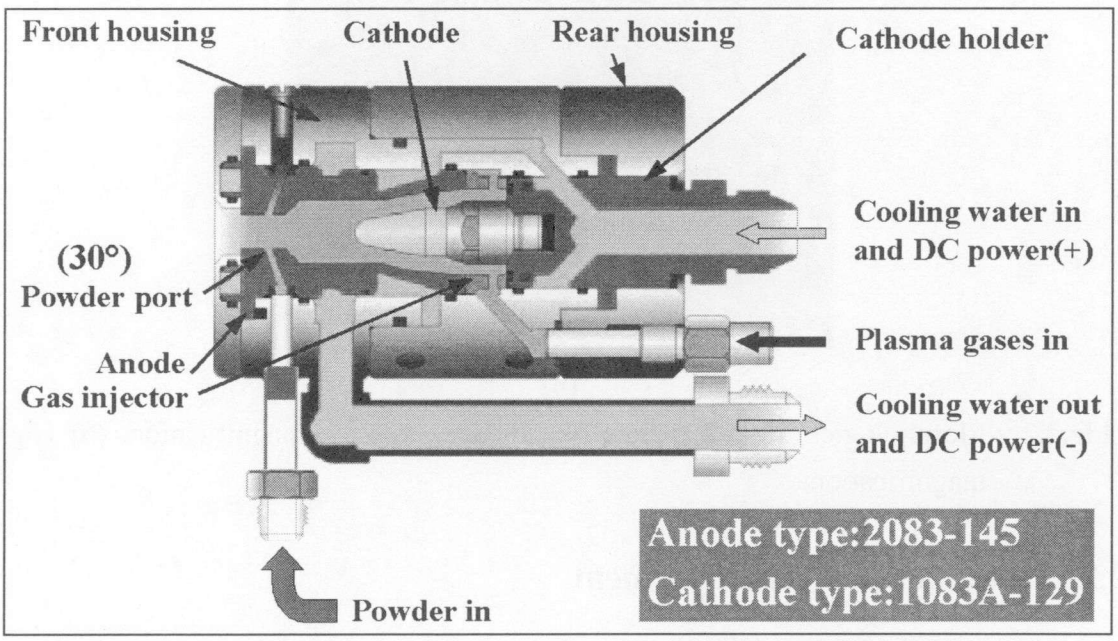

Fig.2.3. Schematic diagram of plasma spray torch applied in this study.

2.2.3. Heat Treatment Procedure of Agglomerated TiO_2 Powder

To investigate the anatase-rutile phase transformation temperature, the TiO_2 feedstock powder was kept in electric furnace for 7200s after reaching at treated

temperature (1123K, 1173K, 1223K or 1273K) with a heating rate of 1.67K/s, and then was cooled with the furnace.

2.2.4. Characterization of Powder and Sprayed Coatings

Electron probe surface roughness analyzer (ERA-8800FE, Elionix Co. Ltd., Japan) and energy dispersive analysis of x-ray (EDAX) were used to examine the structure characteristics of the powders and the sprayed coatings. The phase composition of the powders and the sprayed coatings were investigated by x-ray diffraction using Cu-Kα radiation (λ=1.5406Å) and graphite crystal monochromator (M03XHF, MAC Science Co. Ltd.). The 2θ range was 23°~38°. Quantitative analysis of the phase composition of the sprayed coatings was attempted by comparing the net x-ray diffraction peaks intensities of anatase (101) and rutile (110). The content of anatase phase in the sprayed coatings was calculated using the most common equation given by R. A. Spurr and H. Myers [16].

$$A = \frac{I_A}{1+1.265\frac{I_R}{I_A}} \times 100\% \tag{2.1}$$

where I_A is the highest peak intensity of anatase phase (101 peak), I_R the highest peak intensity of rutile phase (110 peak) and A the content of anatase phase in the sprayed coatings.

The surface roughness of the coating was investigated by a surface roughness analyzer (DEKTAK, ULVAC, Japan).

2.2.5. Definition of Relative Deposition Speed of Feedstock Powder

In thermal spray technology, there have many parameters to evaluate the properties of sprayed coatings, such as cohesion strength, hardness, wear resistance, powder deposition efficiency and so on. The mechanical properties of sprayed coatings are very important in mechanical applications. However, great attention should be paid on not only the functional performance but also the powder deposition speed in the developments of functional coatings.

Therefore, to evaluate the fabrication characteristics of the feedstock powder at various plasma spraying conditions, the powder deposition speed was defined as Equation (2.2). The calculated result was applied to compare the powder deposition efficiency in this study.

$$RDSP = \frac{T_{Thickness} V_{Traverse} W_{Step}}{n V_{Rotation}} \tag{2.2}$$

where *RDSP* is Relative Deposition Speed of Powder, $V_{Rotation}$ relative rotation speed of powder feeder, $V_{Traverse}$ relative traverse speed of plasma gun, W_{Step} relative step width of up-down moving equipment, $T_{Thickness}$ thickness of sprayed coating, n spray pass of the coating.

2.2.6. Photocatalytic Activity Evaluation Method

Generally, the kinetic of photocatalytic reaction follows a Langmuir-Hinshelwood mechanism [17~21] confirming the heterogeneous catalytic character of the system with the rate ν varying proportionally with the surface coverage θ as:

$$v = k\theta = \frac{dC}{dt} = \frac{kKC}{1+KC} \tag{2.3}$$

where C is the reactant concentration, ν the degradation rate of reactant, k the reaction rate constant, θ surface coverage, t reaction time and K surface adsorption equilibrium constant.

Equation (2.3) can be changed to

$$-\left(1+\frac{1}{KC}\right)dC = kdt \tag{2.4}$$

The integration form of Equation (2.4) is

$$\ln(\frac{C_0}{C}) + K(C_0 - C) = kKt \tag{2.5}$$

where C_0 is the initial concentration of reactant. For dilute gas, $K(C_0-C)$ is nearly equivalent to 0, consequently Equation (2.5) becomes Equation (2.6) letting $\tau=kK$.

$$\ln(\frac{C}{C_0}) = -kKt = -t/\tau \tag{2.6}$$

In this research, the photocatalytic activity of the feedstock powders and sprayed coatings was evaluated through the photo mineralization of acetaldehyde applying ultraviolet light. The evaluation set-up is shown in **Fig.2.4**. The irradiation profile of ultraviolet lamp is illustrated in **Fig.2.5**, and the light intensity on the sample surface was set in 1.0mW/cm^2. In the experimental procedure, the decomposition of the concentration (ppm) of acetaldehyde and CO_2 product concentration with time (s) were measured with two kinds of Kitakawa type gas detectors at a certain time interval.

The coatings surface area was standardized as 50×60mm. On the other hand, to

evaluate the photocatalytic activity of powder, the powder was uniformly laid on a silica glass with dimension of 50×60mm, and the weight of powder was 0.5g.

According to Equation (2.6), the smaller the value of τ the better of the photocatalytic activity of the coating/powder. Therefore, the τ can be used as the characteristic decomposition time to evaluate the catalytic effectiveness of the sprayed coating and powder.

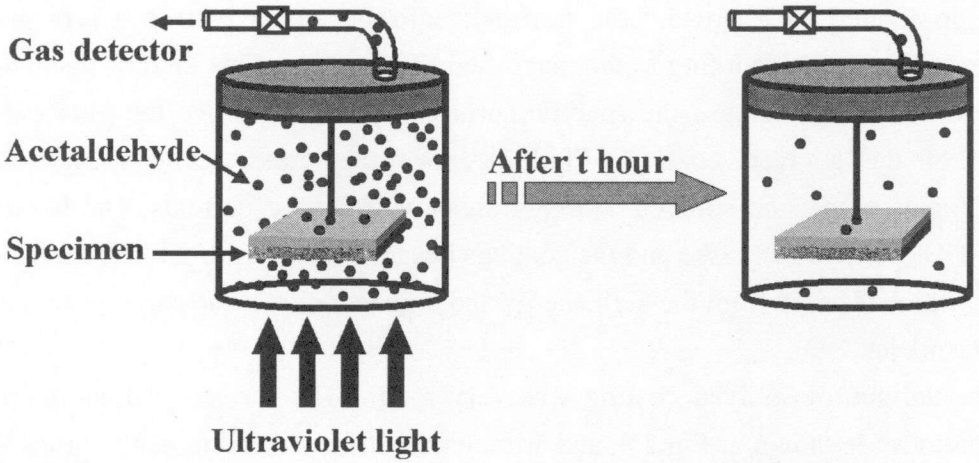

Fig.2.4. Evaluation set-up for photocatalytic activity of feedstock powder and spayed coating.

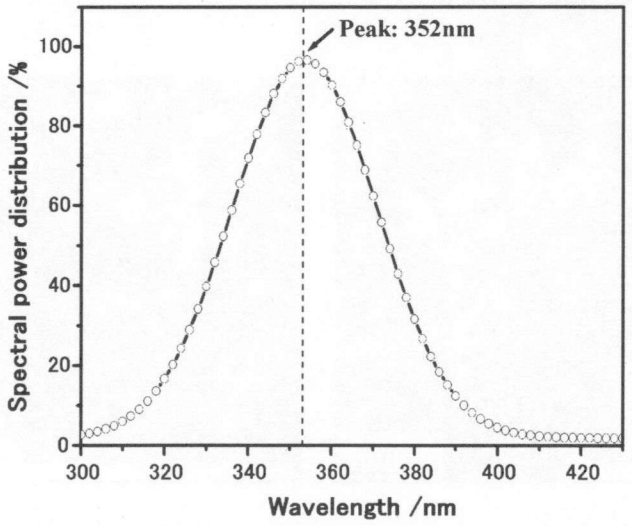

Fig.2.5. Spectral power distribution of ultraviolet lamp used for photocatalytic experiment in this study.

2.3. Results and Discussion

2.3.1. General Features of Plasma Sprayed TiO_2 Coatings

Although the rutile TiO_2, which is generally applied for improving wear resistance or as constructional material, etc, is a kind of well-known material, a few researchers are studying on anatase TiO_2 as functional material in thermal spray field. **Fig.2.6** shows the surface morphologies of TiO_2 coating plasma sprayed under the arc current of 400A. The agglomerated TiO_2 powder did not melt entirely, and a part of 0.2μm primary particles still existed according to the magnified SEM image. This kind of phenomenon will be a benefit to increase the specific surface and then improve the photocatalytic activity of the sprayed coating. **Fig.2.7** shows the cross sections and surface morphologies of plasma sprayed coatings under various arc currents. The fraction of melted TiO_2 particle increased and the coatings became denser with the increasing of arc current, which resulted from the high energy and high velocity of the particles transferred from plasma jet.

The surface of sprayed coating was very rough. The surface profiles of sprayed TiO_2 coatings are shown in **Fig.2.8**, and arithmetical mean deviation of the profiles (Ra) were approximate to 8.8μm, 6.3μm and 5.7μm under the arc current of 400A, 600A and 800A, respectively. Under lower arc current, the surface of the coating became rougher.

The relative deposition speed of anatase TiO_2 powder is shown in **Fig.2.9**. Under the arc current of 400A, the relative deposition speed was approximate to 5μm/pass. With more increased arc current of 600A, the relative deposition speed increased significantly.

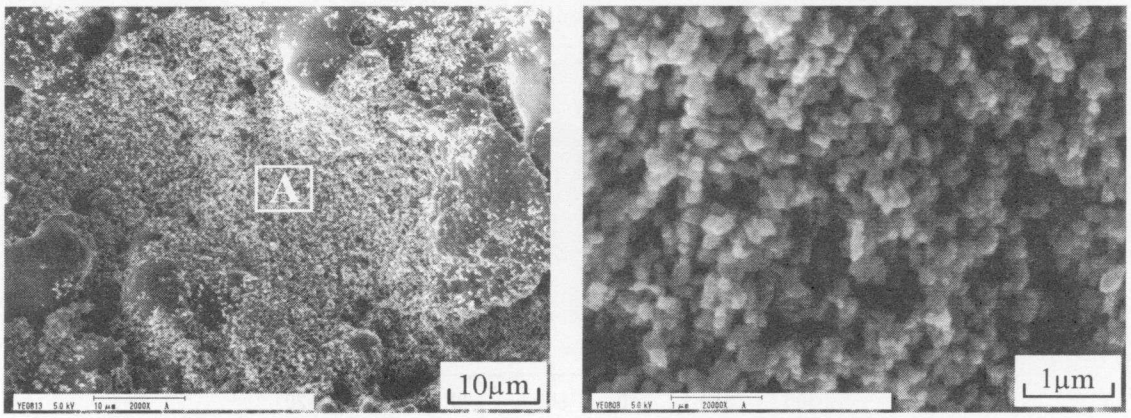

(a) (b)

Fig.2.6. Surface morphologies of plasma sprayed TiO_2 coating under the arc current of 400A. (a) General view, (b) Magnified view of position A in (a)

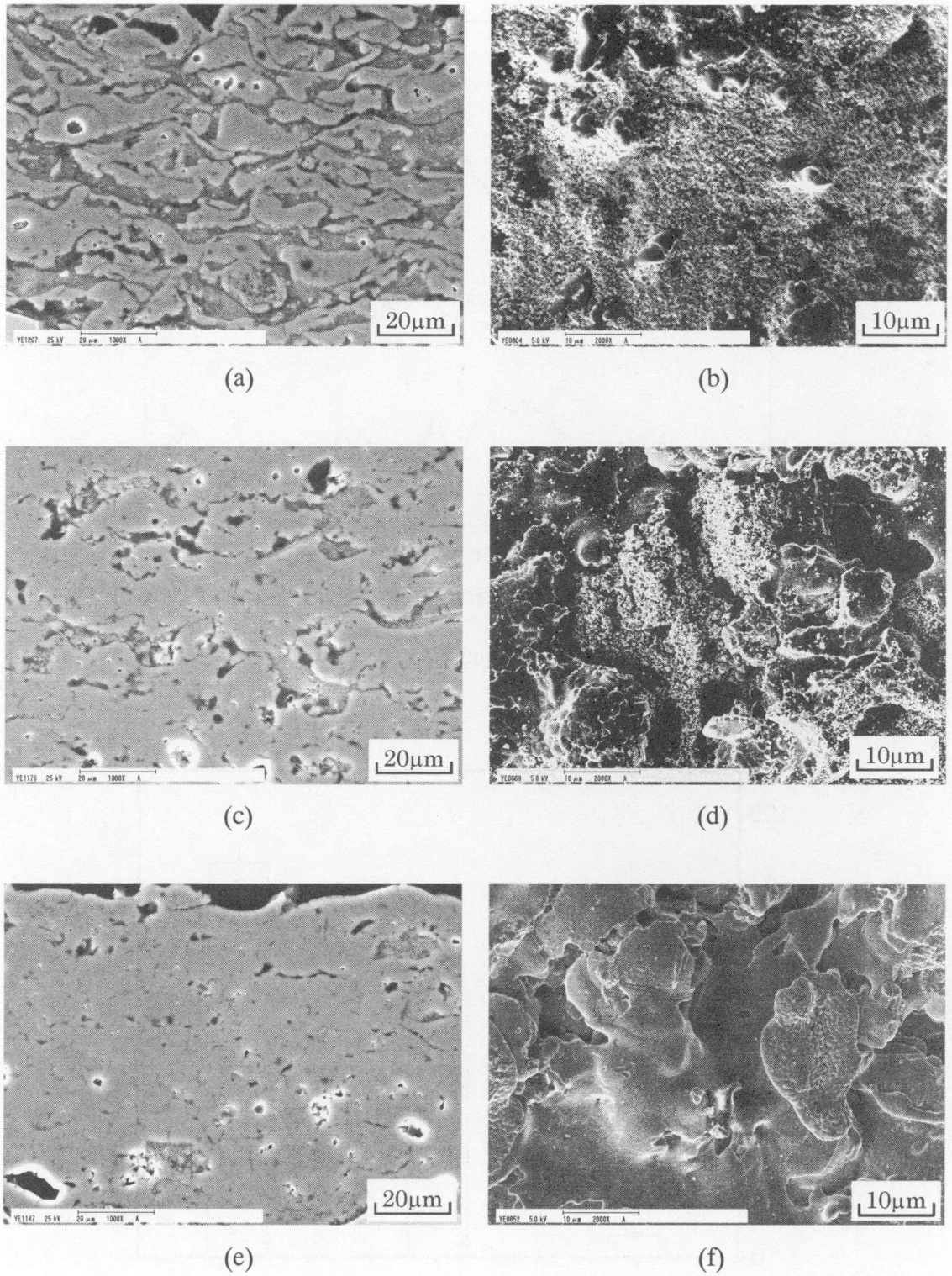

Fig.2.7. SEM micrographs of plasma sprayed TiO_2 coatings. (a), (c) and (e) Cross sections under the arc current of 400A, 600A and 800A, respectively; (b), (d) and (f) Surface morphologies, respectively.

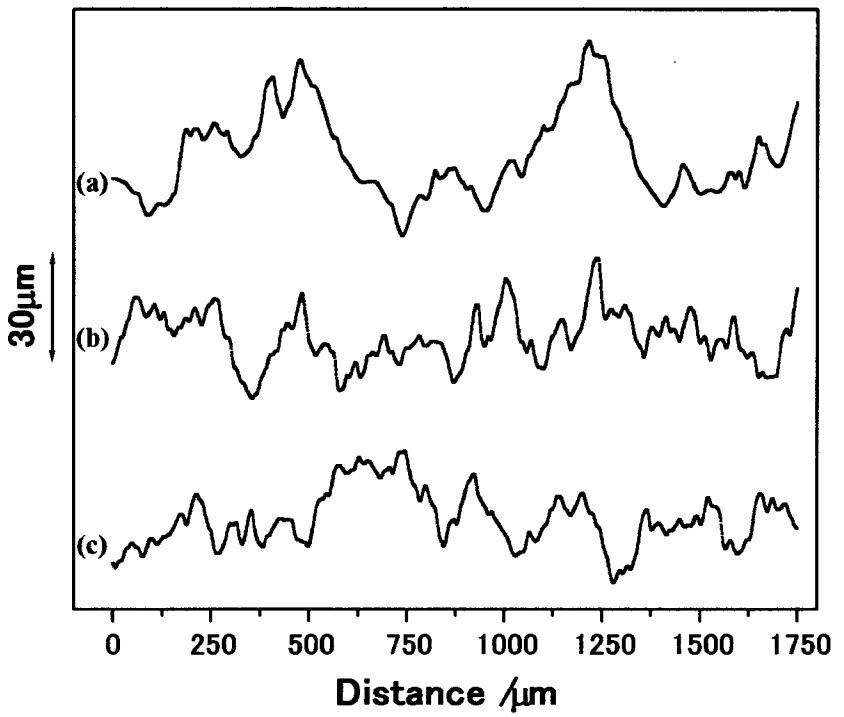

Fig.2.8. Surface profiles of plasma sprayed TiO_2 coatings under various arc currents. (a) 400A, (b) 600A, (c) 800A.

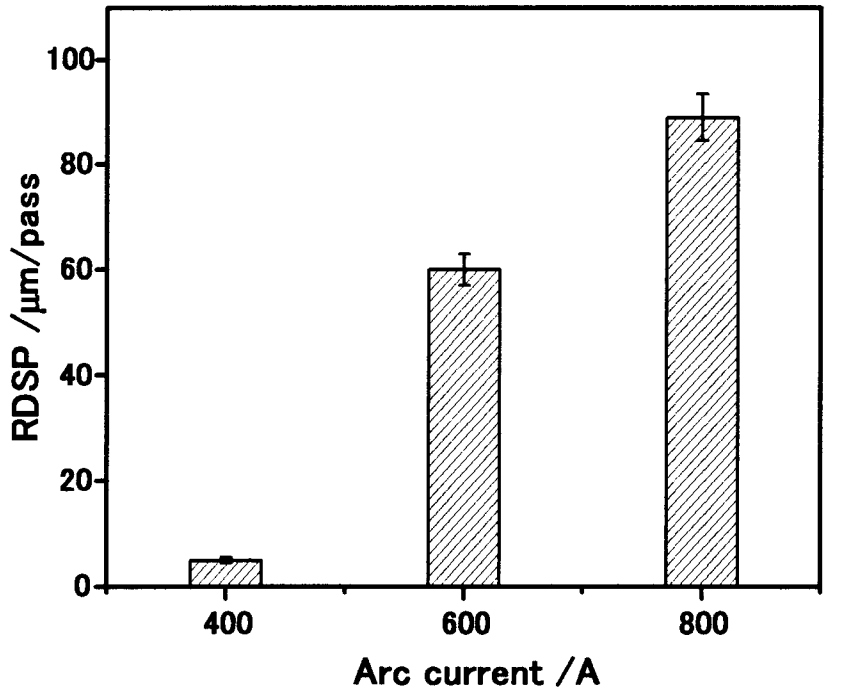

Fig.2.9. Relative deposition speed of anatase TiO_2 powder under the arc current of 400A, 600A and 800A.

2.3.2. Composition of Plasma Sprayed TiO_2 Coatings

The plasma spraying process is characterized by a high temperature, ranging from 10000K and 20000K, by the presence of a plasma reducing gas, mainly a mixture of reducing gas such as Ar, He. As a consequence of these severe conditions, chemical modification such as reduction or composition variations can take place during the plasma spraying process [22, 23].

The x-ray diffraction patterns of TiO_2 coatings plasma sprayed under arc current of 400, 600 and 800A is illustrated in **Fig.2.10**. To compare with the feedstock powder, the x-ray diffraction pattern of anatase TiO_2 powder is also illustrated in it. The peak height of anatase TiO_2 (101 peak) decreased with the increasing of arc current for the phase transformation of anatase to rutile TiO_2, whereas that for rutile TiO_2 (110 peak) increased continuously. Because the photocatalytic activity of anatase phase is better than that of rutile phase [24], the contents of anatase TiO_2 in the sprayed coatings were calculated and summarized in **Fig.2.11** according to the x-ray diffraction patterns and Equations (2.1). The content of anatase TiO_2 in the sprayed coatings was not over 15% and decreased with the increasing of the arc current.

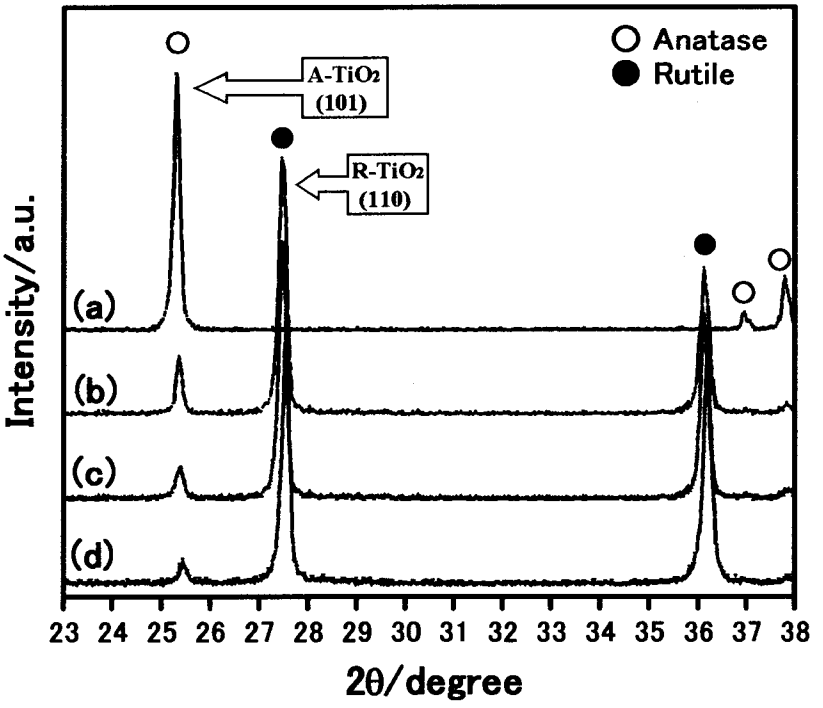

Fig.2.10. X-ray diffraction patterns of TiO_2 powder (a) and plasma sprayed TiO_2 coatings under the arc current of 400A (b), 600A (c) and 800A (d).

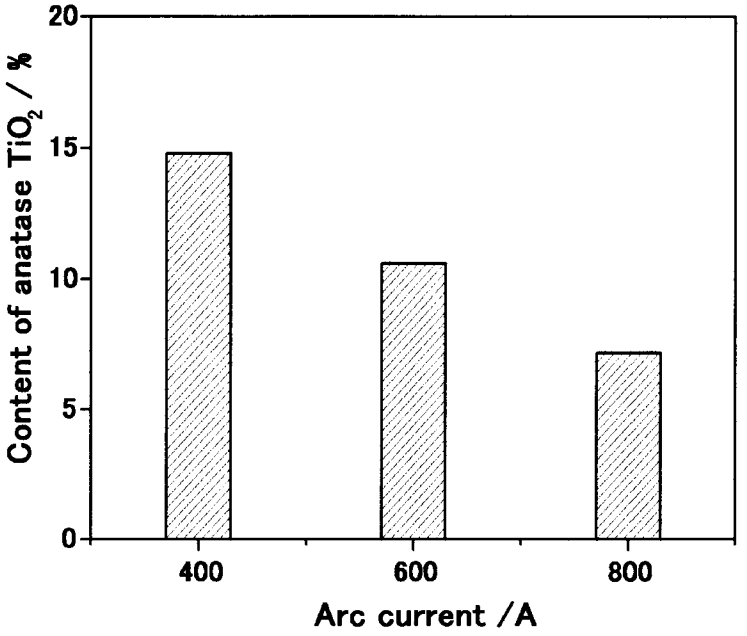

Fig.2.11. Contents of anatase TiO_2 in plasma sprayed TiO_2 coatings under the arc current of 400A, 600A and 800A.

2.3.3. Composition of Heat Treated TiO_2 Powders

Crystal structure variations of TiO_2 are well known, anatase is meta-stable and transform exothermally and irreversibly to rutile over a range of temperatures but usually at 923K to 1273K [25~27], which is governed by particle size, particle morphology, synthetic conditions and purity, etc. Because the photocatalytic activity of anatase phase is better than that of rutile phase, it is very important to know the anatase-rutile transformation temperature of anatase TiO_2 feedstock powder used in this study.

The thermal behaviors of TiO_2 have been observed by differential thermal analysis and furnace heat treatment method and so on. In this study, electric furnace heat treatment at 1123K, 1173K, 1223K and 1273K for 7200s in air with a heating rate of 1.67K/s was selected to investigate the transformation temperature of anatase TiO_2 powder. The x-ray diffraction patterns of heat treated TiO_2 feedstock powders are illustrated in **Fig.2.12**. The anatase phase kept the original phase state at the 1123K. When treated at 1173K, rutile phase appeared. And the anatase phase transformation nearly finished at 1273K. These facts implied that the anatase phase transformation

temperature was approximate to 1173K. For the low anatase-rutile phase transformation temperature, it is not easy to fabricate high performance photocatalytic coatings by plasma spraying technique with the pure anatase TiO_2 powder for the high temperature (over 10000k) of plasma jet using the method inhibiting anatase phase transformation.

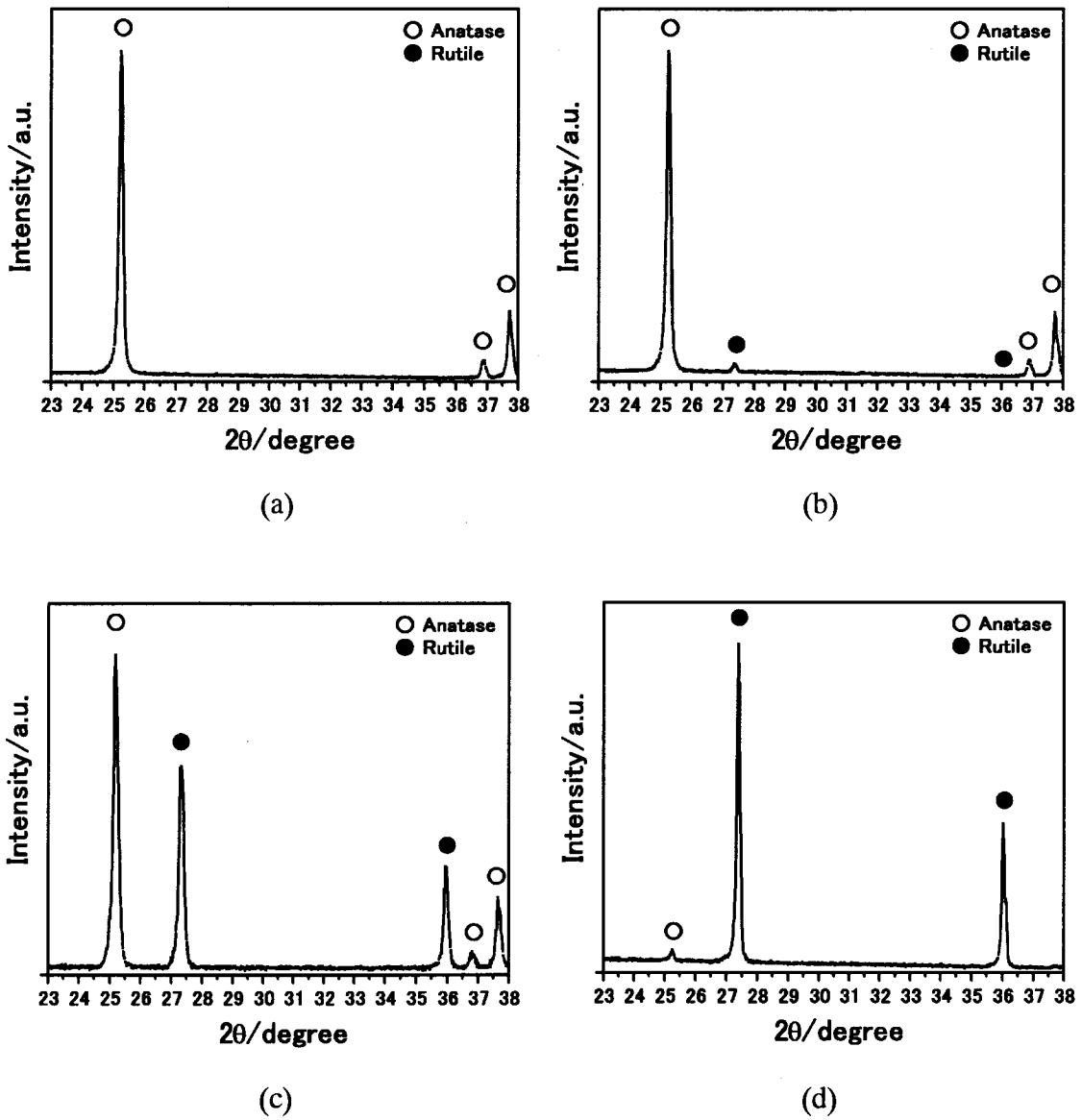

Fig.2.12. X-ray diffraction patterns of heat treated TiO_2 powders for 7200s at various temperatures. (a) 1123K, (b) 1173K, (c) 1223K, (d) 1273K.

2.3.4. Photocatalytic Activity of Plasma Sprayed TiO_2 Coatings

Figure 2.13 illustrates the decomposition characteristics of the acetaldehyde by plasma sprayed TiO_2 coatings under the arc current of 400A, 600A and 800A. In the case of sprayed TiO_2 coatings prepared under the arc current of 400A and 600A, the concentration of acetaldehyde decreased with the irradiation time. Therefore, these two kinds of TiO_2 coatings had photocatalytic activity. The degradation speed by TiO_2 coating sprayed under the arc current of 400A was higher than that by the other one. In the case of TiO_2 coating sprayed under the arc current of 800A, the concentration of acetaldehyde had not considerable change with the irradiation time, which means that this coating had not photocatalytic activity. To compare the photocatalytic activity digitally, the τ values of the plasma sprayed TiO_2 coatings were calculated by Equation (2.6) and the results are shown in **Fig.2.14**. For the highest anatase TiO_2 content and rough surface of the coating sprayed under the arc current of 400A, it had lowest τ value. On the country, with the increasing of arc current to 800A, its τ value was very high.

As a result, it is very important to inhibit the phase transformation of anatase TiO_2 in thermal spray process because rutile TiO_2 has not considerable photocatalytic activity. Therefore, it is not easy to form high photocatalytic performance TiO_2 coatings for the high temperature of plasma jet.

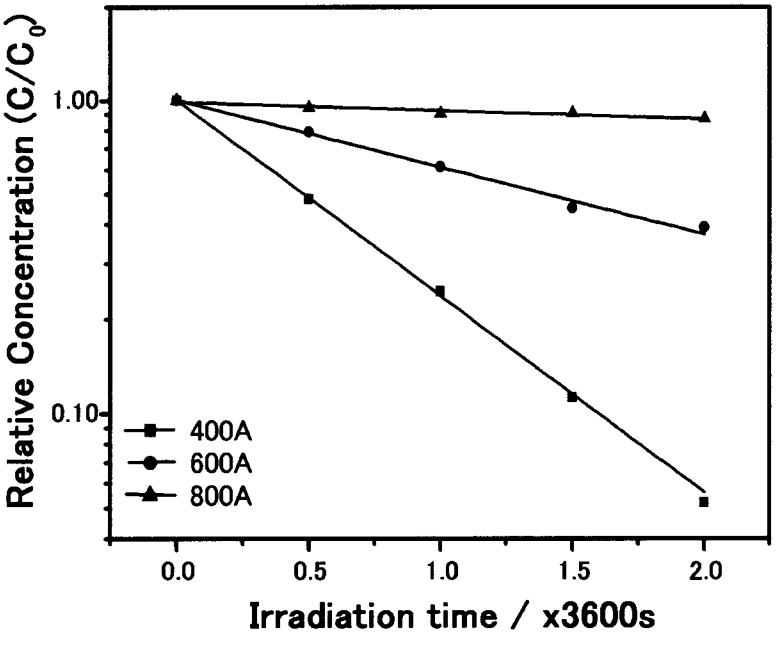

Fig.2.13. Decomposition characteristics of the acetaldehyde by plasma sprayed TiO_2 coatings under the arc current of 400A, 600A and 800A.

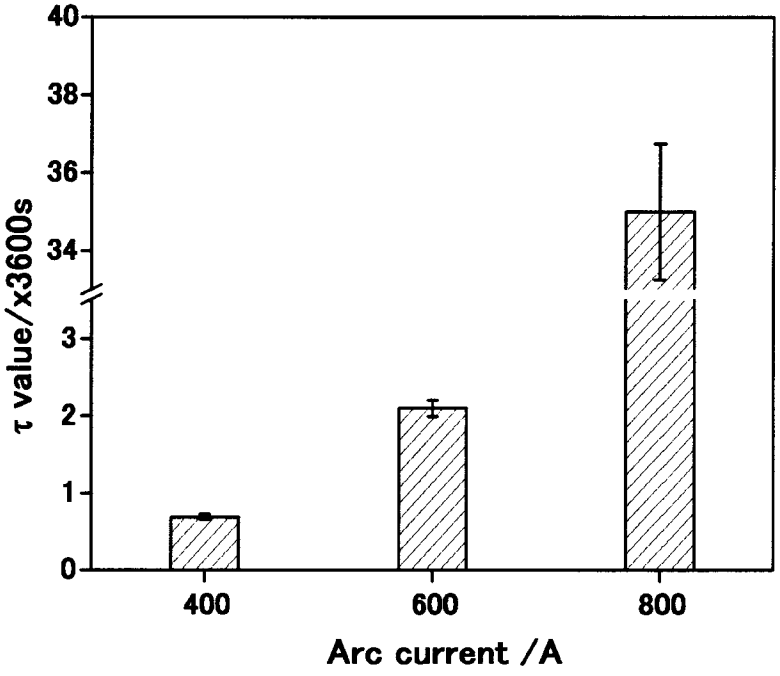

Fig.2.14. τ values of TiO_2 coatings prepared under the arc current of 400A, 600A and 800A.

2.4. Conclusions

TiO_2 coatings were prepared by plasma spraying technique using agglomerated anatase TiO_2 powder. The composition and photocatalytic activity of plasma sprayed TiO_2 coatings were investigated. The content of anatase TiO_2 in the sprayed coatings was approximate to 7-15%, which was influenced by the melting state of TiO_2 powder in plasma spraying process. The anatase to rutile phase transformation temperature of agglomerated anatase TiO_2 powder was approximate to 1173K. The TiO_2 coating sprayed under the arc current of 400A had good photocatalytic activity for the relative high content of anatase phase in it. However, the relative deposition speed, which was approximate to 5μm/pass, was very low. For the high temperature of plasma jet, it is not easy to fabricate high performance photocatalytic coatings by plasma spray using the pure anatase TiO_2 powder applying the technique of inhibiting anatase phase transformation.

References

[1] A. Hasui, Yousya Kougaku, *SanPou Publishing House, 1996 (In Japanese).*

[2] C. J. Li and A. Ohmori, Relationships between the microstructure and properties of thermally sprayed deposits, *Journal of Thermal Spray Technology, Vol. 11(3) (2002) 365-374.*

[3] C. X. Ding, B. T. Huang, and H. L. Lin, Plasma-sprayed wear-resistant ceramic and cermet coating materials, *Thin Solid Films, Vol. 118(4) 1984, 485-493.*

[4] B. Normand, V. Fervel, C. Coddet, and V. Nikitine, Tribological properties of plasma sprayed alumina–titania coatings: role and control of the microstructure, *Surface and Coatings Technology, Vol. 123(2-3)(2000) 278-287.*

[5] N. Berger-Keller, G. Bertrand, C. Filiatre, C. Meunier, and C. Coddet, Microstructure of plasma-sprayed titania coatings deposited from spray-dried powder, *Surface and Coatings Technology, Vol. 168(2-3) (2003) 281-290.*

[6] K. L. Yeung, S. T. Yau, A. J. Maira, Juan M. Coronado, Javier Soria, and Po Lock Yue, The influence of surface properties on the photocatalytic activity of nanostructured TiO_2, *Journal of Catalysis, Vol. 219(1) 2003, 107-116.*

[7] A. Fujishima and K. Honda, Electrochemical photolysis of water at a semi-conductor electrode, *Nature, Vol. 238 (5358) 1972, 37-38.*

[8] A. Fujishima, T.N. Rao, D.A. Tryk, Titanium dioxide photocatalysis, *Journal of Photochemistry and Photobiology C: Photochemistry Reviews, Vol.1 (2000) 1-211.*

[9] M. Anpo and M. Takeuchi, The design and development of highly reactive titanium oxide photocatalysts operating under visible light irradiation, *Journal of Catalysis, Vol. 216(1-2) (2003) 505-516.*

[10] J. Shang, W. Li, and Y. F. Zhu, Structure and photocatalytic characteristics of TiO_2 film photocatalyst coated on stainless steel webnet, *Journal of Molecular Catalysis A: Chemical, Vol. 202(1-2) (2003) 187-195.*

[11] J. Zhao and X. D. Yang, Photocatalytic oxidation for indoor air purification: a literature review, *Building and Environment, Vol. 38(5) (2003) 645-654.*

[12] L. Q. Jing, X. J. Sun, J. Shang, W. M. Cai, Z. L. Xu, Y. G. Du, and H. G. Fu, Review of surface photovoltage spectra of nano-sized semiconductor and its applications in heterogeneous photocatalysis, *Solar Energy Materials and Solar Cells, Vol. 79(2) (2003) 133-151.*

[13] S. Anandan and M. Yoon, Photocatalytic activities of the nano-sized TiO_2-supported Y-zeolites, *Journal of Photochemistry and Photobiology C: Photochemistry Reviews, Vol. 4(1) (2003) 5-18.*

[14] J. Sabate, M. A. Anderson, M. A. Aguado, J. Giménez, S. Cervera-March, C. G. Hill Jr., Comparison of TiO_2 powder suspensions and TiO_2 ceramic membranes supported on glass as photocatalytic systems in the reduction of chromium(VI), *Journal of Molecular Catalysis, Vol. 71(1) 1992, 57-68.*

[15] R.W. Matthews, Purification of water with near-u.v. illuminated suspensions of titanium dioxide, *Water Research, Vol. 24(5) (1990), 653-660.*

[16] R. A. Spurr and H. Myers, Quantitative analysis of anatase-rutile mixtures with an x-ray diffactometer, *Analytical Chemistry, Vol. 29(5) (1957) 760-762.*

[17] L. Y. Shi, C. Z. Li, H. C. Gu, and D. Y. Fang, Morphology and properties of ultrafine SnO_2-TiO_2 coupled semiconductor particles, *Materials Chemistry and Physics, Vol. 62 (2000) 62-67.*

[18] F. L. Zhang, J. C. Zhao, T. Shen, H. Hidaka, E. Pelizzetti, and N. Serpone, TiO_2-assisted photodegradation of dye pollutants II. Adsorption and degradation kinetics of eosin in TiO_2 dispersions under visible light irradiation, *Applied Catalysis B: Environmental, Vol. 15 (1998) 147-156.*

[19] K. E. O'Shea and C. Cardon, The reactivity of phenol in irradiated aqueous suspensions of TiO_2. Mechanistic changes as a function of solutions PH, *Journal of Photochemistry and Photobiology A: Chemistry, Vol. 91 (1995) 67-72.*

[20] A. Sirisuk, C. G. Hill Jr., and M. A. Anderson, Photocatalytic degradation of ethylene over thin films of titania supported on glass rings, *Catalysis Today, Vol. 54 (1999) 159-164.*

[21] V. Augugliaro, J. Blanco Gálvez, J. Cáceres Vázquez, E. García López, V. Loddo, M. J. López Muñoz, S. Malato Rodríguez, G. Marcì, L. Palmisano, M. Schiavello, and J. Soria Ruiz, Photocatalytic oxidation of cyanide in aqueous TiO_2 suspensions irradiated by sunlight in mild and strong oxidant conditions, *Catalysis Today, Vol. 54 (1999) 245-253.*

[22] T. Zhang, Y. Bao, and D. T. Gawne, Process model of plasma enamelling, *Journal of the European Ceramic Society, Vol. 23(7) (2003) 1019-1026.*

[23] P. Fauchais and A. Vardelle, Heat, mass and momentum transfer in coating formation by plasma spraying, *International Journal of Thermal Sciences, Vol. 39(9-11) (2000) 852-870.*

[24] F. X. Ye and A. Ohmori, The photocatalytic activity and photo-absorption of plasma sprayed TiO_2-Fe_3O_4 binary oxide coatings, *Surface Coating Technology, Vol. 160(1) (2002) 62-67.*

[25] R. D. Shannon and J. A. Pask, Kinetics of the anatase-rutile transformation, *Journal of The American Ceramic Society, Vol. 48(8) (1965) 391-398.*

[26] W. F. Sullivan and S. S. Cole, Thermal chemistry of colloidal titanium dioxide, *Journal of The American Ceramic Society, Vol. 42(3) (1959) 127-133.*

[27] Y. Iida and S. Ozaki, Grain growth and phase transformation of titanium oxide during calcination, *Journal of The American Ceramic Society, Vol. 44(3) (1961) 120-127.*

[28] M. Ocana, J. V. Garcia-Ramos, and C. J. Serna, Low-temperature nucleation of rutile observed by raman spectroscopy during crystallization of TiO_2, *Journal of The American Ceramic Society, Vol. 75(7) (1992) 2011-2012.*

CHAPTER 3

Evaluation of Plasma Sprayed Composite TiO_2 Coatings

3.1. Introduction

As mentioned in Chapter 1, titanium dioxide represents one of the most efficient photocatalyst. To prepare high performance photocatalytic TiO_2, the researches can be divided into two broad fields: (1) Improving photocatalytic efficiency of TiO_2 to use UV light. (2) Extending the spectral response into visible region.

The effective photo-excitation of TiO_2 semiconductor particle requires the application of light with energy higher than the band gap energy (E_{BG}) of titanium dioxide. Therefore, the absorption thresholds correspond to 387nm and 413nm for anatase and rutile, respectively. Consequently, only the ultraviolet fraction (3-5%) of the solar irradiation is active in the photo-excitation processes using pure TiO_2 semiconductor as mentioned in Chapter 1. Because of the potential application to the conversion of solar energy to chemical energy, the development of semiconductor photocatalysts that have high reactivity under visible light has received great attention. To extend the spectral response of semiconductor into visible region as like dye-sensitized solar cell and/or to improve the photocatalytic activity, a great deal of effort has been devoted in recent years, such as Cr, V, Fe ion implantation [1~4], plasma surface modification [5,6], doping with N [7], and using binary metal oxides [8~10].

With respect to binary metal oxides, I. Bayer et al. [9] reported that Al_2O_3 acts as an electron acceptor of TiO_2, thus the presence of Al_2O_3 impurity may improve the separation of initiated electrons and holes, and then improves the photocatalytic activity of TiO_2. J. Lin et al. [10] suggested that the mean lifetime of electron-holes photo-generated by UV illumination was longer in the mixture of TiO_2/Y_2O_3 than that in pure TiO_2 according to the transient absorption decay spectra. J. Moser et al. [11] also observed the same phenomenon while study the photocatalytic property of Fe doped TiO_2 semiconductor. On the country, additive into TiO_2 has also negative influence on the photocatalytic activity in spite of the same substance, the reason is still not very clear [12, 13]. To elucidate the effects of Al_2O_3 and Y_2O_3 on the photocatalytic activity of TiO_2, investigations of TiO_2/Al_2O_3 and TiO_2/Y_2O_3 composite coatings prepared by plasma spraying technique were performed in this study.

As discussed in Chapter 2, the relative deposition speed of anatase TiO_2 powder (RDSP) for the preparation of good photocatalytic TiO_2 coating was very low. To improve RDSP and study the effect of Fe elements on the photocatalytic activity of TiO_2, Fe_3O_4 particle with relative low melting point was added into TiO_2.

In this chapter, the phase composition, microstructure and photocatalytic activity of plasma sprayed TiO_2-10%Fe_3O_4, TiO_2-10%Al_2O_3, TiO_2-10%Y_2O_3 coatings were characterized and discussed in detail. Moreover, the composition of heat treated composite TiO_2 powders was investigated.

3.2. Materials and Experimental Procedures

3.2.1 Feedstock Powders and Substrate

TiO_2 particles with average size of 0.2μm were mechanically and uniformly mixed with Fe_3O_4, Al_2O_3 and Y_2O_3 particles with 10% weight content, respectively, and then were agglomerated to TiO_2-10%Fe_3O_4, TiO_2-10%Al_2O_3 and TiO_2-10%Y_2O_3 powders with average size of about 30μm. The substrate was stainless steel (JIS SUS304).The x-ray diffraction result of the TiO_2-10%Fe_3O_4 powder is illustrated in **Fig.3.1**, and powder morphology is also given in it, which was very similar to TiO_2-10%Al_2O_3 and TiO_2-10%Y_2O_3 powders. The additives distributed uniformly in the powders according to EDAX analysis results of powder cross sections. The x-ray diffraction results of the TiO_2-10%Al_2O_3 and TiO_2-10%Y_2O_3 feedstock powders are shown in **Fig.3.2**.

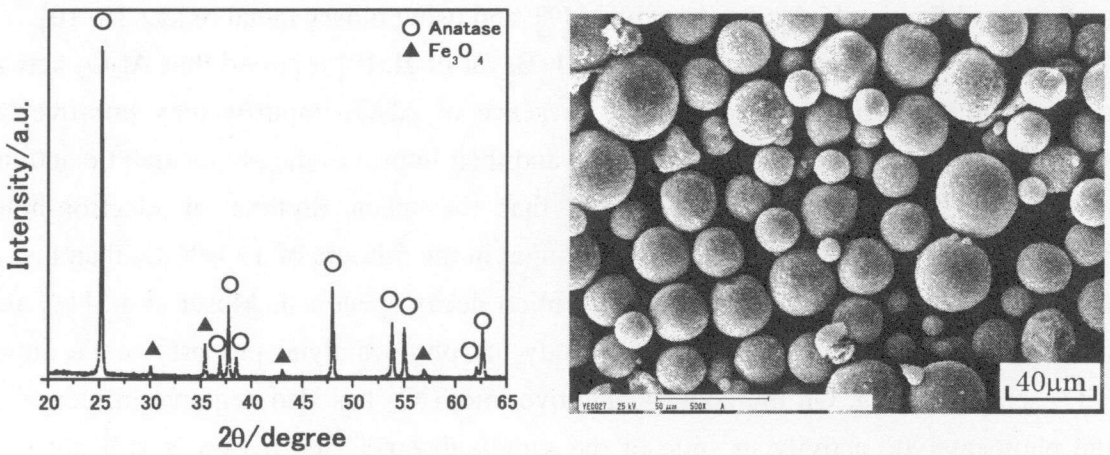

(a) (b)

Fig.3.1. X-ray diffraction pattern (a) and morphology (b) of TiO_2-10%Fe_3O_4 feedstock powder.

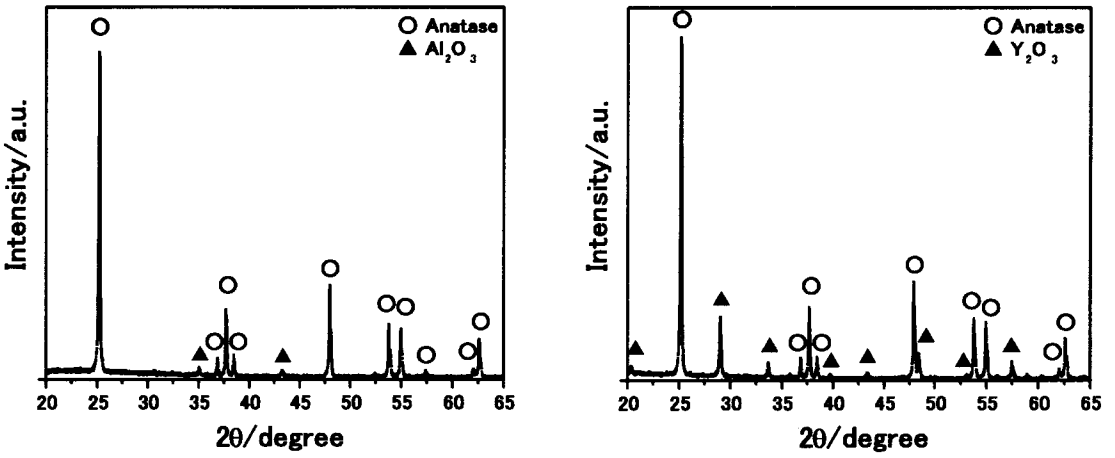

(a) (b)

Fig.3.2. X-ray diffraction patterns of composite TiO_2 feedstock powder. (a) TiO_2-10%Al_2O_3, (b) TiO_2-10%Y_2O_3.

3.2.2. Composite Coatings Preparation and Heat Treatment of Powders

Three kinds of composite powders of TiO_2-10%Fe_3O_4, TiO_2-10%Al_2O_3 and TiO_2-10%Y_2O_3 were plasma sprayed on sandblasted JIS SUS304 steel using the equipment described in Chapter 2. According to the research results of plasma sprayed TiO_2 coatings presented in Chapter 2, the low arc current is preferable to forming high photocatalytic activity coatings. Therefore, to examine the delicate influence of additives, the arc current applied for the composite TiO_2 coating was set as 400A or 500A. The detailed conditions are given in **Table 3.1**.

The anatase-rutile transformation temperature of pure anatase TiO_2 powder was approximate to 1173K (See Chapter 2). To investigate the influence of the additive on the anatase-rutile phase transformation temperature and clarify the composition variations of feedstock powders in thermal spray process, they were kept in the furnace for 7200s after reaching at treated temperature (973K, 1123K, 1273K or 1423K) with a heating rate of 1.67K/s, and then were cooled with the furnace.

Table 3.1 Plasma spraying parameters.

Argon gas pressure (MPa)/ flow (slpm)	0.42/58
Helium gas pressure (MPa)/flow (slpm)	0.21/9
Arc current (A)	400, 500
Arc voltage (V)	28~30
Spraying distance (mm)	70, 100

3.2.3. Characterization of Powders and Sprayed Coatings

The microstructure and phase characterization of powders and sprayed coatings were performed by electron probe surface roughness analyzer (ERA-8800FE, Elionix Co. Ltd., Japan) and x-ray diffraction (M03XHF, MAC Science Co. Ltd.).

The relative deposition speed of feedstock powder (RDSP) was calculated using the Equation (2.2). The photocatalytic activity of sprayed coating was evaluated by the set-up described in Chapter 2 and the τ value was calculated by Equation (2.6).

3.3. Results and Discussion

3.3.1. Heat Treated Composite TiO_2 Powders

Figure 3.3 shows the x-ray diffraction results of TiO_2-10%Fe_3O_4 feedstock powders heat treated at various temperatures. Magnetite (Fe_3O_4) additive reacted with oxygen under 973K and produced Fe_2O_3 (Reaction (3.1) and Fig.3.3(a)), which is in good agreement with the reported data measured by differential scanning calorimetry analysis (DSC) equipment [14]. One part of anatase TiO_2 transformed into rutile at 1123K, which did not observed for pure anatase TiO_2 powder (See Fig.2.12 in Chapter 2). Therefore, conclusion can be drawn that the addition of Fe_3O_4 to TiO_2 would accelerate the anatase-rutile phase transformation. The reaction of Fe_2O_3 with TiO_2 happened below 1123K, and consequently formed stable phase of pseudobrookite Fe_2TiO_5 (Reaction (3.2)).

$$4Fe_3O_4 + O_2 \rightarrow 6Fe_2O_3 \qquad (3.1)$$

$$Fe_2O_3 + TiO_2 \rightarrow Fe_2TiO_5 \qquad (3.2)$$

Figure 3.4 shows the x-ray diffraction results of TiO_2-10%Al_2O_3 feedstock powders heat treated at various temperatures. Comparing the phenomena shown in Fig.3.4 and Fig.2.12, it can see that the addition of Al_2O_3 into TiO_2 seems had not any effect on the thermal behaviors of anatase TiO_2 powder below 1423K. As reported by V. Buscaglia et al. [15, 16], formation of Al_2TiO_5 occurs in an oxidizing atmosphere according to Reaction (3.3) above 1553K. Below 1553K, Al_2TiO_5 decomposes, as it is unstable in comparison to Al_2O_3 and TiO_2. That is why there had not Al_2TiO_5

compound in the heat treated TiO_2-10%Al_2O_3 powders.

$$Al_2O_3 + TiO_2 \rightarrow Al_2TiO_5 \tag{3.3}$$

Figure 3.5 shows the x-ray diffraction results of TiO_2-10%Y_2O_3 feedstock powders heat treated at various temperatures. Over 1273K, TiO_2 reacted with Y_2O_3 and produced $Y_2Ti_2O_7$ (Reaction (3.4) [17, 18]).

$$Y_2O_3 + 2TiO_2 \rightarrow Y_2Ti_2O_7 \tag{3.4}$$

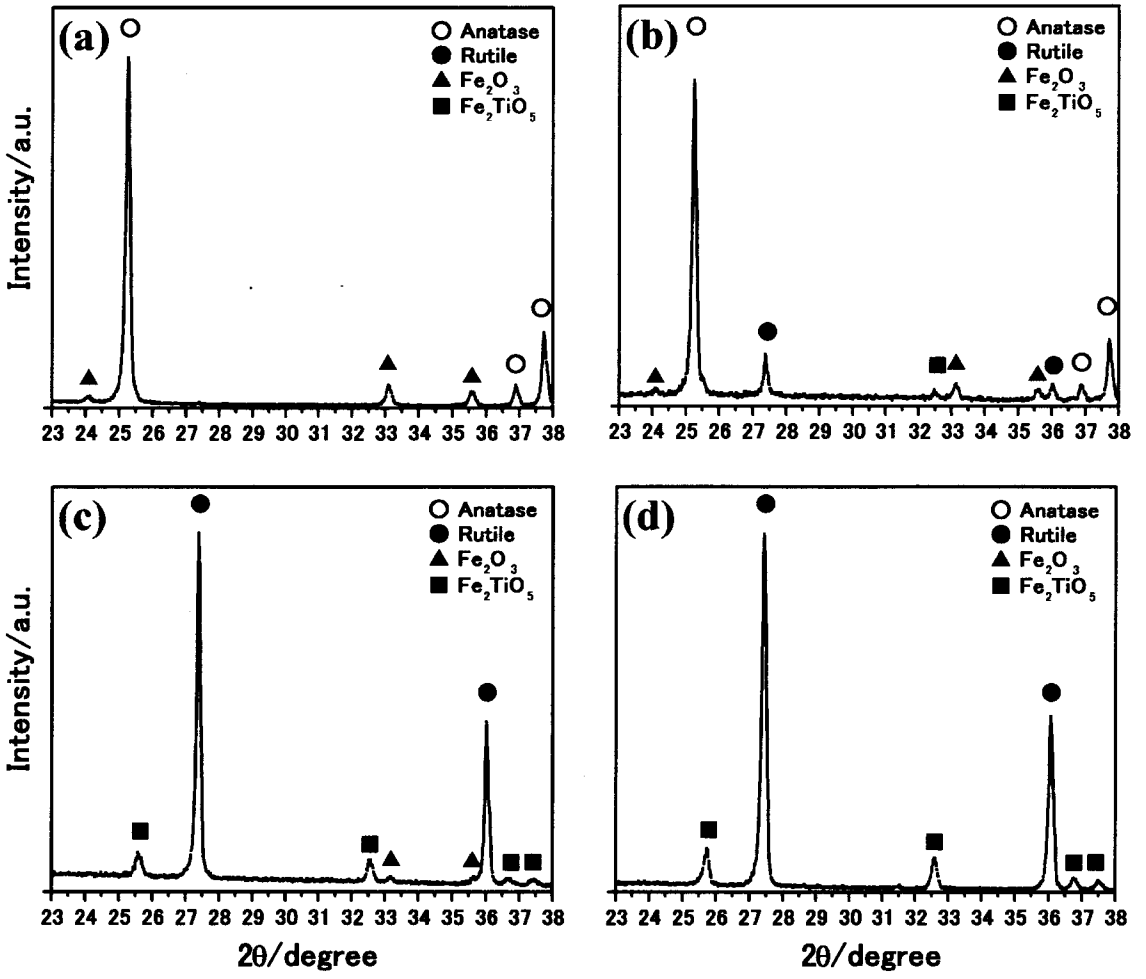

Fig.3.3. X-ray diffraction patterns of heat treated TiO_2-10%Fe_3O_4 feedstock powders at various temperatures. (a) 973K, (b) 1123K, (c) 1273K, (d) 1423K.

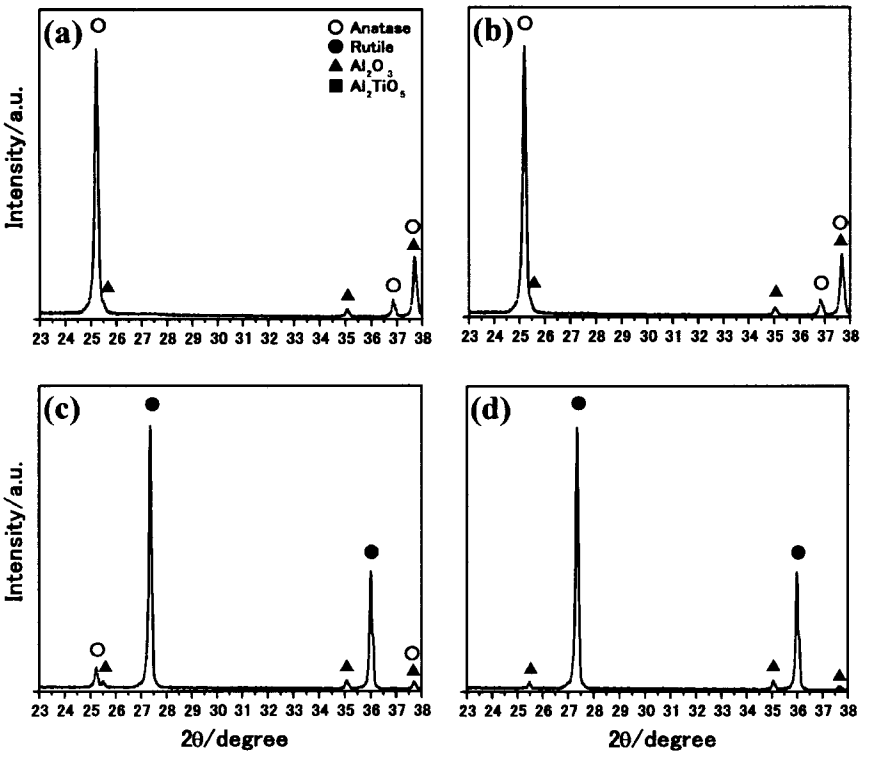

Fig.3.4. X-ray diffraction patterns of heat treated TiO_2-10%Al_2O_3 feedstock powders at various temperatures. (a) 973K, (b) 1123K, (c) 1273K, (d) 1423K.

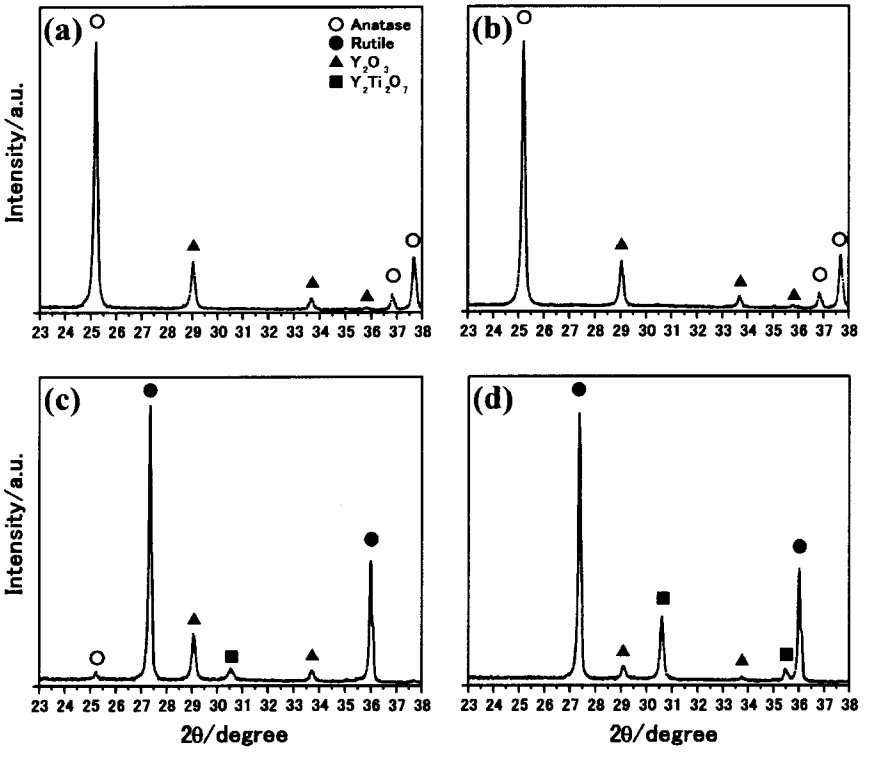

Fig.3.5. X-ray diffraction patterns of heat treated TiO_2-10%Y_2O_3 feedstock powders at various temperatures. (a) 973K, (b) 1123K, (c) 1273K, (d) 1423K.

3.3.2. Characterization of Plasma Sprayed TiO_2-10%Fe_3O_4 Coatings

Figure 3.6 shows the cross sections of plasma sprayed TiO_2-10%Fe_3O_4 coatings. Under the arc current of 400A and spraying distance of 70mm, the coating had porous structure (Fig.3.6(c)). As shown in **Fig.3.7**, partially melted 0.2μm particle still existed in it. This kind of phenomenon will be a benefit to increase the specific surface and then improve the photocatalytic activity of the sprayed coatings. With more increased arc current, the coating became denser, and the content of the partially melted particle decreased.

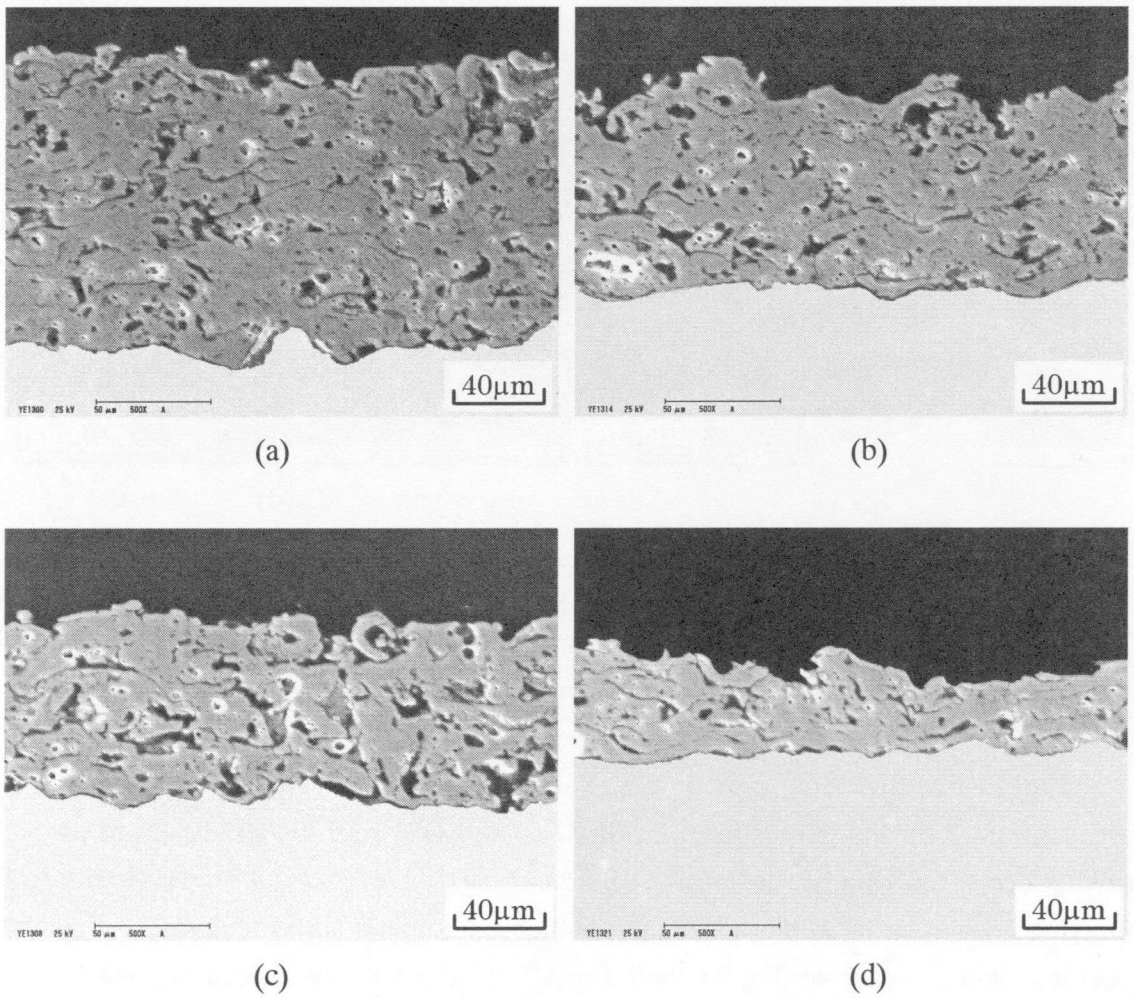

Fig.3.6. Cross sections of plasma sprayed TiO_2-10%Fe_3O_4 coatings. (a) I=500A SD=70mm, (b) I=500A SD=100mm, (c) I=400A SD=70mm, (d)I=400A SD=100mm. (Notes: "I" denotes arc current, "SD" denotes spraying distance.)

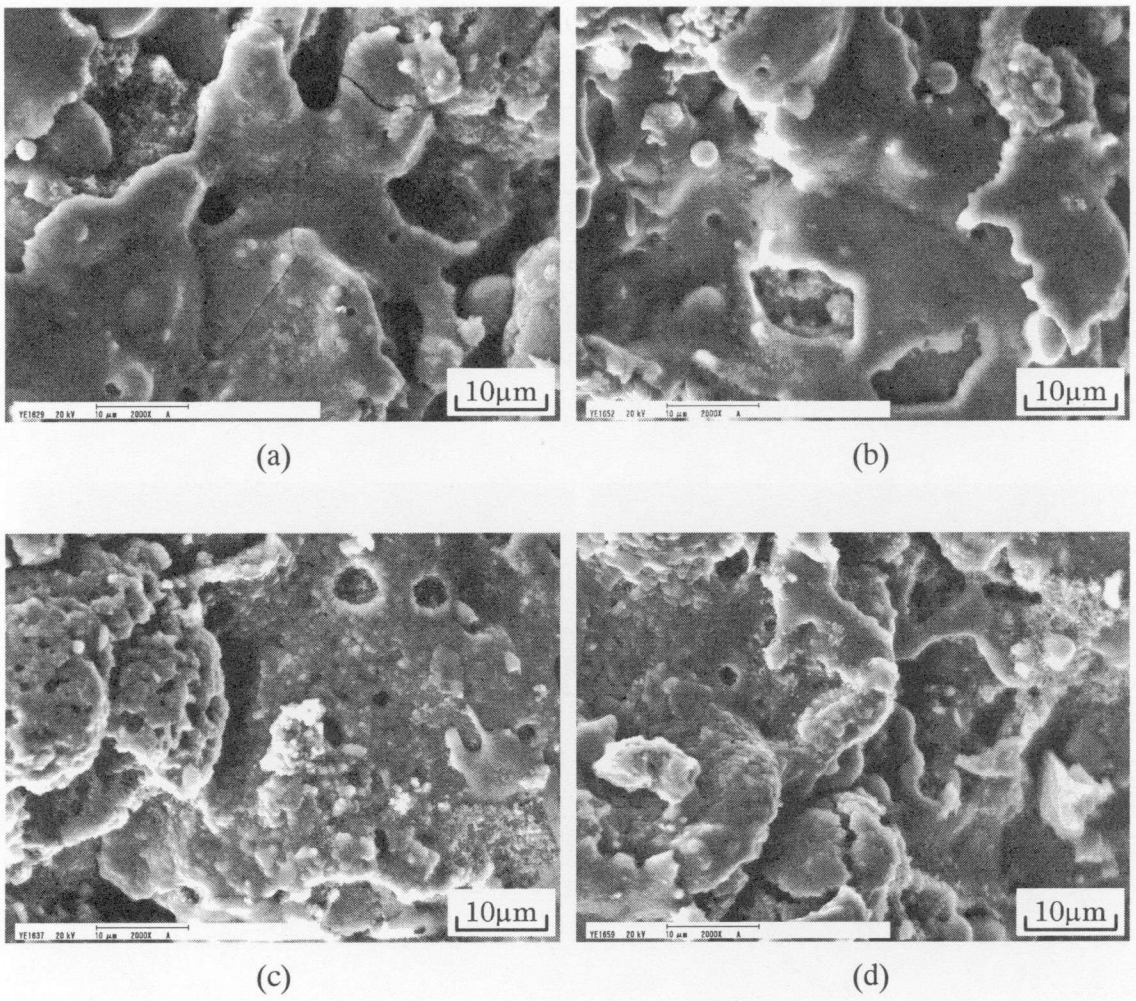

Fig.3.7. Surface views of plasma sprayed TiO_2-10%Fe_3O_4 coatings. (a) I=500A SD=70mm, (b) I=500A SD=100mm, (c) I=400A SD=70mm, (d) I=400A SD=100mm. (Notes: "I" denotes arc current, "SD" denotes spraying distance.)

The relative deposition speed of TiO_2-10%Fe_3O_4 powder (RDSP) was calculated by Equation (2.2), and is illustrated in **Fig.3.8**. The RDSP of TiO_2-10%Fe_3O_4 feedstock powder decreased with the decreasing of arc current, but increased with the decrease of spraying distance from 100mm to 70mm, which are in good agreement with the results (melting state) shown in Fig.3.6 and Fig.3.7. Under the arc current of 400A and spraying distance of 70mm, the RDSP of TiO_2-10%Fe_3O_4 powder was about 2.6 times high than that of pure TiO_2 powder (See Fig.3.8 and Fig.2.9), which means that the powder deposition efficiency was greatly enhanced for the addition of Fe_3O_4.

The x-ray diffraction patterns of plasma sprayed TiO_2-10%Fe_3O_4 coatings under various conditions are illustrated in **Fig.3.9**. The peak height of anatase TiO_2 (101 peak)

was very low. The content of anatase phase, calculated by Equation (2.1), was below 5%. These implied that large part of anatase phase in the powder transformed into rutile phase in thermal spraying process. Therefore, the addition of Fe_3O_4 to TiO_2 would accelerate the anatase-rutile phase transformation, which is in good agreement with the conclusion described in Section 3.3.1. In the sprayed coatings, a compound called $FeTiO_3$ appeared which did not appear in heat treated powder.

Figure 3.10 illustrates the decomposition characteristics of the acetaldehyde by plasma sprayed TiO_2-10%Fe_3O_4 coatings. The concentration of acetaldehyde decreased with the irradiation time. Therefore, prepared TiO_2-10%Fe_3O_4 coatings had photocatalytic activity. The degradation speed by the coating prepared under the arc current of 400A and spraying distance of 70mm was highest. To compare the photocatalytic activity digitally, the τ values were calculated by Equation (2.6) and are shown in **Fig.3.11**. Under the arc current of 400A and spraying distance of 70mm, the sprayed coating has lowest τ value, which means that it had the best photocatalytic activity. Generally, the photocatalytic activity of TiO_2 increase with the increasing of anatase content in it. However, the TiO_2-10%Fe_3O_4 coatings had good photocatalytic activity despite the very low anatase contents comparing with TiO_2 coatings described in Chapter 2. This implied that other factors also control the photocatalytic activity except the content of anatase phase in the sprayed coating. These will be discussed in detail in Chapter 4.

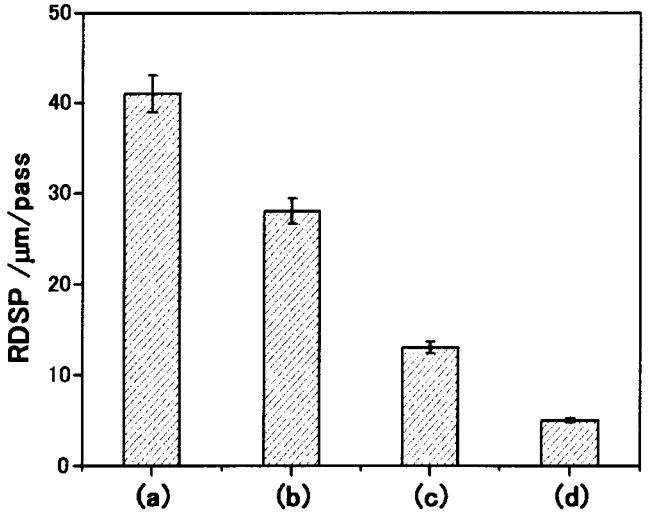

Fig.3.8. Relative deposition speed of TiO_2-10%Fe_3O_4 feedstock powder (RDSP) under various spraying conditions. (a) I=500A SD=70mm, (b) I=500A SD=100mm, (c) I=400A SD=70mm, (d) I=400A SD=100mm. (Notes: "I" denotes arc current, "SD" denotes spraying distance.)

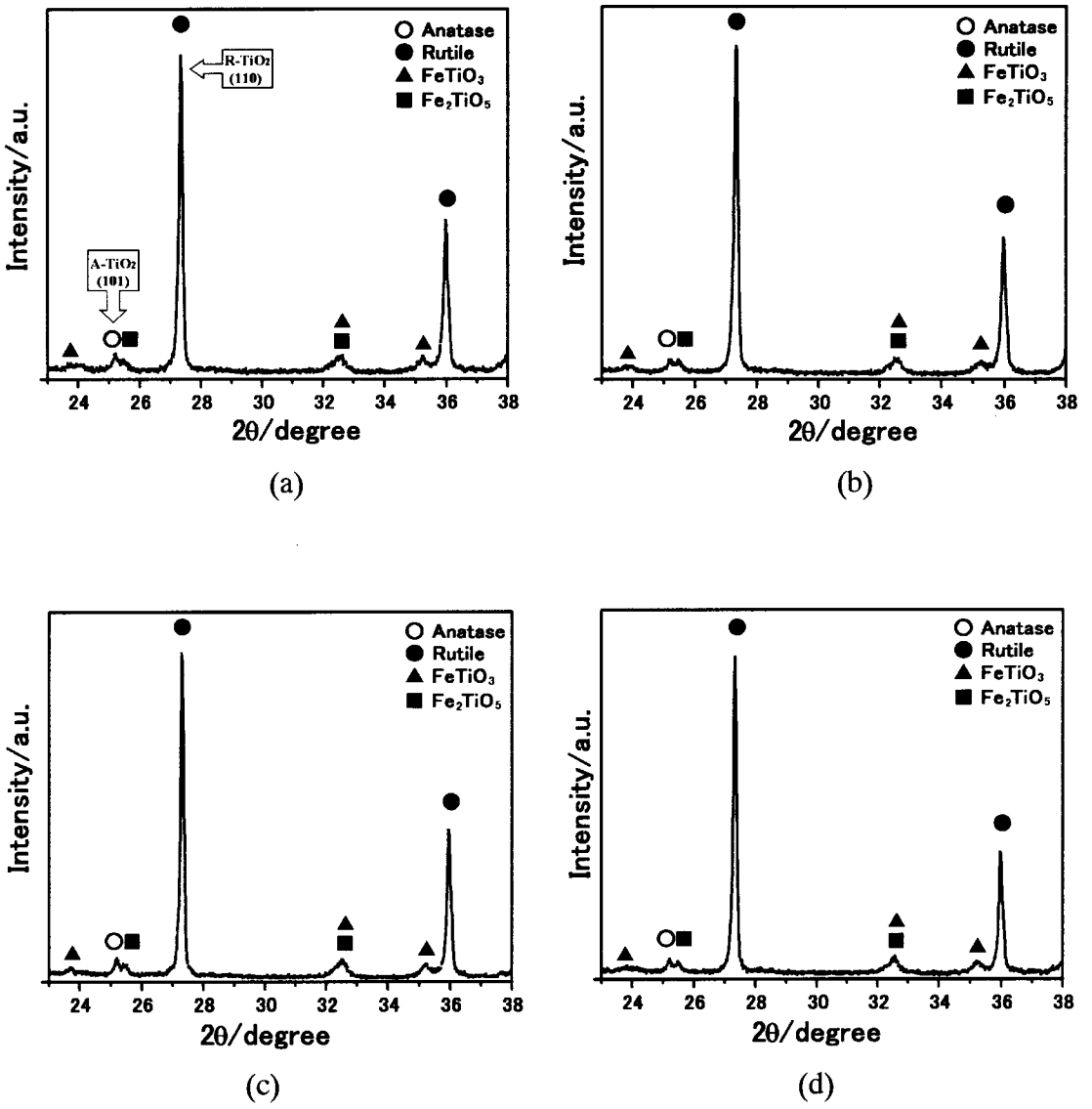

Fig.3.9. X-ray diffraction patterns of plasma sprayed TiO_2-10%Fe_3O_4 coatings under various spraying conditions. (a) I=500A SD=70mm, (b) I=500A SD=100mm, (c) I=400A SD=70mm, (d) I=400A SD=100mm. (Notes: "I" denotes arc current, "SD" denotes spraying distance.)

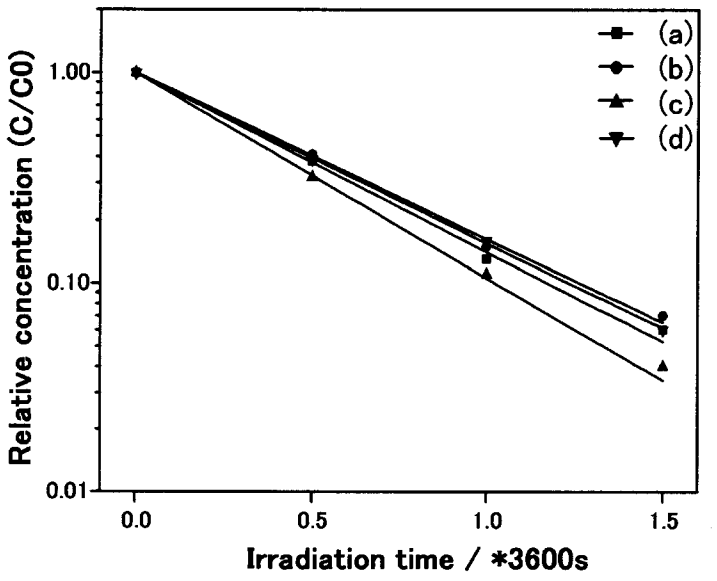

Fig.3.10. Decomposition characteristics of the acetaldehyde by TiO_2-10%Fe_3O_4 coatings prepared under various spraying conditions. (a) I=500A SD=70mm, (b) I=500A SD=100mm, (c) I=400A SD=70mm, (d) I=400A SD=100mm. (Notes: "I" denotes arc current, "SD" denotes spraying distance.)

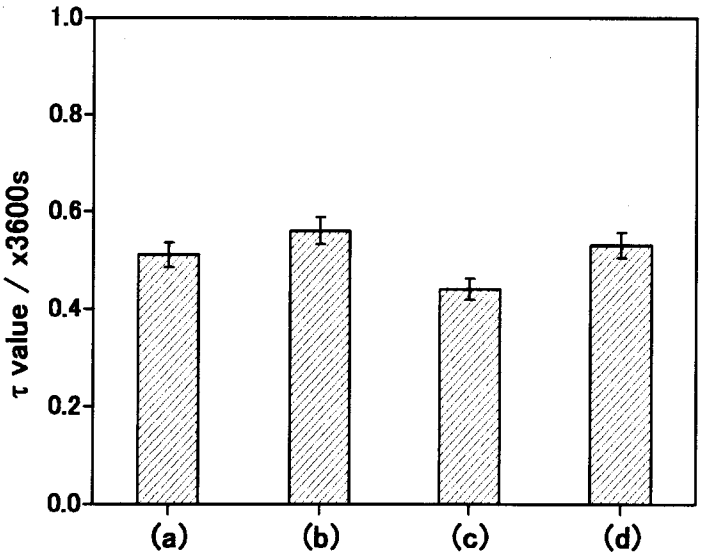

Fig.3.11. τ values of TiO_2-10%Fe_3O_4 coatings prepared under various spraying conditions. (a) I=500A SD=70mm, (b) I=500A SD=100mm, (c) I=400A SD=70mm, (d) I=400A SD=100mm. (Notes: "I" denotes arc current, "SD" denotes spraying distance.)

3.3.3. Characterization of Plasma Sprayed TiO_2-10%Al_2O_3 Coatings

Figure 3.12 shows the typical cross section and surface morphology of plasma sprayed TiO_2-10%Al_2O_3 coating. The melting point of Al_2O_3 (2323K) is about 190K higher than that of rutile TiO_2, thus the TiO_2-10%Al_2O_3 powder was more unmelted than pure TiO_2 powder under the same spraying conditions. As illustrated in **Fig.3.13**, the relative deposition speed of TiO_2-10%Al_2O_3 feedstock powder (RDSP) was nearly the same with that of TiO_2 powder, but was lower than that of TiO_2-10%Fe_3O_4 powder.

The typical x-ray diffraction patterns of plasma sprayed TiO_2-10%Al_2O_3 coatings are illustrated in **Fig.3.14**. Al_2O_3 additive reacted with TiO_2, and produced Al_2TiO_5 compound. For the high solidification speed of impacted particle, Al_2TiO_5 compound did not decompose into TiO_2 and Al_2O_3. The contents of anatase phase in TiO_2-10%Al_2O_3 coatings are shown in **Fig.3.15**. The additive of Al_2O_3 prevented anatase-rutile transformation.

The τ values of TiO_2-10%Al_2O_3 coatings, which were calculated by Equation (2.6) according to the decomposition characteristics of acetaldehyde, are shown in **Fig.3.16**. The coating prepared under the arc current of 400A and spraying distance of 70mm had the highest photocatalytic activity comparing with the other sprayed TiO_2-10%Al_2O_3 coatings, which resulted from the high content of anatase phase in it. Although it increased a few percent comparing with that of TiO_2 coating prepared under the same conditions, the addition of Al_2O_3 had not great influence on the photocatalytic activity of TiO_2.

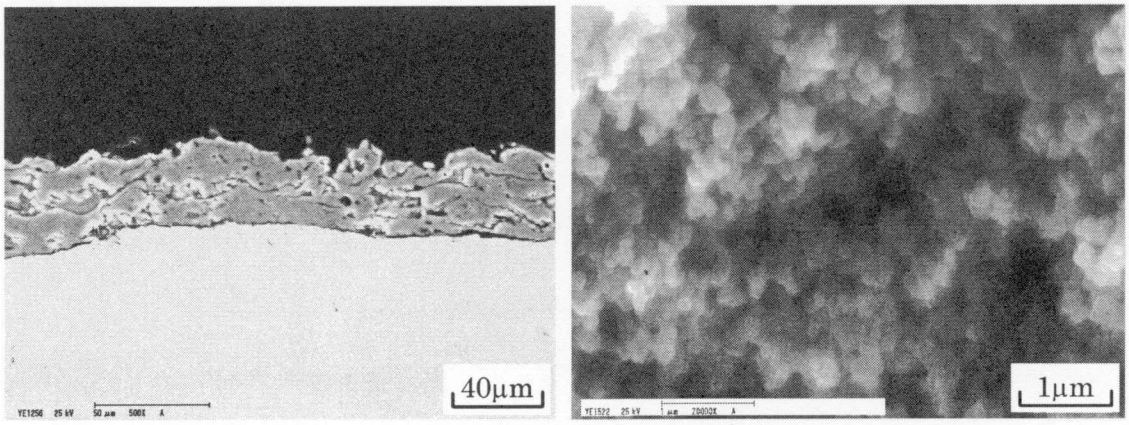

(a) (b)

Fig.3.12. Cross section (a) and surface morphology (b) of plasma sprayed TiO_2-10%Al_2O_3 coating under the arc current of 400A and spraying distance of 70mm.

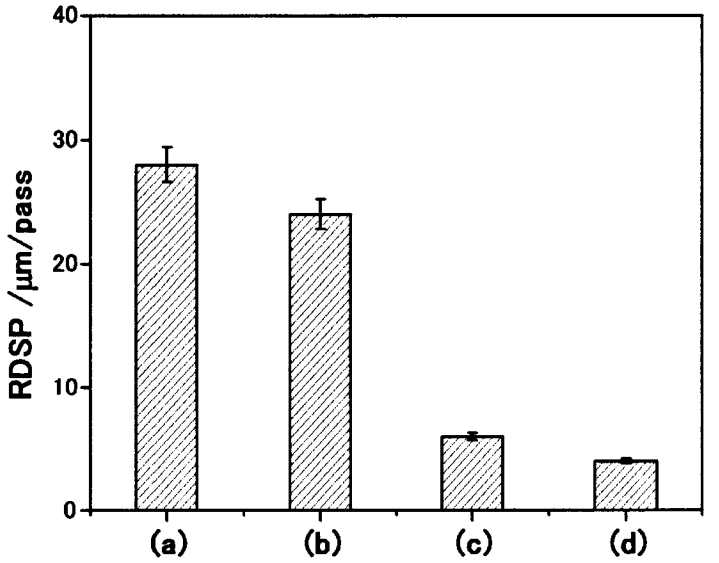

Fig.3.13. Relative deposition speed of TiO_2-10%Al_2O_3 feedstock powder (RDSP) under various spraying conditions. (a) I=500A SD=70mm, (b) I=500A SD=100mm, (c) I=400A SD=70mm, (d) I=400A SD=100mm.

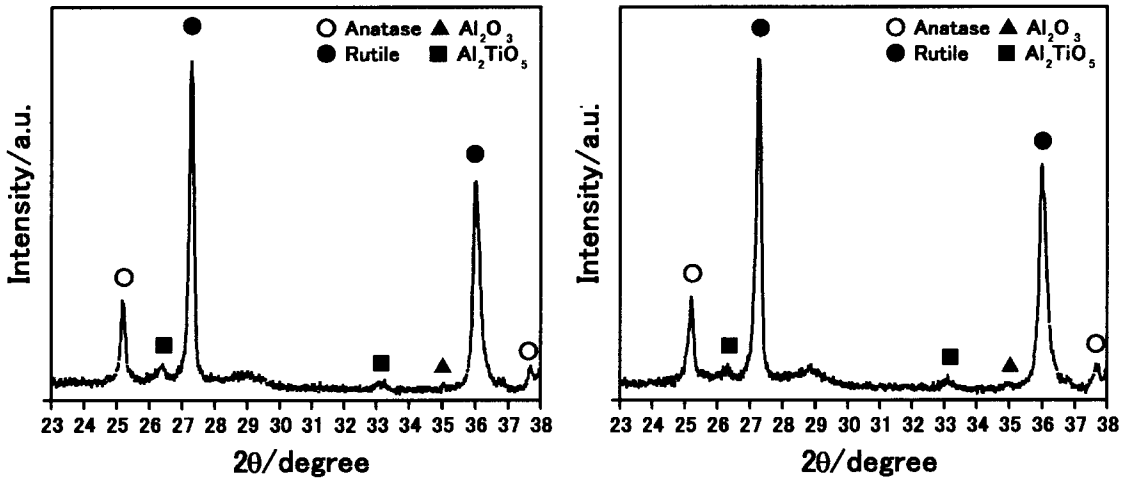

Fig.3.14. X-ray diffraction patterns of plasma sprayed TiO_2-10%Al_2O_3 coatings under various spraying conditions. (a) I=500A SD=70mm, (b) I=400A SD=70mm.

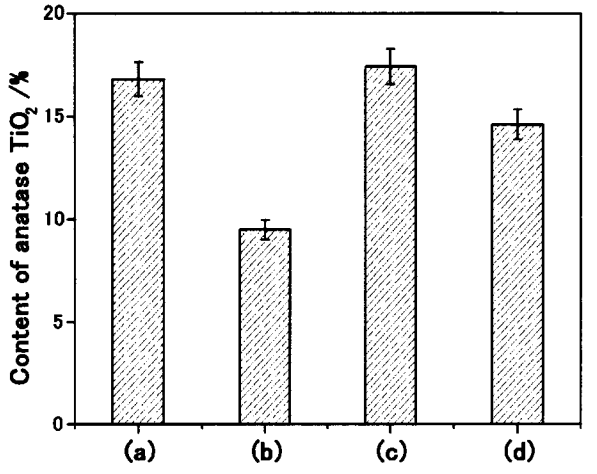

Fig.3.15. Contents of anatase TiO_2 in plasma sprayed TiO_2-10%Al_2O_3 coatings under various conditions. (a) I=500A SD=70mm, (b) I=500A SD=100mm, (c) I=400A SD=70mm, (d) I=400A SD=100mm.

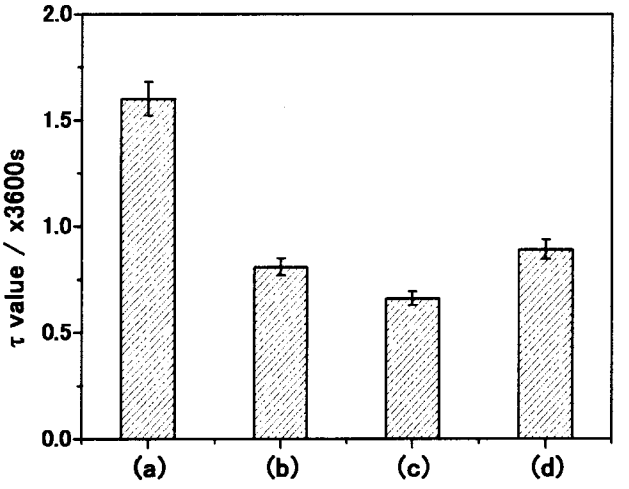

Fig.3.16. τ values of TiO_2-10%Al_2O_3 coatings prepared under various spraying conditions. (a) I=500A SD=70mm, (b) I=500A SD=100mm, (c) I=400A SD=70mm, (d) I=400A SD=100mm.

3.3.4. Characterization of Plasma Sprayed TiO_2-10%Y_2O_3 Coatings

Figure 3.17 shows the cross section and surface morphology of plasma sprayed TiO_2-10%Y_2O_3 coating. Although the melting point of Y_2O_3, which is 2713K, is 580K higher than that of rutile TiO_2, TiO_2-10%Y_2O_3 powder was more melted than pure TiO_2

powder under the same spraying conditions. This also can be inferred from the relative deposition speed of TiO_2-10%Y_2O_3 powder as shown clearly in **Fig.3.18**. Because $Y_2Ti_2O_7$ compound formed (**Fig.3.19**) in thermal spraying process according to the reaction mentioned in Section 3.2.1, a lot of heat gave off, which improved the melting of powder and increased the RDSP. The contents of anatase phase in TiO_2-10%Y_2O_3 coatings are shown in **Fig.3.20**.

According to the τ values of TiO_2-10%Y_2O_3 coatings calculated by Equation (2.6), the photocatalytic activity of TiO_2-10%Y_2O_3 coating was inferior to that of TiO_2 coating under the arc current of 400A and spraying distance of 70mm. It implied that the addition of Y_2O_3 had unfavorable influence on the photocatalytic activity of TiO_2.

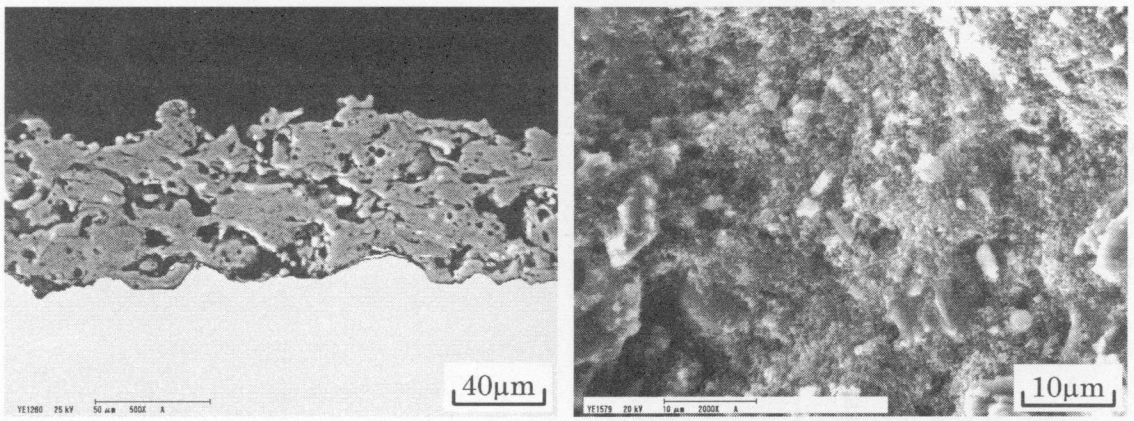

(a) (b)

Fig.3.17. Cross section (a) and surface morphology (b) of TiO_2-10%Y_2O_3 coating plasma sprayed under arc current of 400A and spraying distance of 70mm.

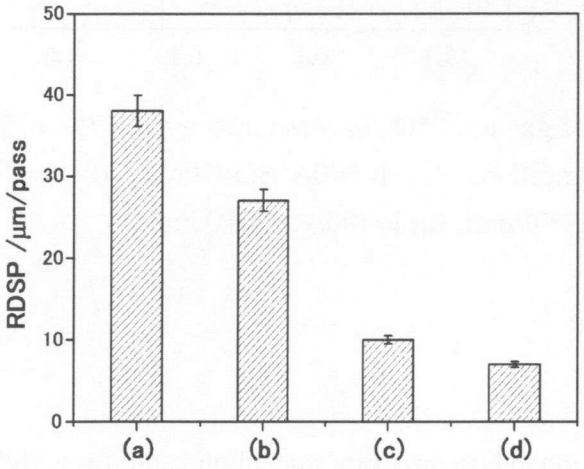

Fig.3.18. Relative deposition speed of TiO_2-10%Y_2O_3 feedstock powder (RDSP) under various spraying conditions. (a) I=500A SD=70mm, (b) I=500A SD=100mm, (c) I=400A SD=70mm, (d) I=400A SD=100mm.

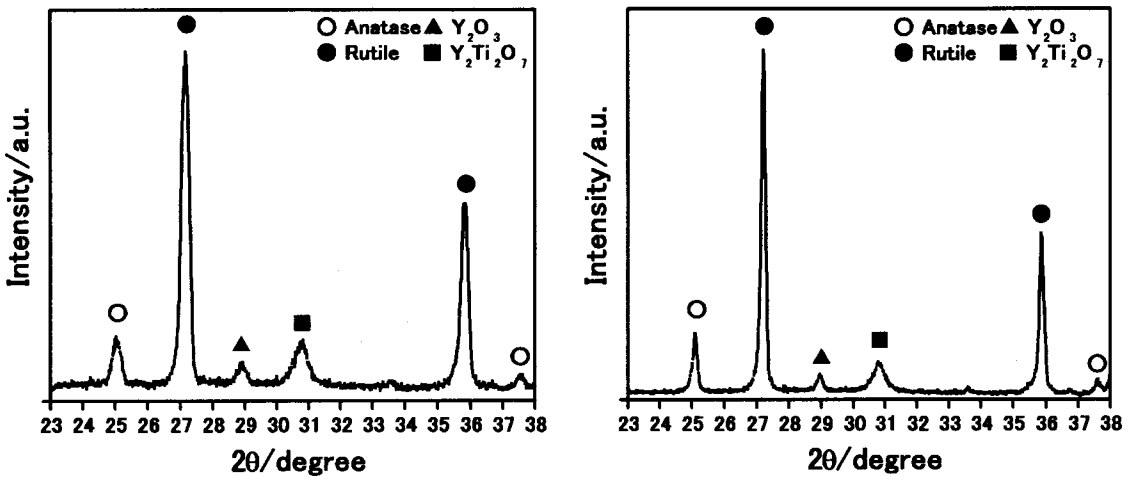

Fig.3.19. X-ray diffraction patterns of plasma sprayed TiO_2-10%Y_2O_3 coatings under various spraying conditions. (a) I=500A SD=70mm, (b) I=400A SD=70mm.

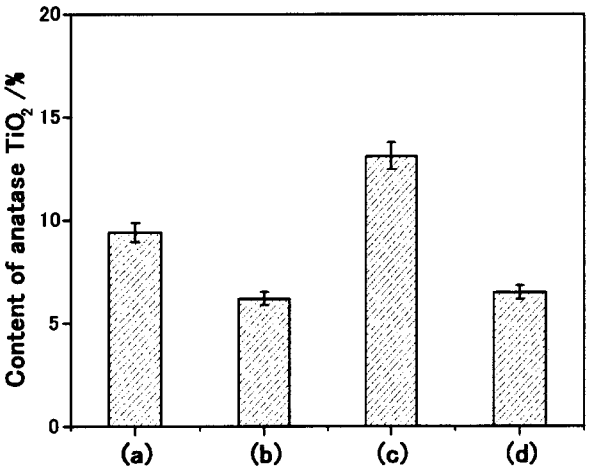

Fig.3.20. Contents of anatase TiO_2 in plasma sprayed TiO_2-10%Y_2O_3 coatings under various conditions. (a) I=500A SD=70mm, (b) I=500A SD=100mm, (c) I=400A SD=70mm, (d) I=400A SD=100mm.

3.4. Conclusions

Phase composition, microstructure and photocatalytic activity of plasma sprayed TiO_2-10%Fe_3O_4, TiO_2-10%Al_2O_3, and TiO_2-10%Y_2O_3 coatings were characterized and discussed in detail. The addition of Fe_3O_4 to TiO_2 improved the anatase-rutile transformation. The anatase content of TiO_2 in the sprayed coating was affected by the

melting degree of TiO_2 particle in thermal spraying process. Although the content of anatase TiO_2 was very low in the sprayed TiO_2-10%Fe_3O_4 coating, the photocatalytic activity was better than that of TiO_2 coating under the same spraying conditions, which implied the photocatalytic activity was not only controlled by anatase content of TiO_2. The original reasons are presented in Chapter 4. The relative deposition speed of TiO_2-10%Fe_3O_4 powder was 2.6 times than that of TiO_2 powder under the arc current of 400A and spraying distance of 70mm. However, the addition of Al_2O_3 and Y_2O_3 particle to TiO_2 particle had not favorable effect on the photocatalytic activity of TiO_2 coating. Therefore, the influence of additive on the photocatalytic activity of TiO_2 is greatly controlled by not only the kind of additive, but also by the synthetic process.

References

[1] D. Dvoranová, V. Brezová, M. Mazúr, and M. A. Malati, Investigations of metal-doped titanium dioxide photocatalysts, *Applied Catalysis B: Environmental, Vol. 37(2) (2002) 91-105.*

[2] H. Yamashita, M. Harada, J. Misaka, M. Takeuchi, K. Ikeue, and M. Anpo, Degradation of propanol diluted in water under visible light irradiation using metal ion-implanted titanium dioxide photocatalysts, *Journal of Photochemistry and Photobiology A: Chemistry, Vol. 148(1-3) (2002) 257-261.*

[3] K. Tennakone, C. A. N. Fernando, S. Wickramanayake, M. W. P. Damayanthi, L. H. K. Silva, W. Wijeratne, O. A. Illeperuma, and S. Punchihewa, Photocatalytic reduction of nitrogen to ammonia with coprecipitated Fe(III) and Ti(IV) hydrous oxides, *Solar Energy Materials, Vol. 17(1) (1988) 47-53.*

[4] F. Gracia, J. P. Holgado, F. Yubero, and A. R. González-Elipe, Phase mixing in Fe/TiO_2 thin films prepared by ion beam-induced chemical vapor deposition: optical and structural properties, *Surface and Coatings Technology, Vol.158-159 (2002) 552-557.*

[5] Y. Choi, S. Yamamoto, H. Saitoh, T. Sumita, and H. Itoh, Influence of carbon-ion irradiation and hydrogen-plasma treatment on photocatalytic properties of titanium dioxide films, *Nuclear Instruments and Methods in Physics Research Section B: Beam Interactions with Materials and Atoms, Vol. 206 (2003) 241-244.*

[6] I. Nakamura, N. Negishi, S. Kutsuna, T. Ihara, S. Sugihara, and K. Takeuchi, Role of oxygen vacancy in the plasma-treated TiO_2 photocatalyst with visible light

activity for NO removal, *Journal of Molecular Catalysis A: Chemical, Vol. 161(1-2) (2000) 205-212.*

[7] R. Asahi, T. Morikawa, T. Ohwaki, K. Aoki, and Y. Taga, Visible-light photocatalysis in nitrogen-doped titanium oxides, *Science, Vol. 293 (2001) 269-271.*

[8] V. Keller, P. Bernhardt, and F. Garin, Photocatalytic oxidation of butyl acetate in vapor phase on TiO_2, Pt/TiO_2 and WO_3/TiO_2 catalysts, *Journal of Catalysis, Vol. 215(1) (2003) 129-138.*

[9] I. Bayer, I. Eroglu, and L. Turker, Experimental insight into the performance characteristics of Ni-mesh semiconductor photo-electrochemical cells, *Solar Energy Materials & Solar Cells, Vol. 62 (2000) 43-49.*

[10] J. Lin and J. C. Yu, An investigation on photocatalytic activities of mixed TiO_2-rare earth oxides for the oxidation of acetone in air, *Journal of Photochemistry and Photobiology A: Chemistry, Vol. 116 (1998) 63-67.*

[11] J. Moser and M. Grätzel, Inhibition of electron-hole recombination in substitutionally doped colloidal semiconductor crystallites, *Helvetica Chimica Acta, Vol. 79 (1987) 1596-1604.*

[12] M. A. Fox and M. T. Dulay, Heterogeneous photocatalysis, *Chemical Reviews, Vol. 93(1) (1993) 341-357.*

[13] W. Y. Choi, A. Termin and M. Grätzel, The role of metal ion dopants in quantum-sized TiO_2: Correlation between photoreactivity and charge carrier recombination dynamics, *Journal Physics Chemistry, Vol.98 (1994) 13669-13679.*

[14] D. Beydoun and R. Amal, Implications of heat treatment on the properties of a magnetic iron oxide-titanium dioxide photocatalyst, *Materials Science and Engineering, Vol. B94 (2002) 71-81.*

[15] V. Buscaglia, M. Alvazzi Delfrate, M. Leoni, and C. Bottino, The effect of $MgAl_2O_4$ on the formation kinetics of Al_2TiO_5 from Al_2O_3 and TiO_2 fine powders, *Journal of Materials Science, Vol. 31 (1996) 1715-1724.*

[16] I. Barrios De Arenas, and O. Gil, Synthesis and properties of in situ Al_2TiO_5/Al_2O_3 composite, *Journal of Materials Processing Technology, (In press).*

[17] S. Yamaguchi, K. Kobayashi, K. Abe, S. Yamazaki, and Y. Iguchi, Electrical conductivity and thermoelectric power measurement of $Y_2Ti_2O_7$, *Solid State Ionics, Vol. 113-115 (1998) 393-402.*

[18] K. Kobayashi, M. Mukaida, T. Tsunoda, and Y. Imai, Theoretical V-I characteristic of the solid-oxide thermocell using the oxide ion and electronic mixed conductors, *Solid State Ionics, Vol. 154-155 (2002) 101-107.*

CHAPTER 4

Influence of Fe_3O_4 Content on the Properties of Plasma Sprayed TiO_2-Fe_3O_4 Coatings

4.1. Introduction

As discussed in Chapter 3, 10wt.% addition of Fe_3O_4 into TiO_2 powder improved the photocatalytic activity of TiO_2 coating in spite of the low content of anatase phase in it, and increased obviously the relative deposition speed of TiO_2 powder. Insomuch that Fe_3O_4 may be regarded as a kind of promising material applying in photocatalytic field. However, the influence of Fe_3O_4 amount on the properties of plasma sprayed TiO_2-Fe_3O_4 coating is still unclear. To study the effects of Fe_3O_4 particles on the photocatalytic activity of TiO_2-Fe_3O_4 coatings in detail, four kinds of composite powders were further designed, these were TiO_2-5%Fe_3O_4, TiO_2-12.7%Fe_3O_4, TiO_2-22.5%Fe_3O_4 and TiO_2-32.6%Fe_3O_4 powders.

Although the plasma spray process has been developed in 1950's, photocatalytic coating preparation applying plasma spray is a new filed. Currently, most application researches in plasma spraying are focused onto the relationship between plasma deposition parameters and coating properties. Indeed, properties and microstructure of plasma sprayed coatings depend on the in-flight treatment of the particles in plasma jet. In fact, particle velocity and temperature at impact play an important role. So in order to produce desired coatings, it is essential to measure and understand in-flight particles behavior [1~3].

The photocatalytic performance is affected by catalyst substance, light absorptive ability, morphology, and surface active site and so on. Because the light absorptive ability of the photocatalyst is a main factor to affect the photocatalytic activity, the diffuse reflectance of feedstock powders, sprayed TiO_2 and TiO_2-Fe_3O_4 coatings was investigated. Generally, the photocatalytic activity increases with the increasing of light absorptive capacity [4].

In this chapter, the influence of Fe_3O_4 on anatase-rutile phase transformation temperature was investigated, and the phase composition of heat treated powder was quantitatively analyzed. Furthermore, the speed and temperature of in-flight particles

were measured. The phase composition, microstructure, photo absorbance and photocatalytic activity of plasma sprayed TiO_2-Fe_3O_4 coatings were characterized and discussed in detail. Moreover, the existence of solid solution, amorphous phase and phase segregation in the sprayed coatings was examined. To discuss the influence of Fe_3O_4 amount on the performance of plasma sprayed TiO_2-Fe_3O_4 coatings systematically, TiO_2 and TiO_2-10%Fe_3O_4 coatings discussed in Chapter 2 and 3 were also mentioned in this chapter.

4.2. Materials and Experimental Procedures

4.2.1 Feedstock Powders and Substrate

The feedstock powders were pure TiO_2 and five kinds of composite TiO_2-Fe_3O_4 powders. These were TiO_2, TiO_2-5%Fe_3O_4, TiO_2-10%Fe_3O_4, TiO_2-12.7%Fe_3O_4, TiO_2-22.5%Fe_3O_4 and TiO_2-32.6%Fe_3O_4 powders. The average sizes of TiO_2-Fe_3O_4 powders were about 32μm. The x-ray diffraction results of the powders are shown in **Fig.4.1**. It is very clear that Fe_3O_4 particles distributed uniformly in the agglomerated TiO_2-Fe_3O_4 powders according to their EDAX maps. The substrate was stainless steel (JIS SUS304).

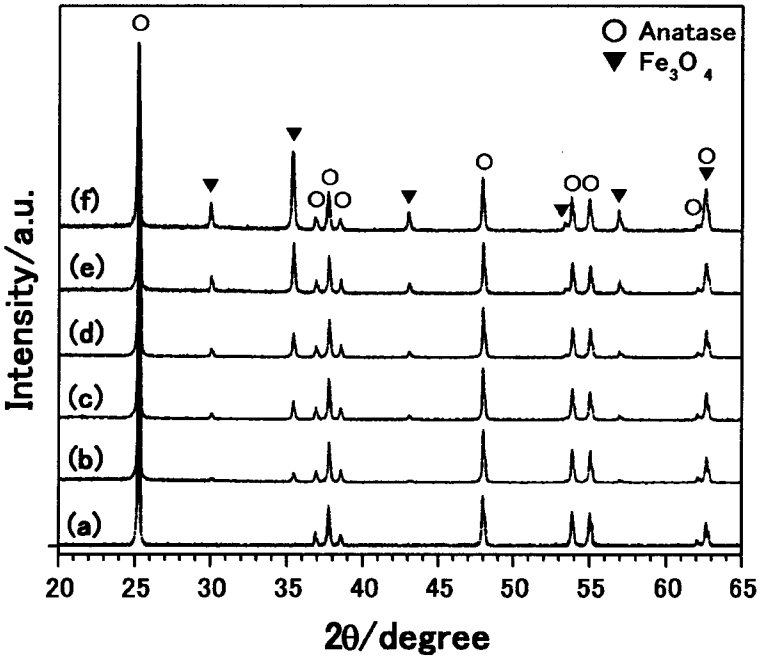

Fig.4.1. X-ray diffraction patterns of TiO_2 and TiO_2-Fe_3O_4 feedstock powders. (a) TiO_2 powder, (b) TiO_2-5%Fe_3O_4 powder, (c) TiO_2-10%Fe_3O_4 powder, (d) TiO_2-12.7%Fe_3O_4 powder, (e) TiO_2-22.5%Fe_3O_4 powder, (f) TiO_2-32.6%Fe_3O_4 powder.

4.2.2. Coatings Preparation

The thermal spraying equipment was a plasma spraying system (Plasmadyne-Mach1 manufactured by Plasmadyne Company). Argon was used as a primary plasma gas and helium was used as the secondary gas. As discussed in Chapter 2 and Chapter 3, low arc current is preferable to high arc current for photocatalytic coating preparation, thus arc current of 400A was applied to study the properties with relation to photocatalyst. For the high melting and solidification speed of powder in plasma spray process, solid solution, amorphous phase and phase segregation exist widely in the coating despite the content is very different. To study the phase changes of TiO_2-32.6%Fe_3O_4 coatings after heat treatment, arc currents of 400A, 600A and 800A were chosen. The detailed plasma spraying parameters are given in **Table 4.1**.

Table 4.1 Plasma spraying parameters.

Argon gas pressure (MPa)/ flow (slpm)	0.42/58
Helium gas pressure (MPa)/flow (slpm)	0.21/9
Arc current (A)	400, 600, 800
Arc voltage (V)	28~30
Spraying distance (mm)	70

4.2.3. Heat Treatment of Feedstock Powders and Sprayed Coatings

The anatase-rutile transformation temperature of agglomerated pure anatase TiO_2 powder was approximate to 1173K as reported in Chapter 2. To investigate the influence of the additive on the anatase-rutile phase transformation temperature and compare the composition variations of feedstock powders in heat treatment process and in thermal spray process, TiO_2 and TiO_2-Fe_3O_4 composite powders were kept in electric furnace for 7200s after reaching at treated temperature (973K, 1123K, 1273K or 1423K) with a heating rate of 1.67K/s, and then were cooled with the furnace.

However, to investigate abundance of solid solution in sprayed coating, specimen was kept a long time in furnace for 21600s at 1273K with a low heating rate of 0.84K/s.

4.2.4. General Characterization

Oxygen concentration in as-received and heat treated TiO_2-Fe_3O_4 coating was studied by electron probe microanalyzer (EPMA) (JXA-8600, JEOL, Japan) in attempt

to investigate the existence of solid solution in it.

Scanning electron microscope (SEM) and energy dispersive analysis of x-ray (EDAX) were used to examine the structure characteristics of the feedstock powders and the sprayed coatings. The phase composition of the heat treated powders and the sprayed coatings were investigated by x-ray diffraction using Cu-Kα radiation (λ=1.5406Å) and graphite crystal monochromator (M03XHF, MAC Science Co. Ltd.). The 2θ range was 23°~38° including the main diffraction line of the possible phase compositions. Quantitative analysis of the phase composition of the heat treated powders was attempted by comparing the integrated x-ray diffraction peaks for anatase (101), rutile (110), α-Fe_2O_3 (104), $FeTiO_3$ (104) and Fe_2TiO_5 (101) phase. The weight contents of anatase TiO_2, rutile TiO_2, α-Fe_2O_3, $FeTiO_3$ and Fe_2TiO_5 compound were calculated by Equations (4.1)~(4.6), respectively. The peak intensity relations have been established experimentally from powders mixture, of which composition was known, and the validity of this method was confirmed.

However, it is extremely complex to consider the plasma sprayed coatings applying Equations (4.1)~(4.6) because amorphous phase, phase segregation or solid solution can not be generally neglected for thermal sprayed composite coating [5~7].

$$\frac{W_{Anatase}}{W_{Rutile}} = C_1 \frac{I_{Anatase(101)}}{I_{Rutile(110)}} \tag{4.1}$$

$$\frac{W_{Fe_2O_3}}{W_{Rutile}} = C_2 \frac{I_{Fe_2O_3(104)}}{I_{Rutile(110)}} \tag{4.2}$$

$$\frac{W_{FeTiO_3}}{W_{Rutile}} = C_3 \frac{I_{FeTiO_3(104)}}{I_{Rutile(110)}} \tag{4.3}$$

$$\frac{W_{Fe_2TiO_5}}{W_{Rutile}} = C_4 \frac{I_{Fe_2TiO_5(101)}}{I_{Rutile(110)}} \tag{4.4}$$

$$W_{Anatase} + W_{Rutile} + W_{Fe_2O_3} + W_{FeTiO_3} + W_{Fe_2TiO_5} = 1 \tag{4.5}$$

$$W_{AnataseToRutile} = \frac{W_{Rutile}}{W_{Anatase} + W_{Rutile}} \times 100\% \tag{4.6}$$

where $I_{Anatase(101)}$ is the integrated intensity of the (101) reflection of anatase phase, $I_{Rutile(110)}$ the integrated intensity of (110) reflection of rutile phase, $I_{Fe2O3(104)}$ the integrated intensity of (104) reflection of α-Fe_2O_3, $I_{FeTiO3(104)}$ the integrated intensity of (104) reflection of $FeTiO_3$ phase, $I_{Fe2TiO5(101)}$ the integrated intensity of (101) reflection of Fe_2TiO_5 phase, $W_{Anatase}$, W_{Rutile}, W_{Fe2O3}, W_{FeTiO3} and $W_{Fe2TiO5}$ the weight fractions of anatase TiO_2, rutile TiO_2, α-Fe_2O_3, $FeTiO_3$ and Fe_2TiO_5, respectively, and C_1, C_2, C_3 and C_4 the constants which are dependent on the crystal structures and lattice parameters of the upper mentioned substances. $W_{AnataseToRutile}$ the weight fraction of anatase transformed into rutile.

The relative deposition speed of feedstock powder (RDSP) was calculated using the Equation (2.2). The photocatalytic activity of sprayed coating was evaluated by the set-up described in Chapter 2.

4.2.5. Particle Speed and Temperature Measurement

The speed and temperature of in-flight particle were measured by DPV-2000 equipment (Tecnar Automation Ltd., Canada) [8]. DPV-2000 applies infrared pyrometry along with a two-slit photo-mask in order to perform in-flight diagnostics on individual particles. A particle passing in front of the photo-mask will generate a two-peaks signal as illustrated in **Fig.4.2.**

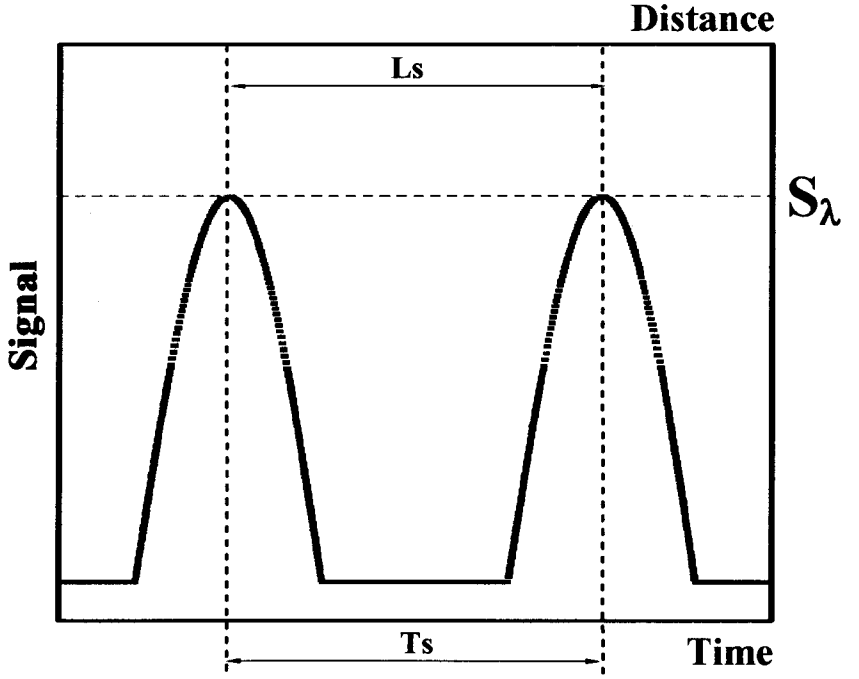

Fig.4.2. Particle velocity and temperature measurement principle of DPV-2000.

According to the signals, the velocity and temperature of particle were calculated by Equations (4.7) and (4.8).

$$Velocity_{particle} = Ls / Ts \tag{4.7}$$

$$Temperature_{particle} = f(S_{\lambda 1} / S_{\lambda 2}) \tag{4.8}$$

Where $Velocity_{Partilce}$ is the velocity of particle, $Temperature_{Partilce}$ the temperature of particle, Ls the distance of two signals from two slits, Ts the time between two signals from two slits, $S_{\lambda 1}$ the intensity of the signal at wavelength of $\lambda 1$, $S_{\lambda 2}$ the intensity of the signal at wavelength of $\lambda 2$.

4.2.6. Diffuse Reflectance Measurement

The UV-VIS-NIR spectra of the feedstock powders and plasma sprayed coatings were recorded using a Shimadzu UV-3100PC scanning spectrophotometer equipped with a diffuse reflectance accessory. The absorption intensity was calculated from the Kubelka-Munk equation (Eq. (4.9)). The integrated energy absorbance from the light source of the sprayed coatings is estimated according to Equation (4.10).

$$f(R_\lambda) = \frac{(1-R_\lambda)^2}{2R_\lambda} \tag{4.9}$$

$$E_{total} = \int E(\lambda) f(R_\lambda) d\lambda \tag{4.10}$$

where λ is the wavelength of light, $f(R_\lambda)$ Kubelka-Munk value, R_λ diffuse reflection of the powder/coating. $E(\lambda)$ spectral irradiance of the light source, and E_{total} relative integrated energy absorbance.

The study of the tail of the absorption curve of semiconductor shows that it has a simple exponential increase. The onset of this increase (point A in **Fig.4.3**) has been suggested as a universal method of deducing the position of the absorption edge [9, 10]. In this study, the wavelength coordinate of the point on the low wavelength side of the curve at which the liner increase in absorbance starts was marked to investigate the absorption shift of feedstock powders and sprayed coatings.

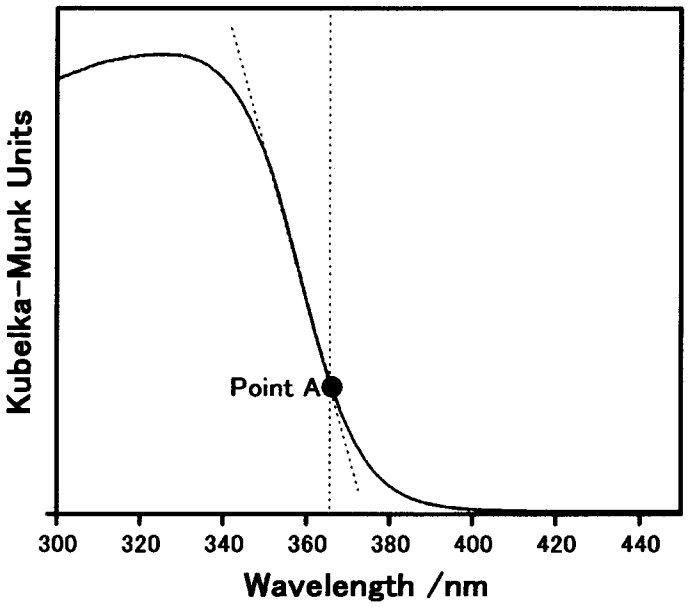

Fig.4.3. Definition of absorption edge in absorption spectrum of semiconductor.

4.3. Results and Discussion

4.3.1. Heat Treated TiO_2 and Composite TiO_2-Fe_3O_4 Powders

Although the TiO_2-10%Fe_3O_4 powder was heat treated and the results were given in Chapter 3, the details of Fe_3O_4 behavior was still unclear. **Fig.4.4** shows the x-ray diffraction results of TiO_2 and TiO_2-Fe_3O_4 feedstock powders heat treated at various temperatures. At 973K, anatase TiO_2 kept its crystal structure, but magnetite (Fe_3O_4) additive disappeared and Fe_2O_3 formed consequently (Fig4.4(A)). One part of anatase TiO_2 transformed into rutile at 1123K in composite powders, which did not occur for pure anatase TiO_2 powder. The content of anatase TiO_2 in the heat treated powders at 1123K, which was calculated according to equations (4.1)~(4.6), decreased with the increasing of Fe_3O_4 amount as shown in **Fig.4.5**. The weight fractions of anatase transformed to rutile increased gradually (Fig.4.5(b)). These implied that the addition of Fe_3O_4 improved the anatase-rutile transformation of TiO_2-Fe_3O_4 powers, and the transformation temperature, which was in the range of 973K to 1123K, decreased at least 50K comparing with pure TiO_2 powder.

At the heat treated temperature of 1273K, anatase phase transformed completely to rutile in composite TiO_2-Fe_3O_4 powders. But anatase TiO_2 phase was still detectable in pure TiO_2 powder. At the higher temperature of 1423K, all Fe_2O_3 reacted with TiO_2 and

produced stable Fe_2TiO_5.

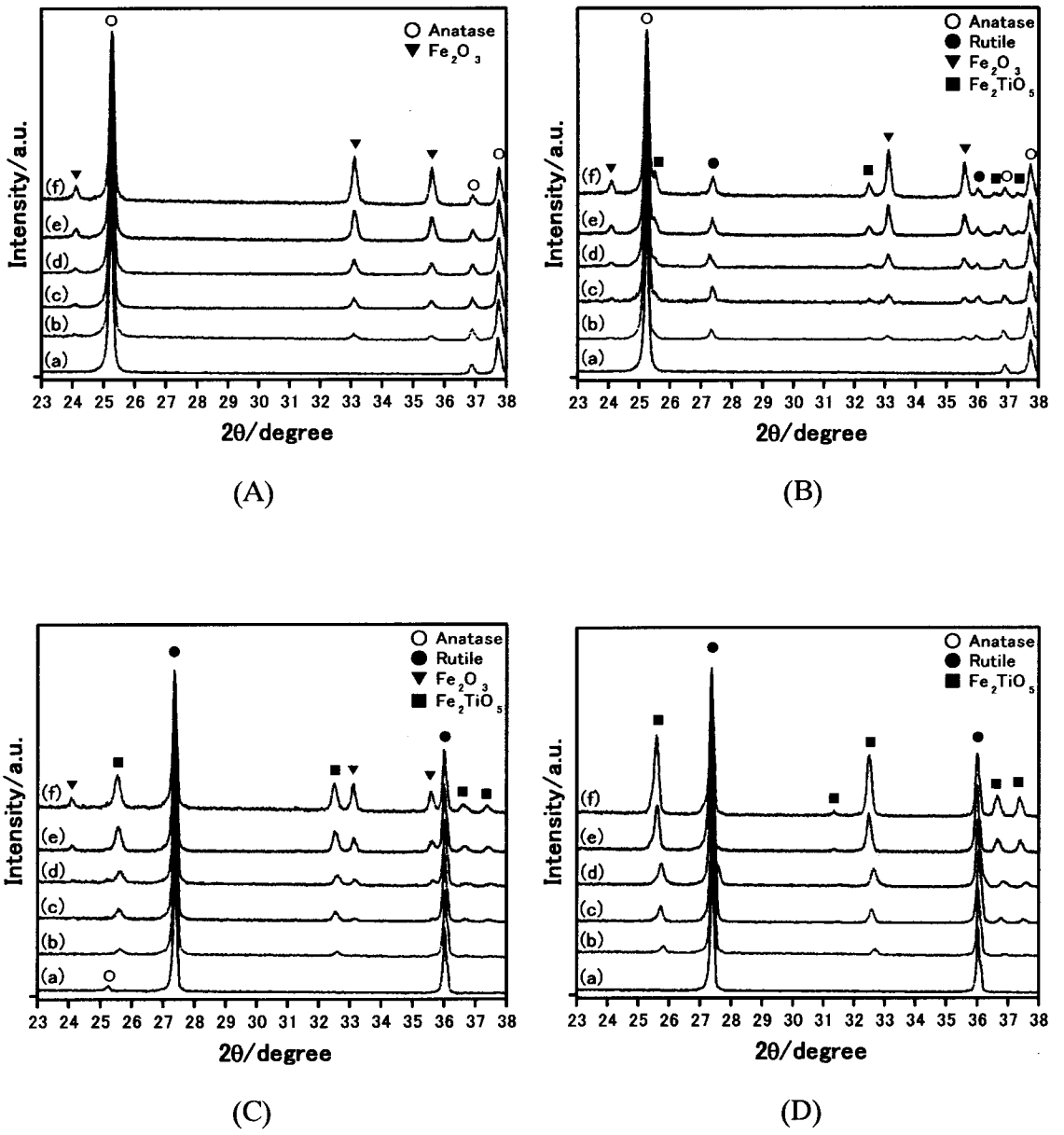

Fig.4.4. X-ray diffraction patterns of heat treated TiO_2 and TiO_2-Fe_3O_4 feedstock powders at various temperatures. (A) 973K, (B) 1123K, (C) 1273K, (D) 1423K. (Notes: (a) TiO_2 powder, (b) TiO_2-5%Fe_3O_4 powder, (c) TiO_2-10%Fe_3O_4 powder, (d) TiO_2-12.7%Fe_3O_4 powder, (e) TiO_2-22.5%Fe_3O_4 powder, (f) TiO_2-32.6%Fe_3O_4 powder.)

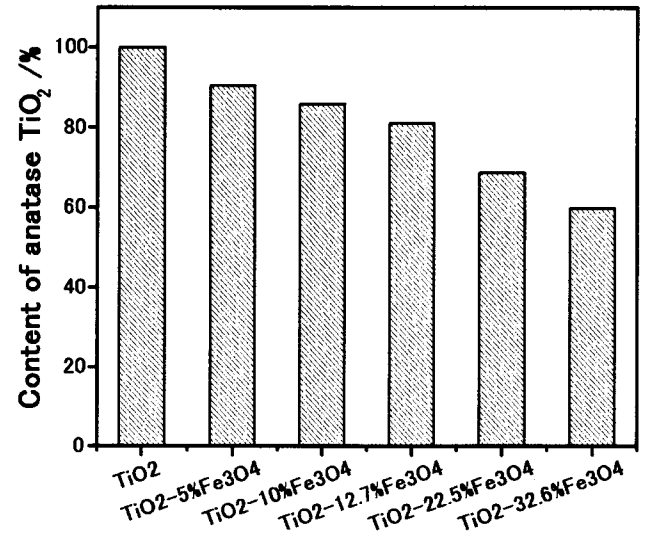

(a)

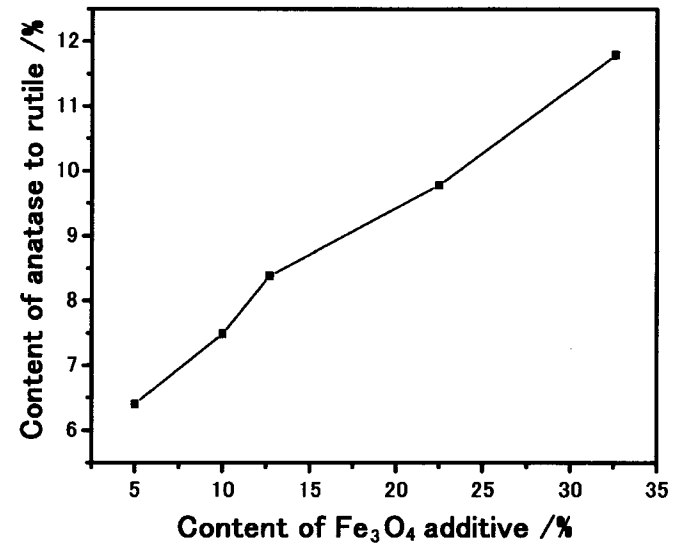

(b)

Fig.4.5. Content of anatase TiO_2 (a) and content of anatase TiO_2 transformed to rutile (b) in TiO_2 and TiO_2-Fe_3O_4 feedstock powders heat treated at 1123K.

4.3.2. Speed and Temperature of In-flight Particles

The addition of Fe_3O_4 to TiO_2 powder had no considerable influence on the speed and temperature of in-flight TiO_2 and TiO_2-Fe_3O_4 particles as shown in **Fig.4.6**. The average temperature of TiO_2 particles under the arc current of 400A was approximate to 2100K. The melting point of rutile TiO_2 is 2131K, thus large part of TiO_2 particles did

not melted at low arc current of 400A, which resulted in the low RDSP as shown in Fig.2.9 in Chapter 2.

On the other hand, the melting point of Fe_2TiO_5 is 1823K [11], and it is 1623K for Fe_2O_3 [12]. Moreover, reactions (4.11) and (4.12) give off heat, which may serve as the melting latent heat. Therefore, the melted proportion of TiO_2-Fe_3O_4 particle was higher than that of TiO_2 particle in spite of the same average temperature of particle, and the TiO_2-Fe_3O_4 particle was more melted with the higher content of Fe_3O_4.

$$4Fe_3O_4 + O_2 \rightarrow 6Fe_2O_3 + heat \tag{4.11}$$

$$Fe_2O_3 + TiO_2 \rightarrow Fe_2TiO_5 + heat \tag{4.12}$$

Because the speed and temperature of plasma jet is higher with higher arc current, the speed and temperature of in-flight particles increased with the increasing of arc current as clearly shown in **Fig.4.7**.

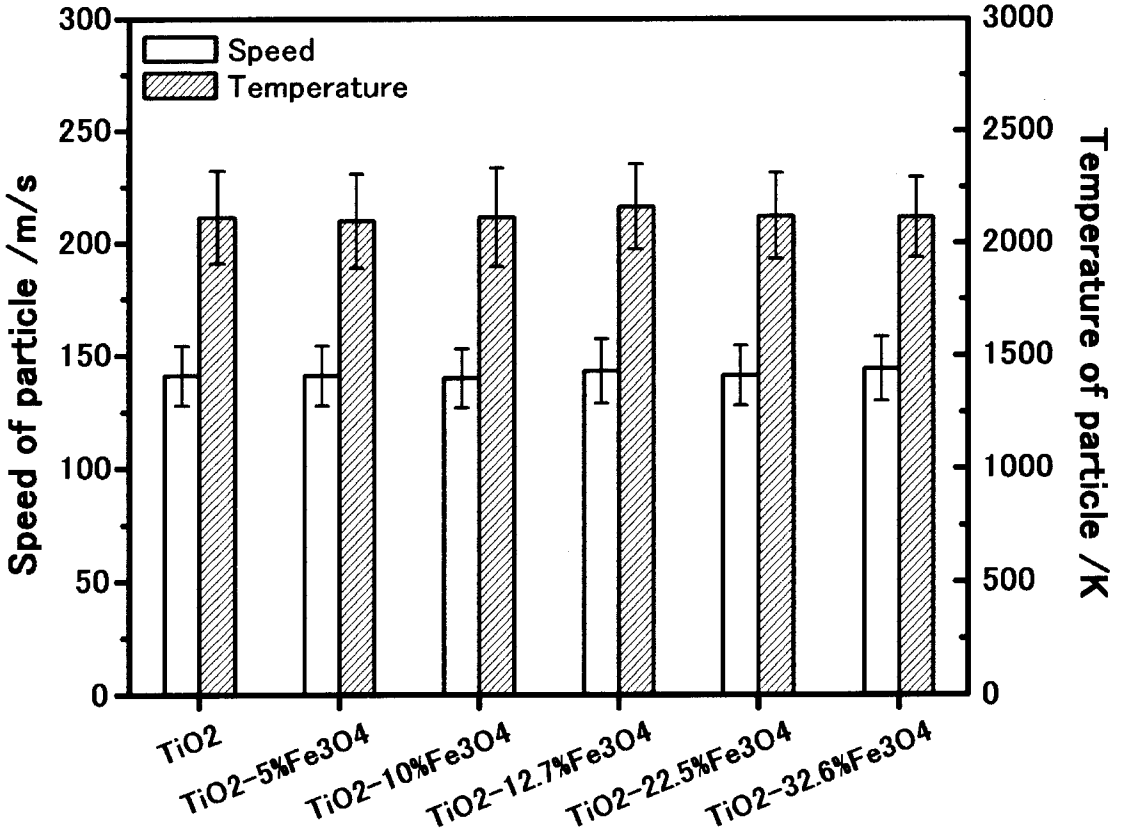

Fig.4.6. Speed and temperature of in-flight TiO_2 and TiO_2-Fe_3O_4 particles under the arc current of 400A.

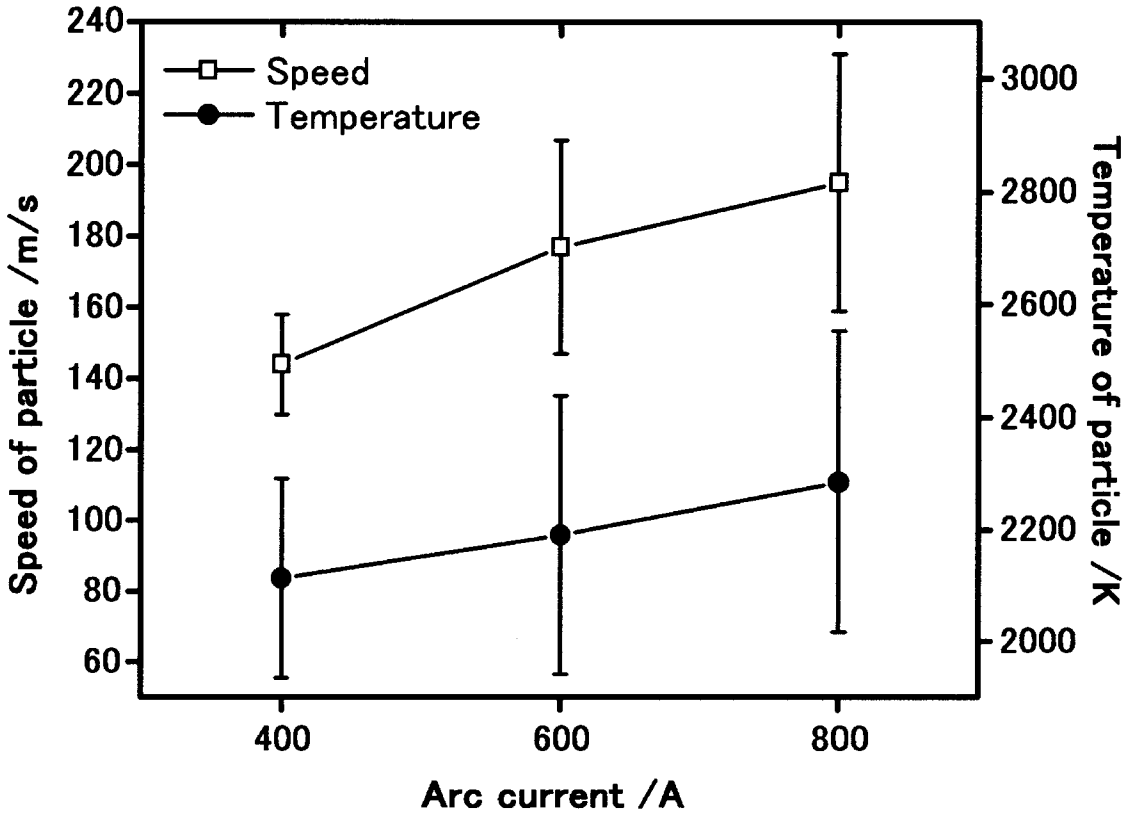

Fig.4.7. Speed and temperature of in-flight TiO_2-32.6%Fe_3O_4 particles under the arc current of 400A, 600A and 800A.

4.3.3. Composition of Plasma Sprayed TiO_2-Fe_3O_4 Coatings

Although the phase characterization results of TiO_2-10%Fe_3O_4 coatings were presented in Chapter 3, the influence of Fe_3O_4 content on the properties of TiO_2-Fe_3O_4 coating was not clear. In this section, detailed information about the compositions of TiO_2, TiO_2-5%Fe_3O_4, TiO_2-10%Fe_3O_4, TiO_2-12.7%Fe_3O_4, TiO_2-22.5%Fe_3O_4 and TiO_2-32.6%Fe_3O_4 coatings is given in order to obtain composition-property relations.

The x-ray diffraction patterns of plasma sprayed TiO_2 and TiO_2-Fe_3O_4 coatings under the arc current of 400A are illustrated in **Fig.4.8.** The relative intensity of anatase phase decreased with the increasing of Fe_3O_4 amount. This implied that the TiO_2-Fe_3O_4 feedstock powders were more melted with the increasing of Fe_3O_4 content, which is in good agreement with the results of the measured temperature of in-flight particles by

DPV-2000 and with the heat treatment results of feedstock powders. $FeTiO_3$ phase appeared with the addition of Fe_3O_4 till 22.5%, and became undetectable with the additive amount to 32.6%. The relative intensity of $FeTiO_3$ was highest in TiO_2-10%Fe_3O_4 coating comparing with other coating, which indicates that this coating had the highest content of $FeTiO_3$ compound. However, $FeTiO_3$ phase, which is thermally metastable compound, did not appear in heat treated TiO_2-Fe_3O_4 powders (See Fig.4.4). Thus it can be inferred plasma spraying technique is a method to form metastable substance.

The peak intensity of Fe_2TiO_5 phase increased continuously and obviously with the increasing of Fe_3O_4 amount, and finally became the main phase with the almost complete disappearance of ilmenite $FeTiO_3$ in the sprayed coating. For the high content of Fe_3O_4 in the TiO_2-32.6%Fe_3O_4 powder and high coating formation speed, a little Fe_3O_4 remained in the coating.

The crystal system of TiO_2 belongs to tetragonal ($a=b\neq c$). It has been reported that because TiO_2 contains interstitial channels in the *c* direction, certain transition metals diffuse through these channels into lattices. The diffusing ions have been found to locate preferentially on either the substitutional or interstitial sites. Moreover, $FeTiO_3$ is derived from α-Fe_2O_3 by replacing every other layer of the Fe atoms in (0001) planes by a layer of Ti atoms. Therefore, the formation of $FeTiO_3$ is possible in spite of the large ion radius of Fe^{2+}(0.83Å) [13] especially in plasma spraying processes for the instantaneous melting and solidification of the feedstock particles.

Furthermore, the formation of Fe_2TiO_5 is reported by the fact that certain percentage of Fe^{3+} ion diffuses into TiO_2 producing a substitutional solid solution where Fe^{3+} is dispersed in the lattice of TiO_2 due to the ion radius similarity of Fe^{3+}(0.67Å) and Ti^{4+}(0.64Å). The substitution of Fe^{3+} in the matrix of TiO_2 is a favorable process and is easier in rutile TiO_2 for the open channel [14]. This reason may result in the high amount of Fe_2TiO_5 in the sprayed coatings when more anatase TiO_2 transformed into rutile.

For the high temperature of plasma jet, elements evaporation (particle mass loss) is a common phenomenon in plasma spraying processes [15, 16], Fe and Ti elements analysis of sprayed TiO_2-Fe_3O_4 coatings were carried out in this study. **Fig.4.9(a)** illustrates typical EDAX analysis pattern of plasma sprayed TiO_2-Fe_3O_4 coating. The weight ratios of Fe/(Ti+Fe) in TiO_2-Fe_3O_4 coatings were obtained and are shown in **Fig.4.9(b)**. The weight fractions of Fe/(Ti+Fe) in the feedstock powders were calculated according to the powder nominal composition. The results indicates that the measured weight ratio of Fe/(Ti+Fe) in the sprayed coating was comparable to that of the corresponding powder. Therefore, it can be considered that the Fe and Ti elements did

not disappear in plasma spraying processes.

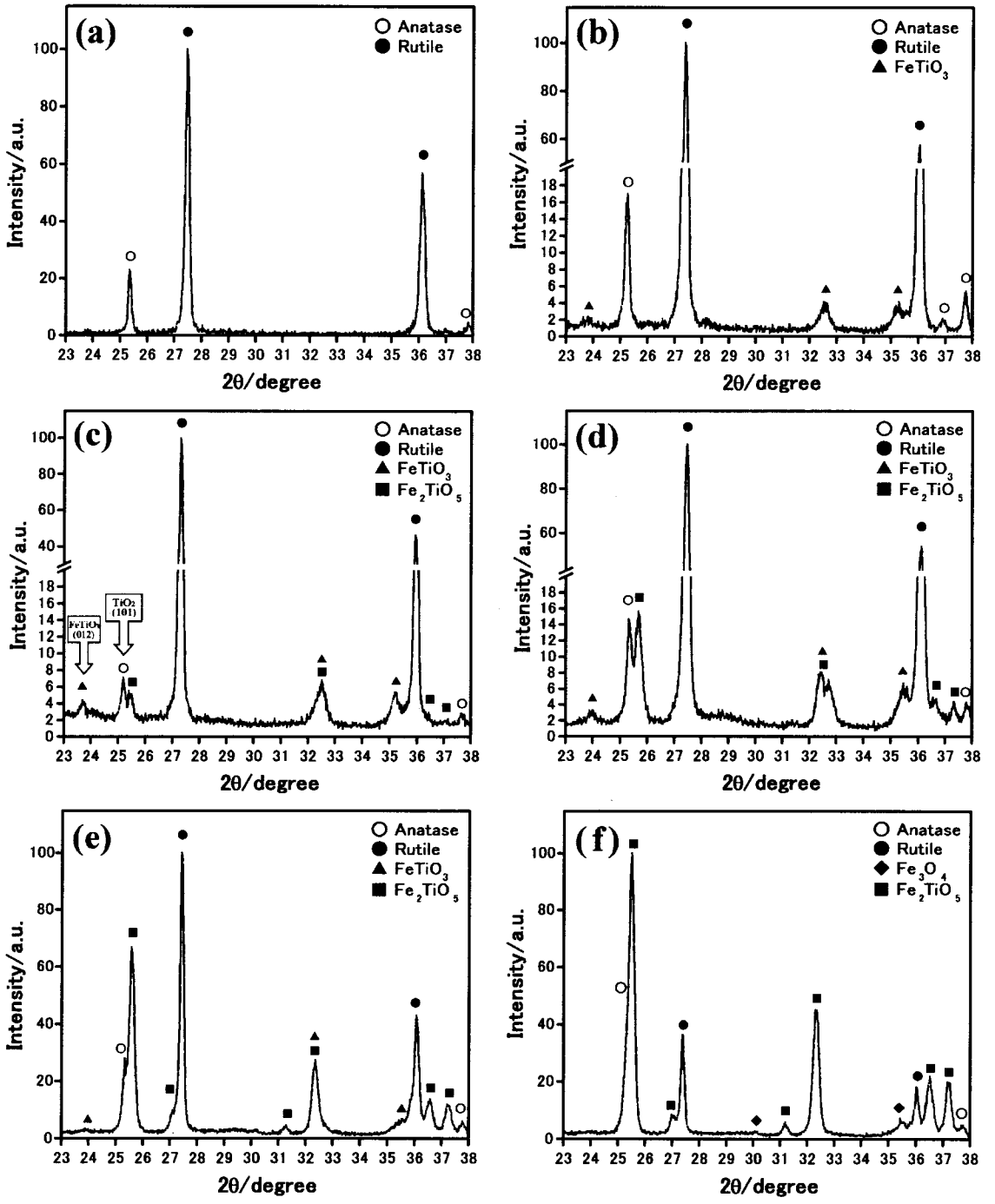

Fig.4.8. X-ray diffraction patterns of TiO_2 and TiO_2-Fe_3O_4 coatings plasma sprayed under the arc current of 400A and spraying distance of 70mm. (a) TiO_2 coating, (b) TiO_2-5%Fe_3O_4 coating, (c) TiO_2-10%Fe_3O_4 coating, (d) TiO_2-12.7%Fe_3O_4 coating, (e) TiO_2-22.5%Fe_3O_4 coating, (f) TiO_2-32.6%Fe_3O_4 coating.)

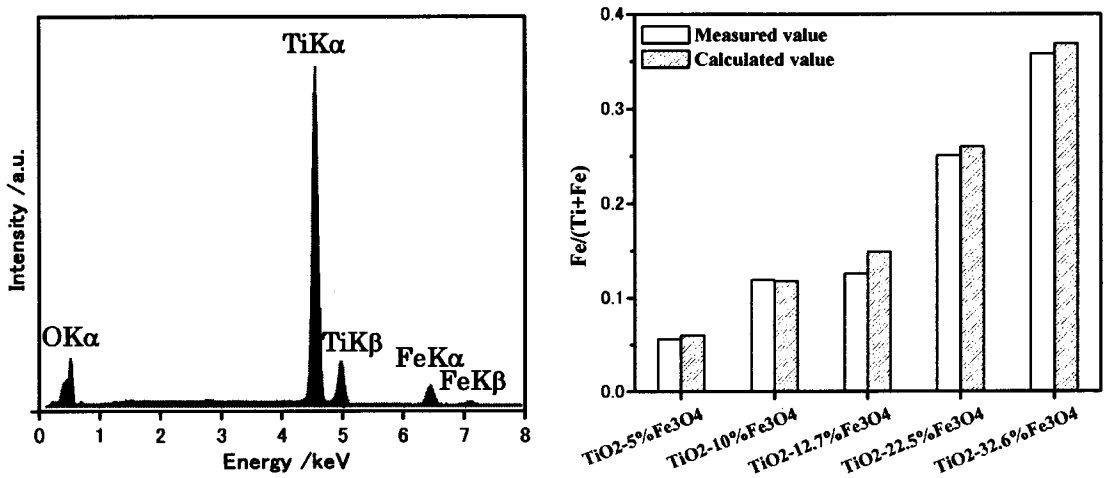

Fig.4.9. Typical EDAX analysis pattern of TiO_2-Fe_3O_4 coating (a), and the weight fractions of Fe/(Ti+Fe) in the TiO_2-Fe_3O_4 powders (Calculated value) and in the sprayed coatings (Measured value) (b).

4.3.4. Heat Treatment of Plasma Sprayed TiO_2-Fe_3O_4 Coatings

During the short residence time in the plasma jet, the feed particles are completely/partially melted. The droplets impact on a substrate and experience a cooling rate of 10^4~10^6K/s, therefore, solid solution, amorphous phase and phase segregation exists widely in composite coating [6, 7]. The existence of these kinds of phenomena in sprayed TiO_2-32.6%Fe_3O_4 coatings was investigated. As clearly shown in **Fig.4.10**, the relative intensity of the main diffraction of rutile phase (110) increased obviously when the coating was heat treated at 1273K, and became higher than that of Fe_2TiO_5 phase (101). The ratio of main diffraction intensity of rutile phase (110) and Fe_2TiO_5 phase (101) of heat treated TiO_2-32.6%Fe_3O_4 coating was comparable to that of heat treated TiO_2-32.6%Fe_3O_4 powder.

The XRD peaks of sprayed TiO_2-32.6%Fe_3O_4 coatings were not broad, which implied amorphous phase did not exist in it. According to the EDAX analysis results (**Fig.4.11**), Ti and Fe elements distributed uniformly along the perpendicular line to the coating surface, which indicated that TiO_2 and Fe_2TiO_5 phase segregations did not happen. It was confirmed again that Fe/(Ti+Fe) in the sprayed coating was comparable to that in TiO_2-32.6%Fe_3O_4 feedstock powder. As shown in **Fig.4.12**, large amount of Ti segregated from TiO_2 and/or Fe_2TiO_5 phase after heat treatment of coating, and then the weight fraction of TiO_2 increased obviously. Therefore, it was considered that solid

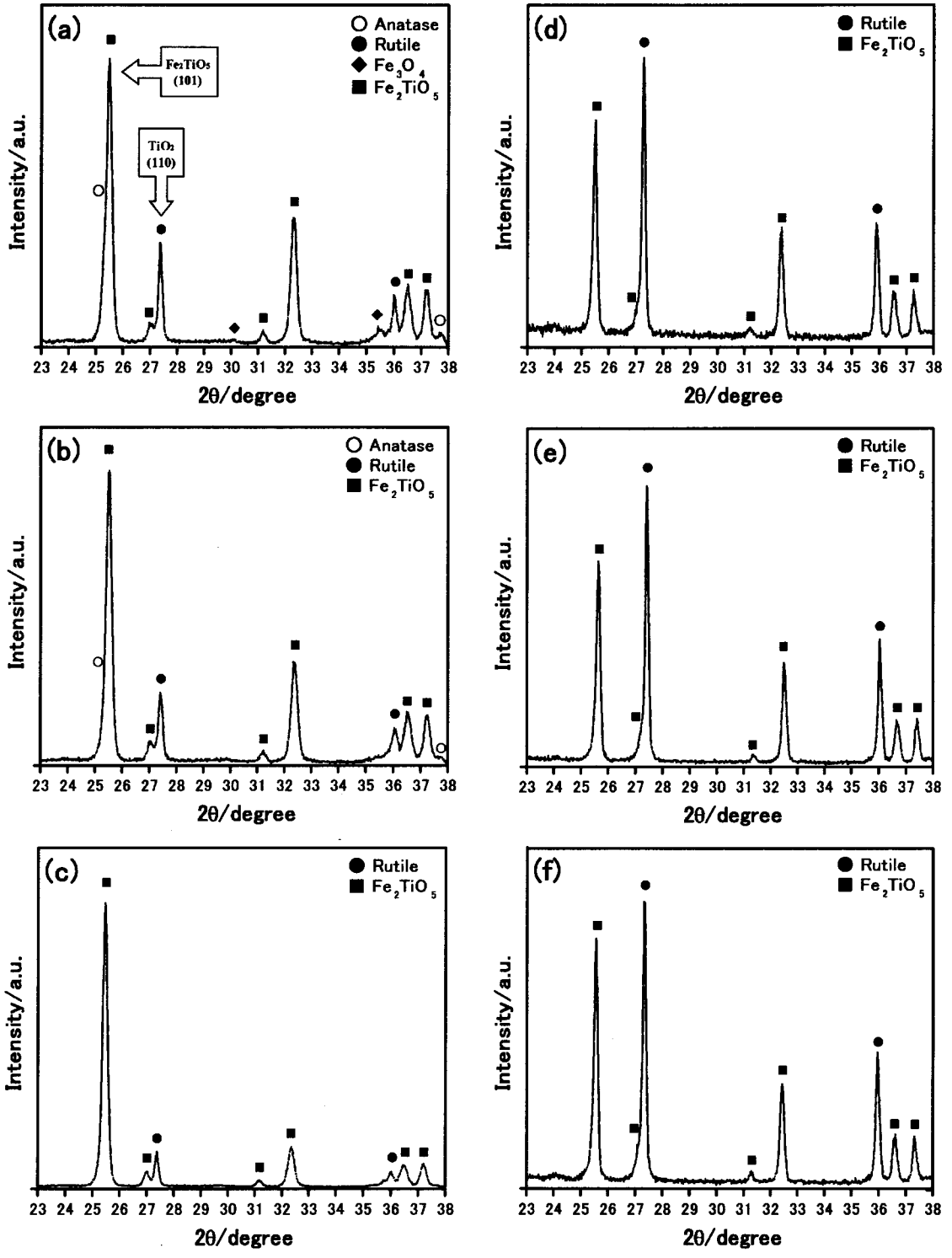

Fig.4.10. Phases changes of TiO_2-32.6%Fe_3O_4 coatings. (a) Coating sprayed at 400A, (b) Coating sprayed at 600A, (c) Coating sprayed at 800A, (d) Heat treated at 1273K of (a), (e) Heat treated at 1273K of (b), (f) Heat treated at 1273K of (c).

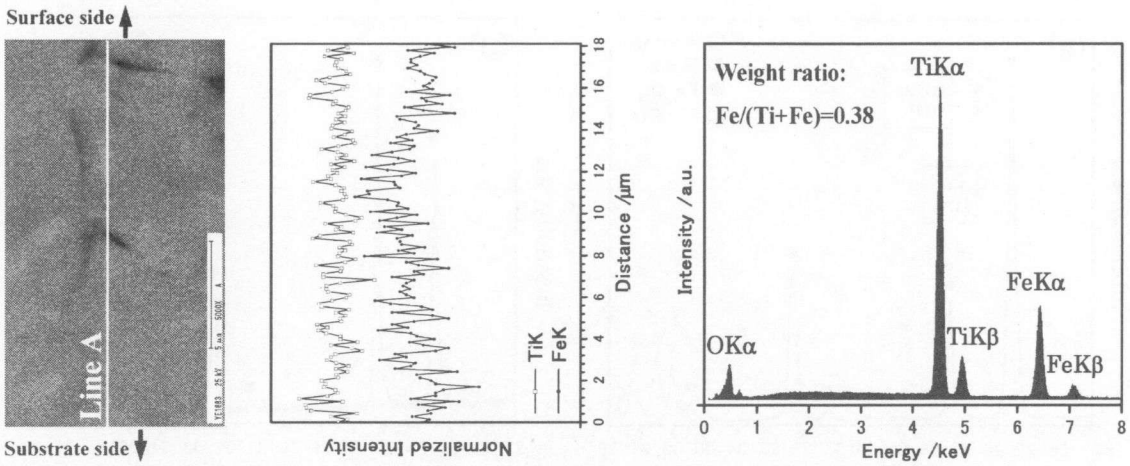

(a) (b) (c)

Fig.4.11. Cross section (a), Ti and Fe elements distribution (b) of *line A* in (a) and EDAX spectrum (c) of TiO_2-32.6%Fe_3O_4 coating plasma sprayed under the arc current of 600A.

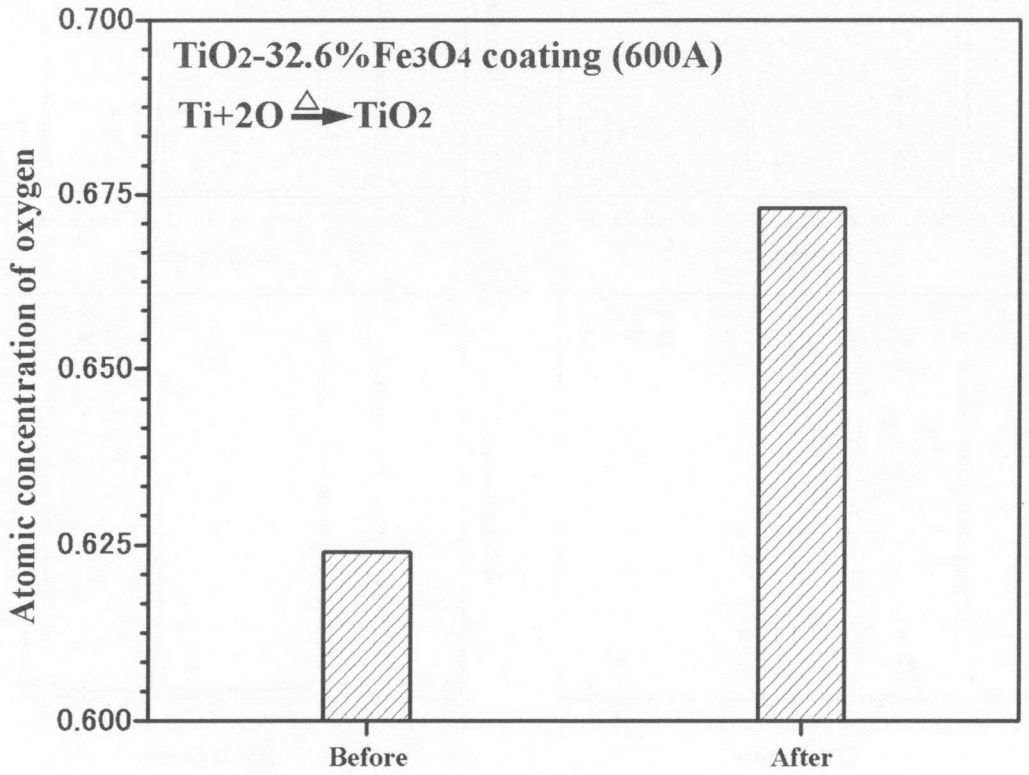

Fig.4.12. Atomic concentration change of oxygen before and after heat treatment at 1273K×21600s of TiO_2-32.6%Fe_3O_4 coating plasma sprayed under the arc current of 600A.

solution existed in the sprayed TiO_2-32.6%Fe_3O_4 coating. As shown in Fig. 4.10 (a), (b) and (c), the relative intensity of the main diffraction of rutile phase (110) decreased with the increasing of arc current. This implied the abundance of solid solution in the sprayed coatings increased with the increase of arc current, which results from the higher speed and temperature of particle transferred from plasma jet at high arc current (See Fig.4.7). The existence of solid solution may make the quantitative analysis of the coatings using the abnormal intensities absolutely meaningless.

As a result, special attentions should be paid on the quantitative measurement using the XRD method for thermal sprayed composite coating.

4.3.5. General Features of Plasma Sprayed TiO_2-Fe_3O_4 Coatings

Figure 4.13 illustrates the relative deposition speed of TiO_2 and TiO_2-Fe_3O_4 powders (RDSP). The RDSP increased with the amount increase of Fe_3O_4 additive. The RDSP of TiO_2-10%Fe_3O_4 powder, which was 13μm/pass, was over two times than that of TiO_2 powder. With the content of Fe_3O_4 to 32.6%, the RDSP was improved eight times. Conclusion has been drawn that the addition of Fe_3O_4 to TiO_2 improved obviously the TiO_2 powder deposition efficiency.

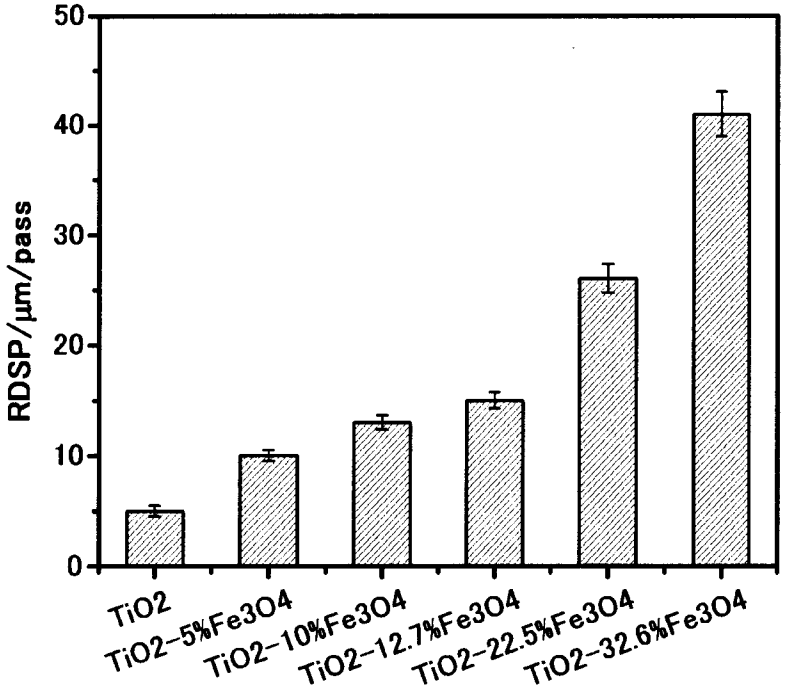

Fig.4.13. Relative deposition speed of TiO_2 and TiO_2-Fe_3O_4 powders (RDSP) under the arc current of 400A and spraying distance of 70mm.

Figure 4.14 shows the surface morphologies and cross sections of TiO_2, TiO_2-12.7%Fe_3O_4 and TiO_2-32.6%Fe_3O_4 coatings prepared by plasma spraying. The "U" denotes unmelted zone, "M" denotes melted zone in Fig.4.14 (b). TiO_2 coating is not very dense, and TiO_2 powders were not melted fully. In the TiO_2-Fe_3O_4 coatings, unmelted or partially melted TiO_2-Fe_3O_4 powders were fewer than that of TiO_2 powders under the same spraying conditions. These facts are in good agreement with the results presented in Section 4.3.2 and illustrated in Fig.4.13.

The solidification processes involve extraction of heat from the melt in a manner. The major growth morphologies are dendrites and eutectic [17, 18]. **Fig.4.15** displays a well-defined dendritic crystal in plasma sprayed TiO_2-Fe_3O_4 coating. As discussed in Section 4.3.2, one part of TiO_2 did not melted. Thus the unmelted TiO_2 may become nuclei, and then the nuclei grow into spherical crystals which rapidly become unstable and dendritic in form. These dendrites grow freely in the melt and finally impinge on one another.

4.3.6. Energy Absorbance of Plasma Sprayed TiO_2-Fe_3O_4 Coatings

According to the diffuse reflectance spectra of the feedstock powders (**Fig.4.16**), the Fe_3O_4 additive did not change the absorption edge (wavelength coordinate of black circle in Fig.4.16) and the light absorbance dropped suddenly in the wavelength range of 340nm to 400nm. These implied that Fe_3O_4 particle cannot shift the photo-absorptive ability of TiO_2 to the visible spectral range. The diffuse reflectance spectra of the sprayed coatings are shown in **Fig.4.17**, and to investigate the absorptive relation between light source used in this study and the sprayed coating, the spectral power distribution for UV-lamp is also illustrated in Fig.4.17. In the case of TiO_2 coating, the light absorbance dropped suddenly in the wavelength range of 340nm to 400nm. However, the dropping speed decreased continuously and the optical absorption edge (black circle) shifted to longer wavelength with the content increase of Fe_3O_4 additive. To compare the light absorptive capacity, the integrated energy absorbance of the sprayed TiO_2 and TiO_2-Fe_3O_4 coatings from the ultraviolet lamp used in this study is estimated according to Equations (4.9) and (4.10). As shown in **Fig.4.18**, the relative integrated energy absorbance increased with the content increase of the Fe_3O_4 additive, which means that more irradiation light energy can be utilized. It partly ascribed to $FeTiO_3$ and Fe_2TiO_5 compound as reported by N. Smirnova et al. [19], F. X. Ye et al. [20] and B. Pal et al. [14].

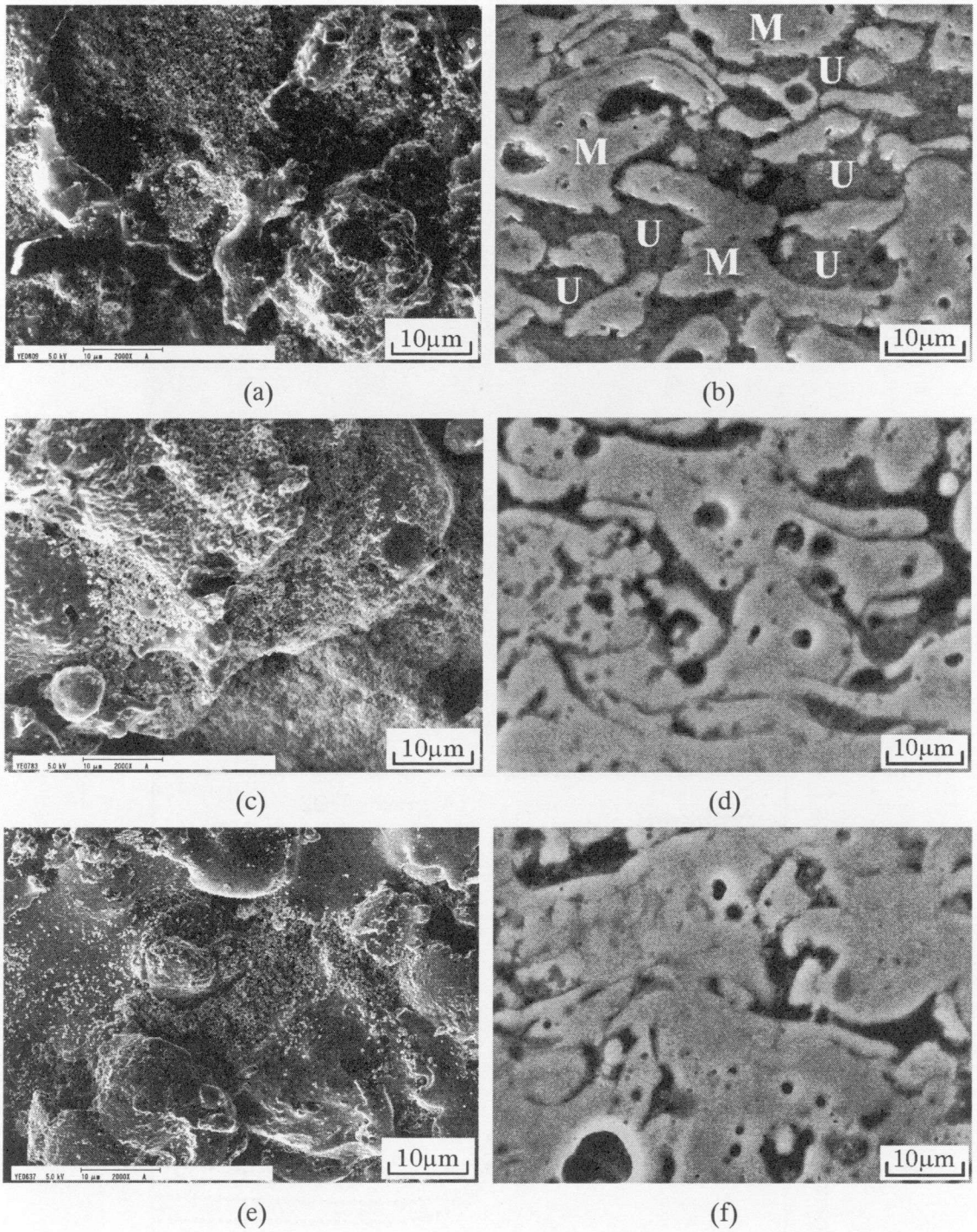

(a) (b)

(c) (d)

(e) (f)

Fig.4.14. Surface morphologies and cross sections of plasma sprayed coatings under the arc current of 400A and spraying distance of 70mm. (a), (c), (e) Surface morphologies of TiO_2, TiO_2-12.7%Fe_3O_4, and TiO_2-32.6%Fe_3O_4 coatings, respectively. (b), (d), (f) Cross sections of TiO_2, TiO_2-12.7%Fe_3O_4, and TiO_2-32.6%Fe_3O_4 coatings, respectively. (Notes: "U" denotes unmelted zone, "M" denotes melted zone in (b)).

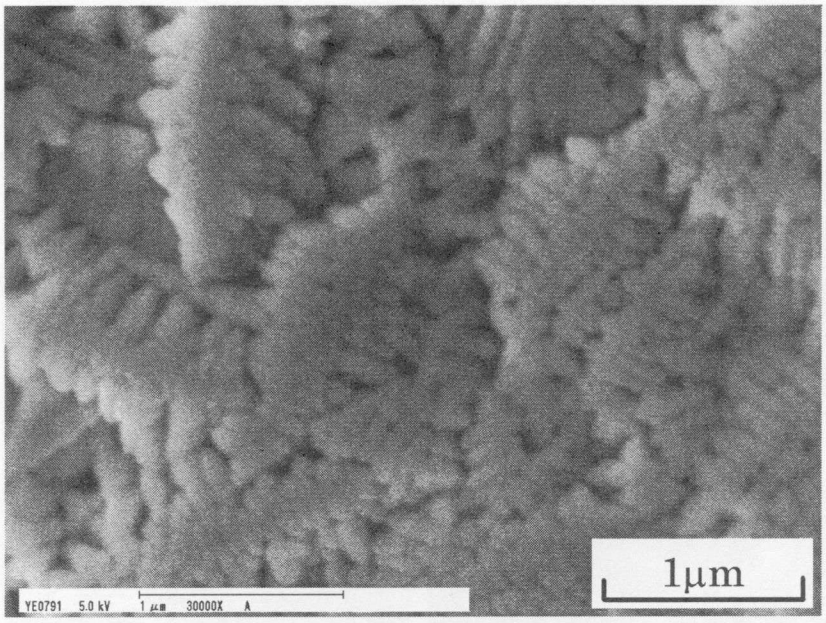

Fig.4.15. Dendritic crystal appeared in TiO_2-Fe_3O_4 coating sprayed under the arc current of 400A.

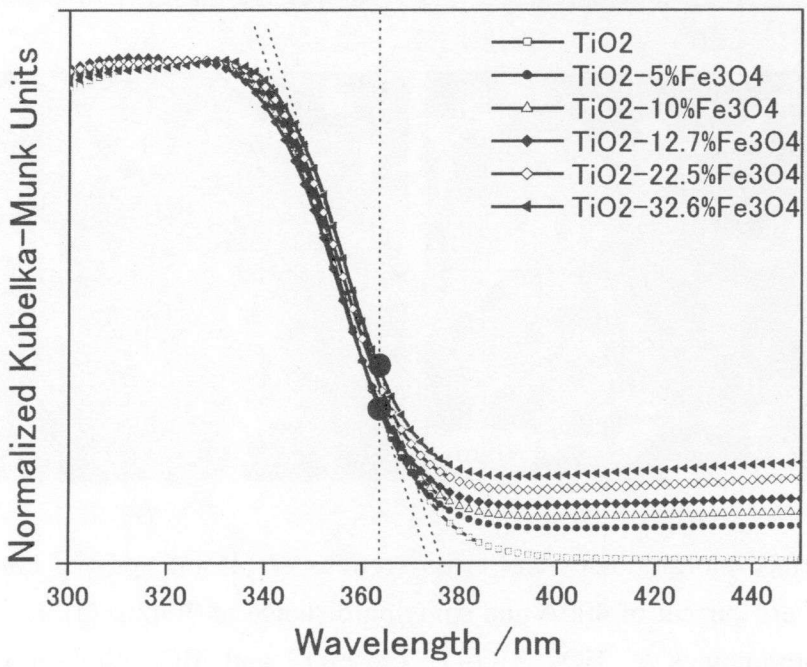

Fig.4.16. Diffuse reflectance spectra of the feedstock TiO_2 and TiO_2-Fe_3O_4 powders.

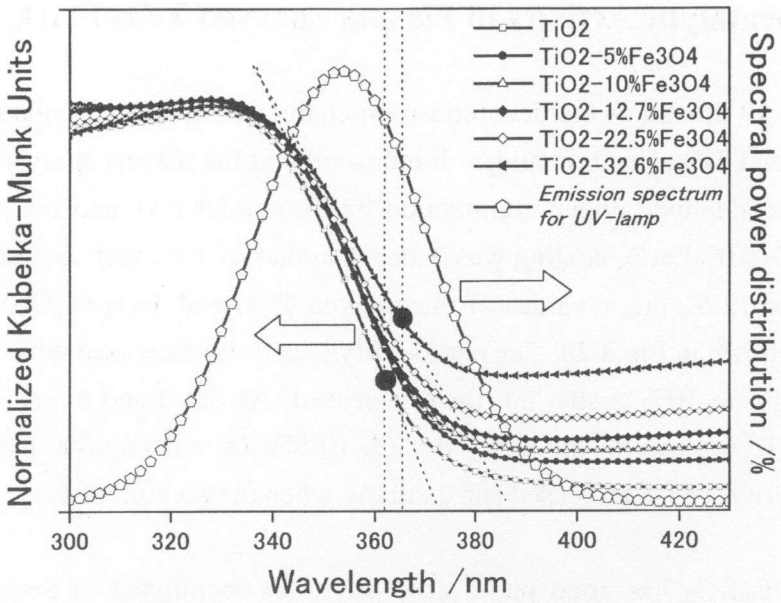

Fig.4.17. Diffuse reflectance spectra of TiO_2, TiO_2-Fe_3O_4 coatings sprayed under the arc current of 400A and spraying distance of 70mm, and the spectral power distribution for the ultraviolet lamp used in this study.

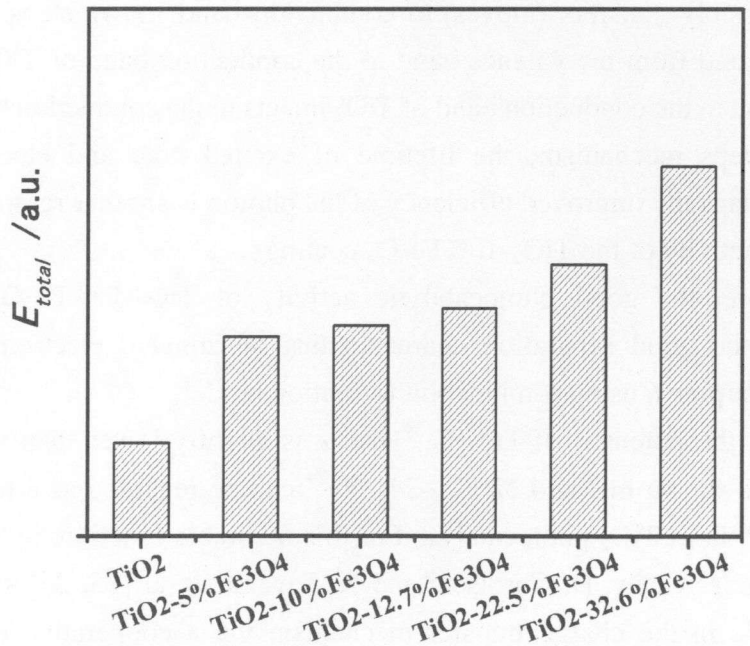

Fig.4.18. Integrated energy absorbance of TiO_2 and TiO_2-Fe_3O_4 coatings sprayed under the arc current of 400A and spraying distance of 70mm from the ultraviolet lamp used in this study.

4.3.7. Photocatalytic Activity of Plasma Sprayed TiO_2-Fe_3O_4 Coatings

Figure 4.19 illustrates the decomposition characteristic of the acetaldehyde by the sprayed TiO_2 and TiO_2-Fe_3O_4 coatings. It indicated that the plasma sprayed coatings can decompose acetaldehyde under illumination by ultraviolet rays and the photocatalytic activity of TiO_2-10%Fe_3O_4 coating was better than that of the other coatings. According to the Equation (2.6), the τ values of the sprayed TiO_2 and TiO_2-Fe_3O_4 coatings were calculated as shown in **Fig.4.20**. The photocatalytic activity increased with the increasing of Fe_3O_4 weight to 10% firstly, but then decreased. As discussed in section 4.3.3, the amount of $FeTiO_3$ phase in the sprayed TiO_2-10%Fe_3O_4 coating was highest, and the content of Fe_2TiO_5 phase increased substantially when the amount of Fe_3O_4 additive was over 12.7%.

Because $FeTiO_3$ has good photo absorptivity as mentioned in Section 4.3.6, the good photocatalytic efficiency of TiO_2-10%Fe_3O_4 coating possibly resulted from the high content of ilmenite $FeTiO_3$ phase in the coating, but not directly from the Fe_3O_4 particles. Furthermore, the band gap of bulk $FeTiO_3$, which is 2.85eV [21], is lower than that of TiO_2. As a possible phenomenon shown in **Fig.4.21**, when the semiconductor is irradiated, the electron possibly transfers (moves) to conduction band in two steps. First step: the electron is initiated from the valence band to the conduction band of TiO_2, and second step: the electron in the conduction band of TiO_2 injects to the conduction band of $FeTiO_3$. For this two-steps mechanism, the lifetime of excited hole and electron pair was prolonged. Perhaps the improved efficiency of the photon is another reason for the good photocatalytic activity of the TiO_2-10%Fe_3O_4 coatings.

Furthermore, the good photocatalytic activity of TiO_2-10%Fe_3O_4 coating also resulted from the good separation characteristics of initiated electron-hole pairs as discussed in **Chapter 6** using p-n junction formation model.

Moreover, the potential of Fe^{2+}/Fe^{3+} redox is slightly lower than the conduction band of TiO_2 as shown in **Fig.4.22** [22~24], Fe^{2+} can be regarded as a trap of initiated electrons like Pt in Pt/TiO_2 photocatalyst. For this favorable function, initiated electrons separate with holes easily. D. Cordischi and K. Sayama et. al [25, 26] suggested ferric ions play a role in the charge transfer mechanism via a cooperative effect with the Ti^{4+}/Ti^{3+} couple, according to the Reaction (4.13)~(4.16). Fe^{2+}/Fe^{3+} attended the oxidation-reduction reaction and then increased the photocatalytic activity of TiO_2-10%Fe_3O_4 coating.

$$Ti^{4+} + Fe^{2+} \rightarrow Ti^{3+} + Fe^{3+} \qquad (4.13)$$

$$Fe^{2+} + h\nu \rightarrow Fe^{2+,*} \tag{4.14}$$

$$Fe^{2+,*} + Ox \rightarrow Fe^{3+} + R \tag{4.15}$$

$$Ti^{3+} + Ox \xrightarrow{h\nu} Ti^{4+} + R \tag{4.16}$$

where Ox and R are oxidized and reduced adsorbed species, respectively.

The band gap of pure Fe_2TiO_5 is 2.18eV, which is lower than that of TiO_2 and $FeTiO_3$. Although the light absorbance increases with the amount increasing of Fe_2TiO_5 compound, the photocatalytic activity was reduced dramatically when the content of Fe_2TiO_5 is high. As is known [14], this kind of phenomenon may result from the unfavorable charge transfer process to adsorbed substance during light illumination where excess accumulation of electron and hole undergoes recombination immediately without taking part in the photocatalytic reaction. Therefore, the electron-hole pair formation and separation process is a key factor in photocatalytic reaction.

As a result, the photocatalytic efficiency of sprayed TiO_2-Fe_3O_4 coating is improved with an increase in the $FeTiO_3$ content in the sprayed coatings. However, when the content of Fe_3O_4 additive was over 10%, photocatalytic activity was reduced to large extent due to the presence of large amount of inactive Fe_2TiO_5 compound in the TiO_2-Fe_3O_4 coatings.

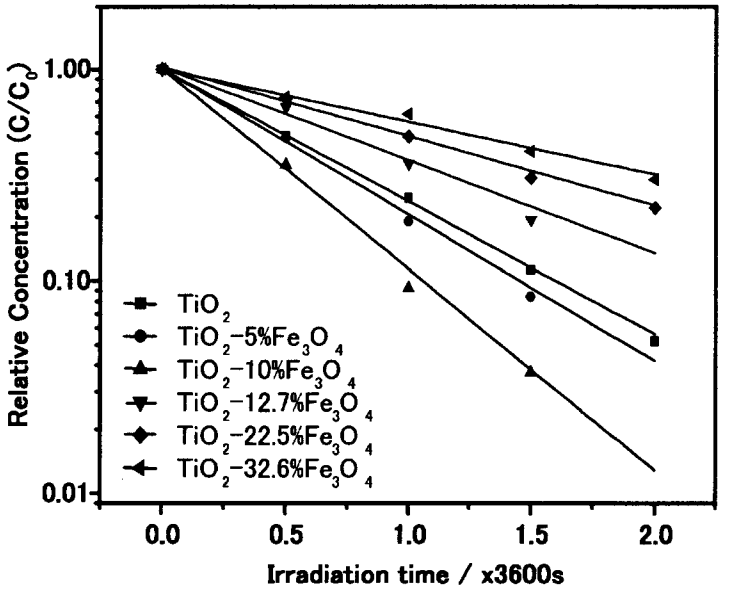

Fig.4.19. Photocatalytic decomposition characteristics of the acetaldehyde by the sprayed TiO_2 and TiO_2-Fe_3O_4 coatings.

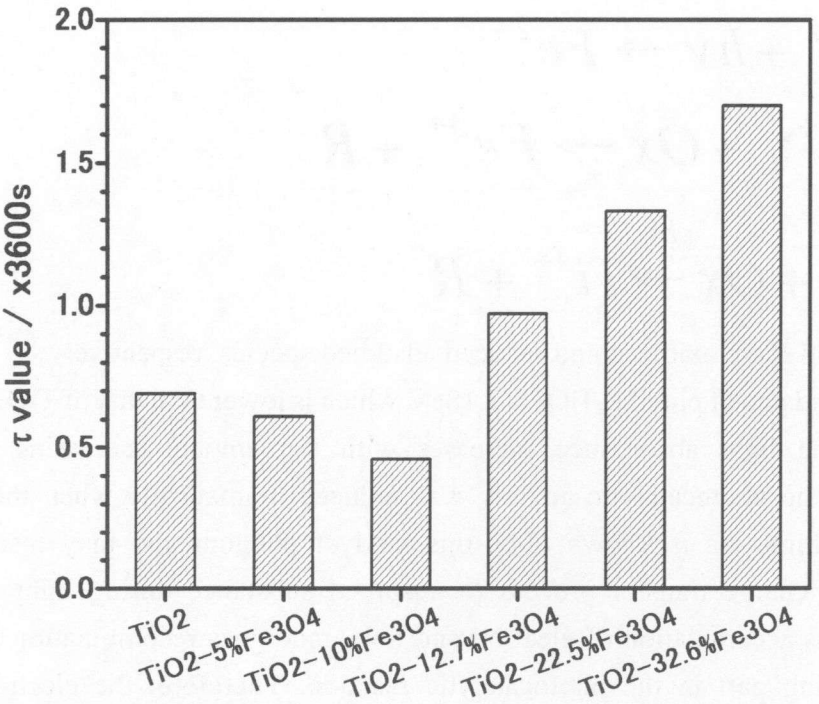

Fig.4.20. τ values of the plasma sprayed TiO_2 and TiO_2-Fe_3O_4 coatings.

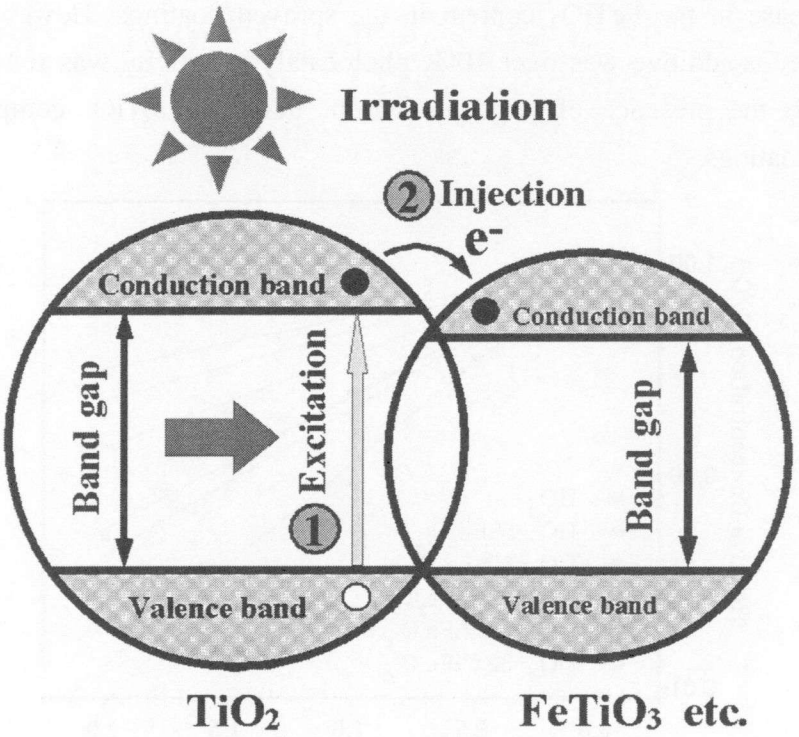

Fig.4.21. A proposed two-steps electron transfer model for the good photocatalytic activity of TiO_2-10%Fe_3O_4 coating.

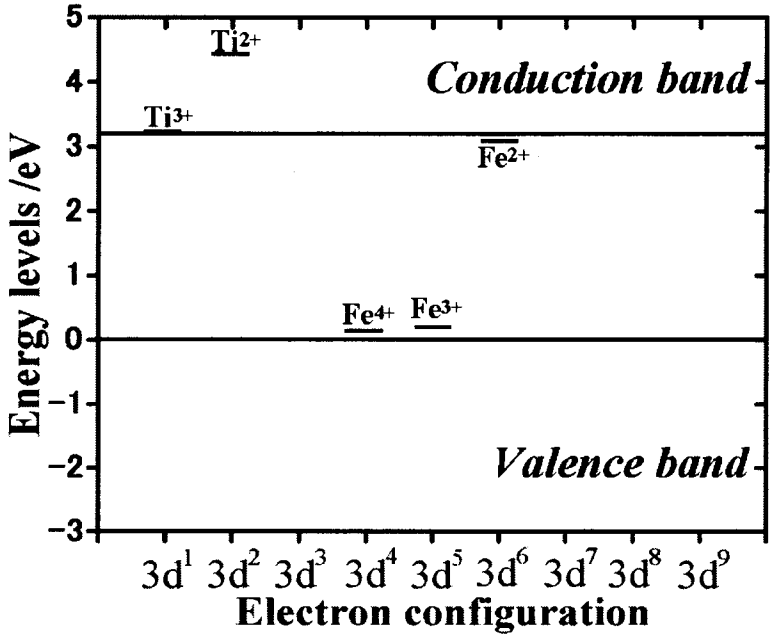

Fig.4.22. Energy levels of various redoxes in anatase TiO_2.

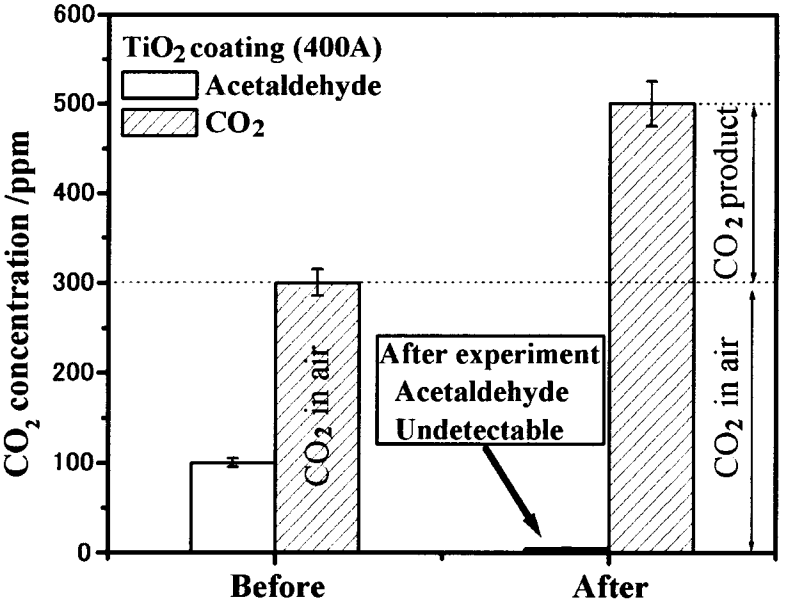

Fig.4.23. Variation of CO_2 concentration before and after photo-degradation experiment.

4.3.8. Generation of CO_2 in Photo Degradation Processes

Figure 4.23 shows the variation of CO_2 concentration before and after photo-degradation experiment (an example). In the figure, "after experiment" was the time

when the acetaldehyde was undetectable in evaluation experiment of photocatalytic activity of sprayed coating.

If 100ppm acetaldehyde decomposes completely to CO_2 and H_2O, the concentration of CO_2 should be 200ppm according to the reaction (4.17).

$$2CH_3CHO + 5O_2 \xrightarrow[TiO_2]{h\nu} 4CO_2 + 4H_2O \qquad (4.17)$$

After photo-degradation experiment, 200ppm CO_2 increased (Fig.4.23), which implied that the acetaldehyde decomposed completely using plasma sprayed TiO_2 coating.

4.4. Conclusions

The anatase-rutile phase transformation temperature of TiO_2 and TiO_2-Fe_3O_4 feedstock powders was studied systematically. TiO_2 and TiO_2-Fe_3O_4 coatings were prepared on stainless steel substrate by plasma spray. The results clearly showed that the anatase-rutile transformation temperature of TiO_2-Fe_3O_4 powders was in the range of 973K to 1123K, which was at least 50K lower than that of pure anatase TiO_2 powder. The TiO_2-Fe_3O_4 coatings consisted of anatase TiO_2, rutile TiO_2, and pseudobrookite Fe_2TiO_5 phase which appeared when the content of Fe_3O_4 additive was equal to or over 10%. With relative low amount addition of Fe_3O_4, ilmenite $FeTiO_3$ phase existed in the sprayed coatings. The content of anatase TiO_2 in the sprayed coatings decreased with the increasing of Fe_3O_4 content. The photocatalytic activity was improved with an increase of $FeTiO_3$ content in the coating, which was explained by the good photo absorbance capacity and by the two-steps electron transfer model. Moreover, initiated electrons could separate with holes easily because Fe^{2+} can be regarded as a trap of initiated electrons. However, the presence of large amount of Fe_2TiO_5 compound substantially reduced the photocatalytic efficiency of the sprayed TiO_2-Fe_3O_4 coatings for the unfavorable electron-hole transfer process.

References

[1] G. Renouare-Vallet, F. Gitzhofer, M. Boulos, P. Fauchais, M. Vardelle, and L. Bianchi, Optimization of axial injection conditions in a supersonic induction plasma torch: Application to SOFCs, *Proceedings of the 2003 International Thermal Spray Conference, May 5-8 2003, Orlando, Florida, USA, 195-202.*

[2] A. Refke, G. Barbezat, J. Dorier, M. Gindrat, and C. Hollenstein, Characterization of LPPS process under various spray conditions for potential applications, *Proceedings of the 2003 International Thermal Spray Conference, May 5-8 2003, Orlando, Florida, USA, 581-588.*

[3] J. E. Craig, R. A. Parker, D. Lee, T. Wakeman, J. Heberlein, and D. Guru, Particle temperature and velocity measurements by two-wavelength streak imaging, *Proceedings of the 2003 International Thermal Spray Conference, May 5-8 2003, Orlando, Florida, USA, 1107-1112.*

[4] Z. Zou, J. Ye, K. Sayama, and H. Arakawa, Photocatalytic and photophysical properties of a novel series of solid photocatalysts, $BiTa_{1-x}Nb_xO_4$ ($0 \leqslant x \leqslant 1$), *Chemical Physics Letters, Vol. 343(3-4) (2001) 303-308.*

[5] B. D. Cullity, Elements of x-ray diffraction, *Second edition, 1978, P397-419.*

[6] X. H. Xiang, J. C. Zhu, Z. D. Yin, and Z. H. Lai, Fabrication and microstructure of ZrO_2/NiCrCoAlY graded coating by plasma spraying, *Surface and Coatings Technology, Vol. 88 (1996) 66-69.*

[7] Y. Z. Yang, Z. G. Liu, Z. Y. Liu, and Y. Z. Chuang, Interfacial phenomena in the plasma spraying Al_2O_3+13wt.%TiO_2 ceramic coating, *Thin Solid Films, Vol. 388(1-2) (2001) 208-212.*

[8] http://www.tecnar-automation.com/en/dpv-f-e.html.

[9] P. D. Fochs, The measurement of the energy gap of semiconductor from their diffuse reflection spectra, *The Proceedings of Physics Society, Section B/ the Physics Society, Vol. B69 (1956) 70-75.*

[10] S. P. Tandon and J. P. Gupta, Diffuse reflectance spectrum of cuprous oxide, *Physica Status Solidi, Vol. 37 (1970) 43-45.*

[11] Erest M. Levin, Carl R. Robbins, and Howard F. McMurdie, Phase diagrams for ceramists, *Volume one, Edited and published by The American Ceramic Society, Inc. 1964, P62.*

[12] Powder Diffraction File, Card 33-0664, Melting point of Fe_2O_3 is 1623-1633K.

[13] K. H. Yoon, J. Cho, and D. H. Kang, Physical and photoelectrochemical properties of the TiO_2-ZnO system, *Materials Research Bulletin, Vol. 34(9) (1999)1451-1461.*

[14] B. Pal, M. Sharon, and G. Nogami, Preparation and characterization of TiO_2/Fe_2O_3 binary mixed oxides and its photocatalytic properties, *Materials Chemistry and Physics, Vol. 59(3) (1999) 254-261.*

[15] V. V. Sobolev, J. M. Guilemany, and A. J. Martín, In-flight behaviour of steel particles during plasma spraying, *Journal of Materials Processing Technology, Vol. 87(1-3) (1999) 37-45.*

[16] K. Ramachandran and V. Selvarajan, Trajectory and temperature history of the particles of different sizes and their injection velocities in a thermal plasma, *Computational Materials Science, Vol. 6(1) (1996) 81-91.*

[17] K. Fisher, Fundamentals of solidification, *Fourth revised edition, Trans Tech Publications Ltd., 1998, 1-16 and 63-92.*

[18] B. H. Kear, Z. Kaiman, R. K. Sadangi, G. Skandan, J. Colaizzi, and W. E. Mayo, Plasma-sprayed nanostructured Al_2O_3/TiO_2 powders and coatings, *Journal of Thermal Spray Technology, Vol. 9(4) (2000) 483-487.*

[19] N. Smirnova, A. Eremenko, O. Rusina, W. Hopp, et al., Synthesis and characterization of photocatalytic porous Fe^{3+}/TiO_2 layers on glass, *Journal of Sol-gel Science and Technology, Vol. 22(1-2) (2001) 109-113.*

[20] F. X. Ye and A. Ohmori, The photocatalytic activity and photo-absorption of plasma sprayed TiO_2-Fe_3O_4 binary oxide coatings, *Surface and Coatings Technology, Vol. 160(1) (2002) 62-67.*

[21] D. S. Ginley and M. A. Butler, The photoelectrolysis of water using iron titanate anodes, *Journal of Applied Physics, Vol. 48(5) (1977) 2019-1021.*

[22] K. Mizushima, M. Tanaka, and S. Lida, Energy levels of iron group impurities in TiO_2, *Journal of The Physics Society of Japan, Vol. 32(6) (1972) 1519-1524.*

[23] S. D. Mo, L. B. Lin, and D. L. Lin, Electron states of iron group impurity in doped rutile (TiO_2), *Journal Physics Chemistry Solids, Vol. 55(11) (1994) 1309-1313.*

[24] J. Moser and M. Grätzel, Inhibition of electron-hole recombination in substitutionally doped colloidal semiconductor crystallites, *Helvetica Chimica Acta, Vol. 70 (1987) 1596-1604.*

[26] D. Cordischi, N. Burriesci, F. Dalba, M. Petrera, G. Polizzotti, and M. Schiavello, Structural characterization of Fe/Ti oxide photocatalysts by x-ray, ESR, and Mossbauer methods, *Journal of Solid State Chemistry, Vol. 56 (1985) 182-190.*

[27] K. Sayama, R. Yoshida, H. Kusama, K. Okabe, Y. Abe and H. Arakawa Photocatalytic decomposition of water into H_2 and O_2 by a two-step photoexcitation reaction using a WO_3 suspension catalyst and an Fe^{3+}/Fe^{2+} redox system, *Chemical Physics Letters, Vol. 227 (1997) 387-391.*

CHAPTER 5

Evaluation of Plasma Sprayed TiO_2-$FeTiO_3$ Coatings

5.1. Introduction

Titanium-substituted iron oxides are widespread in nature and represent an important mineral resource for the commercial extraction of both iron and titanium [1]. The $FeTiO_3$ structure, which is of rhombohedral crystal structure, is derived from α-Fe_2O_3 by replacing every other layer of the Fe atoms in (0001) planes by a layer of Ti atoms [2, 3]. Ilmenite is an incongruently melting material with the melting point of approximate 1683K [4]. Although high temperature electrical conductivity and magnetic properties of ilmenite $FeTiO_3$ have been investigated in detail [2~6], very little work has been done as a chemical catalyst and photocatalyst [7]. The characterization of photocatalytic performance of TiO_2-$FeTiO_3$ composite cannot be found until now.

To elucidate the influence of $FeTiO_3$ on the photocatalytic activity of plasma sprayed TiO_2-Fe_3O_4 coatings, $FeTiO_3$ and TiO_2-$FeTiO_3$ powders were designed. The phase composition, microstructure and photocatalytic activity of plasma sprayed $FeTiO_3$, TiO_2-30%$FeTiO_3$ and TiO_2-50%$FeTiO_3$ coatings were discussed in detail in this chapter. The photocatalytic activity of TiO_2, TiO_2-30%$FeTiO_3$ and $FeTiO_3$ powders was also evaluated.

5.2. Materials and Experimental Procedures

5.2.1 Feedstock Powders and Substrate

$FeTiO_3$ particles with average size of 1.4μm were agglomerated to $FeTiO_3$ feedstock powder with average size of 32.5μm. To manufacture TiO_2-30%$FeTiO_3$ and TiO_2-50%$FeTiO_3$ feedstock powders, TiO_2 particle with average size of 0.2μm was mechanically and uniformly mixed with 1.4μm $FeTiO_3$ particles with corresponding weight ratio. The average size of TiO_2-30%$FeTiO_3$ and TiO_2-50%$FeTiO_3$ was 30.4μm and 28.9μm, respectively. The x-ray diffraction patterns of the $FeTiO_3$, TiO_2-30%$FeTiO_3$ and TiO_2-50%$FeTiO_3$ feedstock powders are shown in **Fig.5.1**. The morphology of TiO_2-30%$FeTiO_3$ powder is given in **Fig.5.2**, which was very similar to $FeTiO_3$ and

TiO_2-50%$FeTiO_3$ powder. The substrate was stainless steel (JIS SUS304).

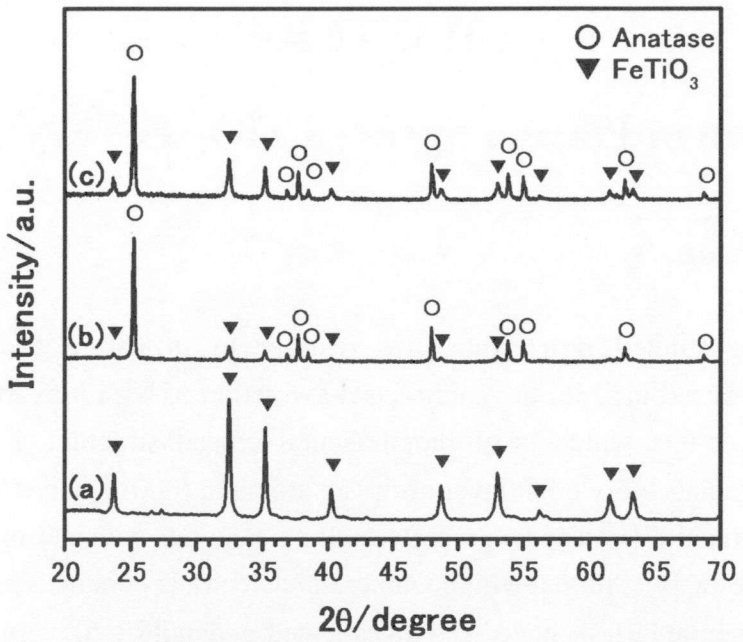

Fig.5.1. X-ray diffraction patterns of the $FeTiO_3$ (a), TiO_2-30%$FeTiO_3$ (b) and TiO_2-50%$FeTiO_3$ (c) feedstock powders.

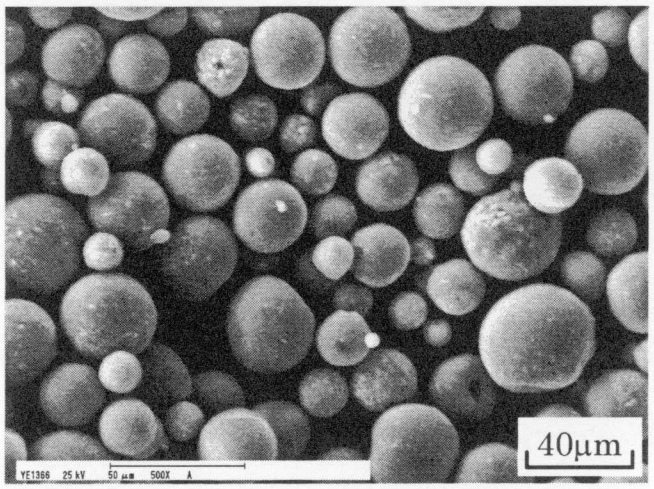

Fig.5.2. The morphology of TiO_2-30%$FeTiO_3$ powder.

5.2.2. Plasma Spraying Equipment

The thermal spraying equipment was a plasma spraying system (Plasmadyne-Mach1 manufactured by Plasmadyne Company). Argon was applied as primary gas, and helium was applied as secondary gas. The thermal spraying parameters are given in **Table 5.1**.

Table 5.1 Plasma spraying parameters.

Argon gas pressure (MPa) /flow (slpm)	0.42/58
Helium gas pressure (MPa) /flow (slpm)	0.21/9
Arc current (A)	400, 600, 800
Arc voltage (V)	28~30
Spraying distance (mm)	70

5.2.3. Characterization of Powders and Sprayed Coatings

Electron probe surface roughness analyzer (ERA-8800FE, Elionix Co. Ltd., Japan) and energy dispersive analysis of x-ray (EDAX) were used to examine the structure characteristics of the feedstock powders and the sprayed coatings. The phase composition of the feedstock powders and the sprayed coatings was investigated by x-ray diffraction using Cu-Kα radiation (λ=1.5406Å) and graphite crystal monochromator (M03XHF, MAC Science Co. Ltd.). To evaluate powder deposition efficiency, the relative deposition speed of powder was also calculated by Equation (2.2) given in Chapter 2. The photocatalytic activity of sprayed coatings was evaluated using the acetaldehyde degradation set-up, and the τ value was calculated by Equation (2.6).

5.3. Results and Discussion

5.3.1. Typical Microstructure of $FeTiO_3$ and TiO_2-$FeTiO_3$ Coatings

Figure 5.3 shows the cross sections of TiO_2-30%$FeTiO_3$ coatings sprayed under the arc current of 400A, 600A and 800A. It indicates that the coating became denser with the increasing of arc current. As clearly shown in **Fig.5.4,** many primary particles existed in the coating sprayed under the arc current of 400A for the low energy transfer from plasma jet. The relative deposition speed of TiO_2-30%$FeTiO_3$ powder, which was approximate to 4μm/pass, had no significant variation comparing with that of TiO_2 powder as shown in **Fig.5.5**. With the increase of arc current to 600A or 800A, the relative deposition speed of TiO_2-30%$FeTiO_3$ powder (RDSP) increased obviously.

Figure 5.6 shows the cross sections and surface morphologies of $FeTiO_3$ and TiO_2-50%$FeTiO_3$ coatings sprayed under the arc current of 400A. It indicated that the $FeTiO_3$ powder was more melted than the TiO_2-50%$FeTiO_3$ powder, which also can be inferred from Fig.5.5.

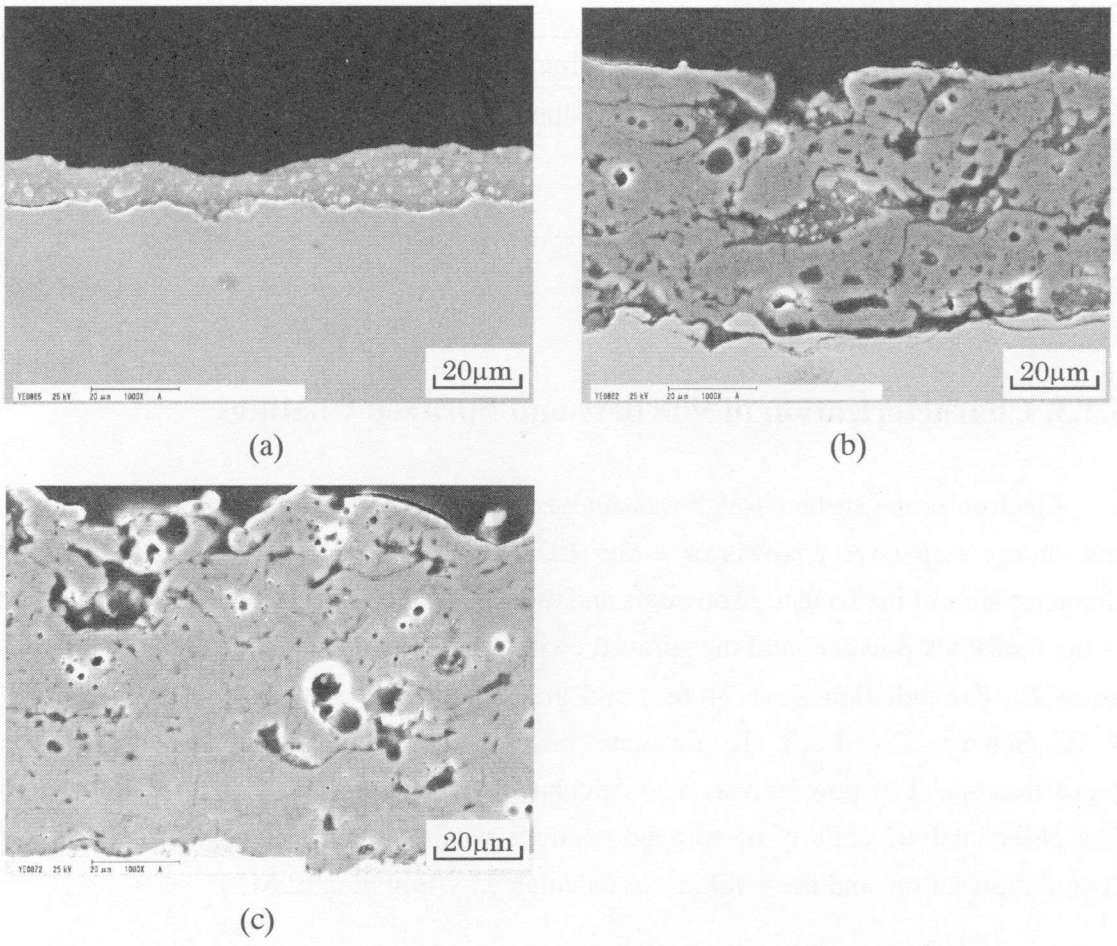

Fig.5.3. Cross sections of TiO_2-30%$FeTiO_3$ coatings sprayed under the arc current of 400A(a), 600A(b) and 800A(c).

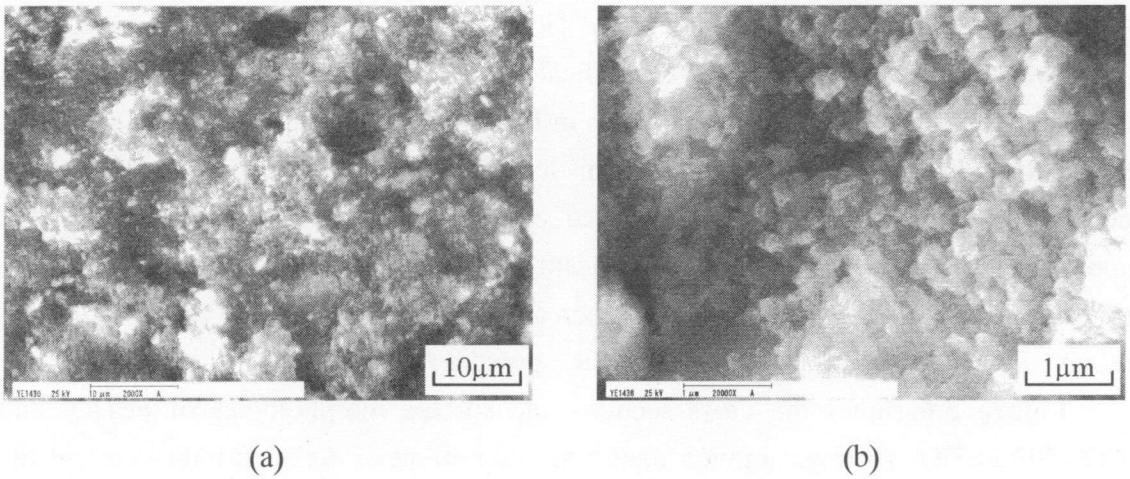

Fig.5.4. Surface morphologies of TiO_2-30%$FeTiO_3$ coating sprayed under the arc current of 400A ((a) low magnification, (b) high magnification.).

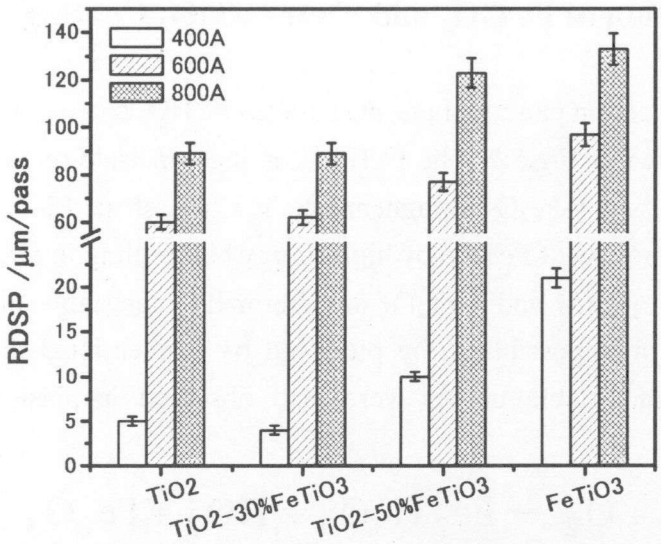

Fig.5.5. Relative deposition speed of TiO_2, TiO_2-30%$FeTiO_3$, TiO_2-50%$FeTiO_3$ and $FeTiO_3$ powder under the arc current of 400A, 600A and 800A.

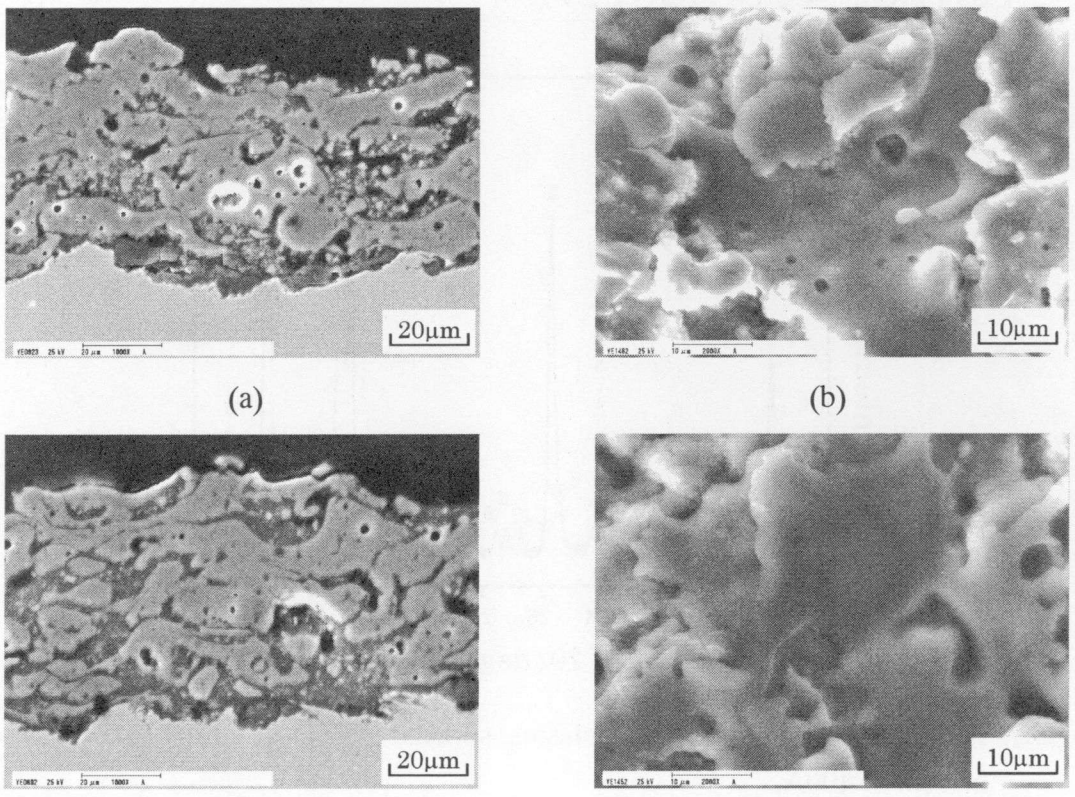

Fig.5.6. Cross sections and surface morphologies of $FeTiO_3$ (a, b) and TiO_2-50%$FeTiO_3$ (c, d) coatings under the arc current of 400A.

5.3.2. Composition of $FeTiO_3$ and TiO_2-$FeTiO_3$ Coatings

The x-ray diffraction pattern of plasma sprayed $FeTiO_3$ coating under the arc current of 400A is illustrated in **Fig.5.7.** The $FeTiO_3$ coating consisted of rutile TiO_2, $FeTiO_3$, Fe_2TiO_5, $Fe_2Ti_3O_9$ and γ-Fe_2O_3 (Maghemite). Y. Chen et al. [2–4] reported that the thermal oxidation process of $FeTiO_3$ by high energy ball milling in air consists Reactions (5.1)~(5.3). The $Fe_2Ti_3O_9$ and γ-Fe_2O_3 are thermally metastable products which are normally difficult or impossible to be produced by conventional thermal equilibrium processes. These metastable phases were also observed in plasma sprayed $FeTiO_3$ coatings.

$$4FeTiO_3 + O_2 \rightarrow Fe_2Ti_3O_9 + TiO_2 + Fe_2O_3 \quad (5.1)$$

$$Fe_2O_3 + TiO_2 \rightarrow Fe_2TiO_5 \quad (5.2)$$

$$Fe_2Ti_3O_9 \rightarrow Fe_2TiO_5 + 2TiO_2 \quad (5.3)$$

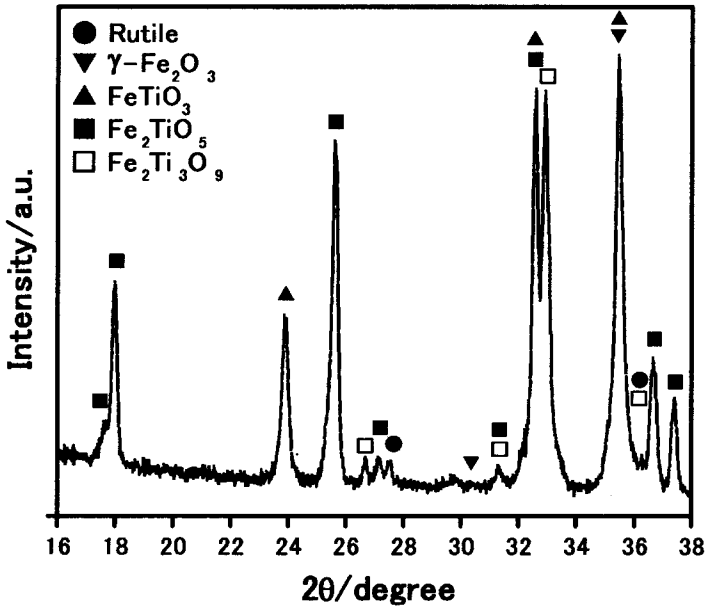

Fig.5.7. X-ray diffraction pattern of plasma sprayed $FeTiO_3$ coating under the arc current of 400A.

The TiO_2-30%$FeTiO_3$ coating under the arc current of 400A consisted of anatase TiO_2, rutile TiO_2 and $FeTiO_3$ as illustrated in **Fig.5.8.** Under the arc current of 400A, large part of anatase TiO_2 and $FeTiO_3$ still existed in it, and Fe_2TiO_5 and $Fe_2Ti_3O_9$ phase were

undetectable. With the increasing of arc current to 600A or 800A, Fe_2TiO_5, $Fe_2Ti_3O_9$ and Fe_2O_3 phases appeared in the sprayed coatings.

With the increase of the weight content of $FeTiO_3$ to 50% in the TiO_2-$FeTiO_3$ feedstock powder, $Fe_2Ti_3O_9$ and Fe_2TiO_5 phases appeared in spite of the low arc current of 400A as illustrated in **Fig.5.9**.

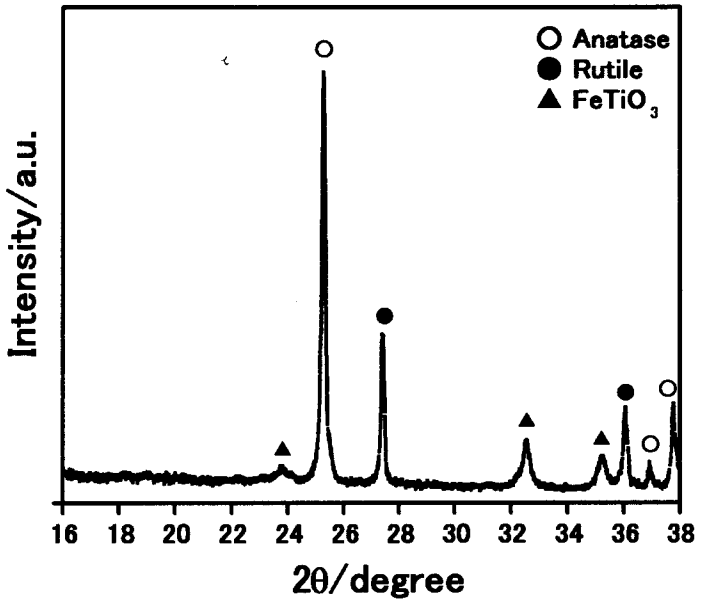

Fig.5.8. X-ray diffraction pattern of plasma sprayed TiO_2-30%$FeTiO_3$ coating under the arc current of 400A.

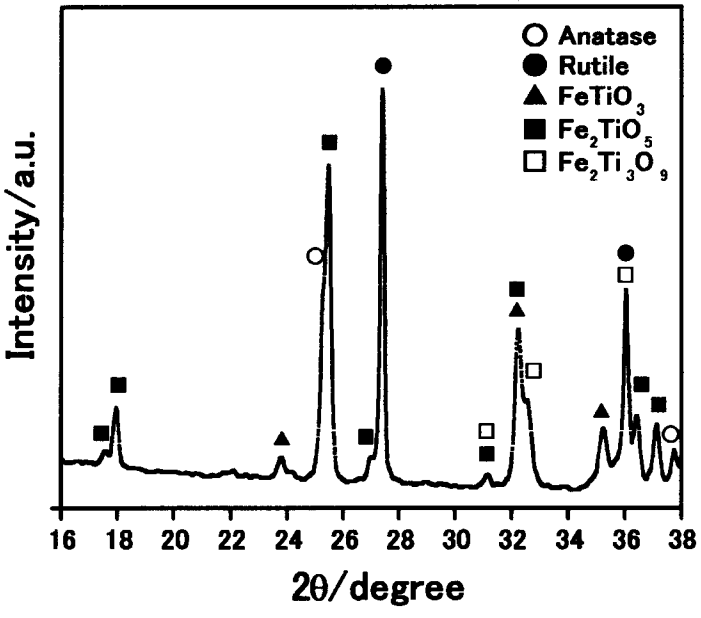

Fig.5.9. X-ray diffraction pattern of plasma sprayed TiO_2-50%$FeTiO_3$ coating under the arc current of 400A.

5.3.3. Photocatalytic Activity of $FeTiO_3$ and TiO_2-$FeTiO_3$ Coatings

Figure 5.10 illustrates the decomposition characteristics of the acetaldehyde by TiO_2, TiO_2-30%$FeTiO_3$ and $FeTiO_3$ feedstock powders.

Although $FeTiO_3$ can absorb visible light, the initiated electron may easily recombine with hole generated in $FeTiO_3$. Thus the pure $FeTiO_3$ powder did not show photocatalytic activity. The photocatalytic activity of TiO_2 powder was higher than that of TiO_2-30%$FeTiO_3$ powder. Because the TiO_2-30%$FeTiO_3$ powder was manufactured by agglomeration of TiO_2 particle with $FeTiO_3$ particle using polyvinyl alcohol (PVA) as binder, the TiO_2 was separated with $FeTiO_3$ particle by binder. Therefore, it is inferred that the initiated electron in the conduction band of TiO_2 can not inject to the conduction band of $FeTiO_3$, which resulted in the relative low photocatalytic activity of TiO_2-30%$FeTiO_3$ feedstock powder comparing with that of agglomerated TiO_2 powder. However, the PVA (C, H, O organic substance) have little influence on the properties of the sprayed coating, because PVA vaporizes over 550K and decomposes in plasma spraying processes.

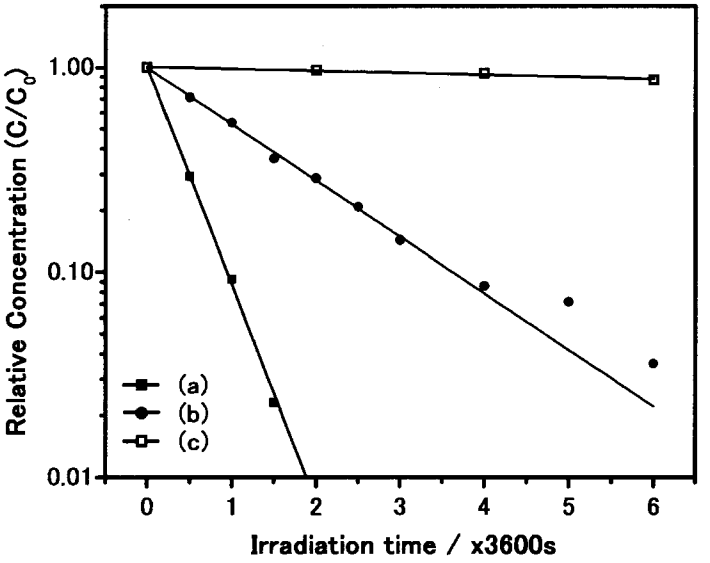

Fig.5.10. Decomposition characteristics of the acetaldehyde by agglomerated TiO_2 (a), TiO_2-30%$FeTiO_3$ (b), and $FeTiO_3$ (c) feedstock powders.

Figure 5.11 illustrates the decomposition characteristic of the acetaldehyde by plasma sprayed $FeTiO_3$ coating under the arc current of 400A. The τ values of the plasma sprayed $FeTiO_3$ coatings are shown in **Fig.5.12**. The results reveal that the $FeTiO_3$ coatings nearly had not photocatalytic activity.

The decomposition characteristics of the acetaldehyde by plasma sprayed TiO_2-30%$FeTiO_3$ and TiO_2-50%$FeTiO_3$ coatings are illustrated in **Fig.5.13**, and their τ values are shown in **Fig.5.14**. Because the TiO_2-30%$FeTiO_3$ coating sprayed under the arc current of 400A consisted of TiO_2 and $FeTiO_3$ only, and did not contain the unfavorable phase of Fe_2TiO_5 as discussed in Section 5.3.2 and large part of PVA combusted for the high temperature of plasma jet according to the EDAX analysis results, the photocatalytic activity was better than that of the other sprayed coatings.

As a result, the compositions of the sprayed coatings have great influence on the photocatalytic activity. Although pure $FeTiO_3$ compound has not photocatalytic property, the existence of $FeTiO_3$ could improve the photocatalytic activity of anatase TiO_2 if $FeTiO_3$ contacts coherently with TiO_2, which was explained using two-steps electron transfer model given in Chapter 4.

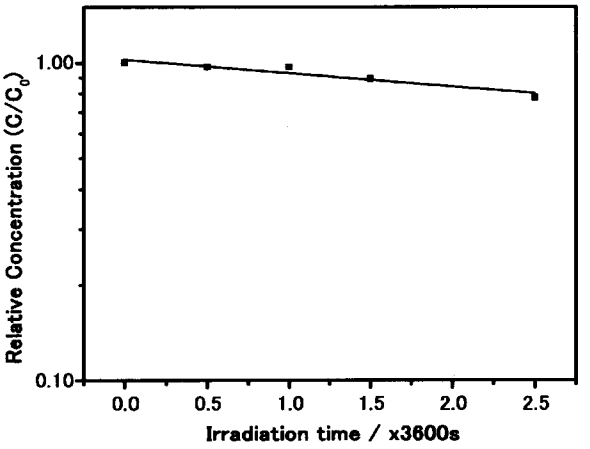

Fig.5.11. Decomposition characteristic of the acetaldehyde by $FeTiO_3$ coating sprayed under the arc current of 400A .

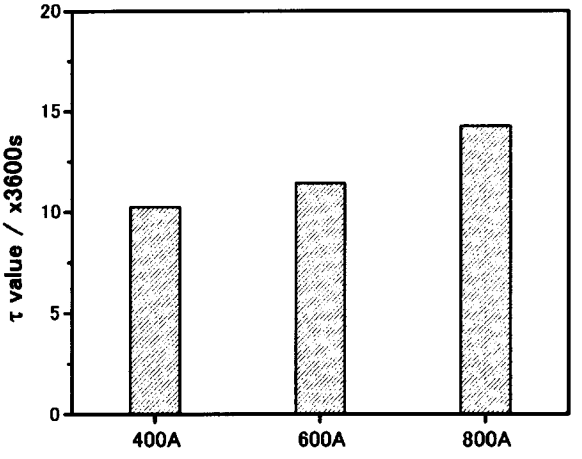

Fig.5.12. τ values of plasma sprayed $FeTiO_3$ coatings under the arc current of 400A, 600A and 800A.

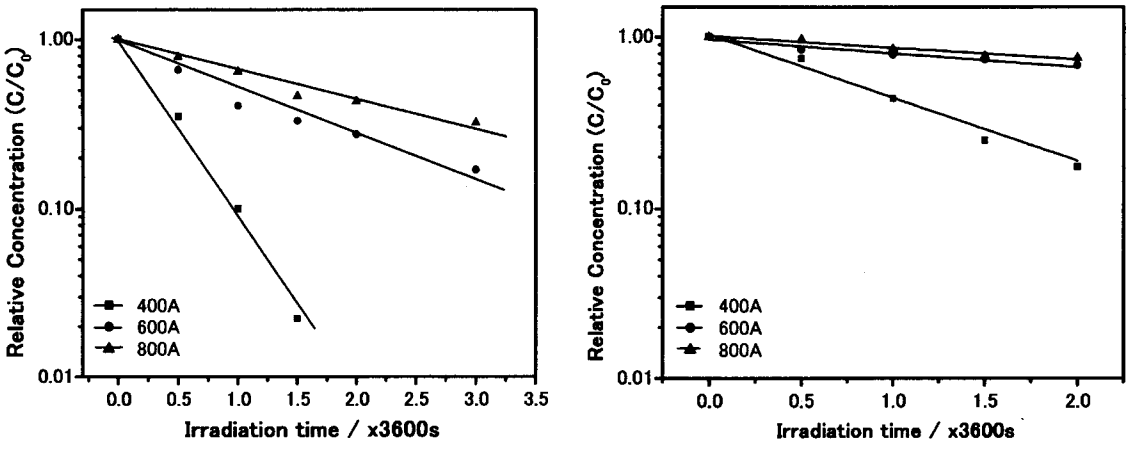

Fig.5.13. The decomposition characteristics of the acetaldehyde by the sprayed TiO_2-30%$FeTiO_3$ coatings (a) and TiO_2-50%$FeTiO_3$ coatings (b) under the arc current of 400A, 600A and 800A.

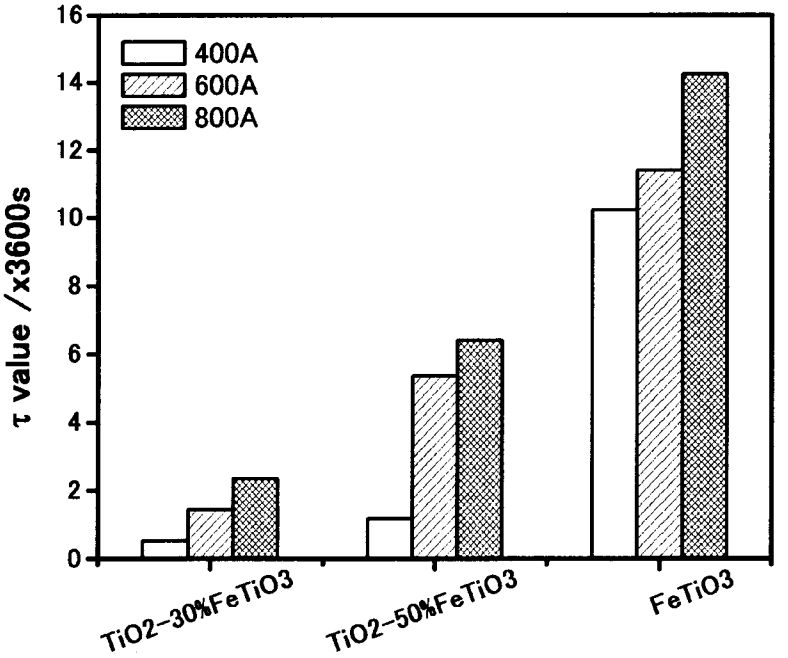

Fig.5.14. τ values of plasma sprayed $FeTiO_3$, TiO_2-30%$FeTiO_3$ and TiO_2-50%$FeTiO_3$ coatings under the arc current of 400A, 600A, 800A.

5.4. Conclusions

The composition and photocatalytic activity of plasma sprayed $FeTiO_3$, TiO_2-30%$FeTiO_3$ and TiO_2-50%$FeTiO_3$ coatings were investigated. The influence of $FeTiO_3$ compound on the photocatalytic activity of TiO_2 coating was clarified. The TiO_2-30%$FeTiO_3$ coating sprayed under the arc current of 400A had good photocatalytic activity because the coating did not contain the unfavorable Fe_2TiO_5 phase. However, the relative deposition speed of TiO_2-30%$FeTiO_3$ powder under the arc current of 400A, which was approximate to 4μm/pass, was very low. Although pure $FeTiO_3$ compound nearly did not show photocatalytic performance, the existence of $FeTiO_3$ could improve the photocatalytic activity of anatase TiO_2 if $FeTiO_3$ contacts coherently with TiO_2, which was explained using two-steps electron transfer model given in Chapter 4.

References

[1] W. Q. Guo, S. Malus, D. H. Ryan, and Z. Altounian, Crystal structure and cation distributions in the $FeTiO_3$-Fe_2TiO_5 solid solution series, *Journal of Physics Condensed Materials, Vol. 11 (1999) 6337-6347.*

[2] R. W. Taylor, Phase equilibria in the system FeO-Fe_2O_3-TiO_2 at 1573K, *The American Mineralogist, Vol. 49 (1964) 1016-1030.*

[3] Y. Ishikawa and S. Akimoto, Maganetic properties of the $FeTiO_3$-Fe_2O_3 solid solution series, *Journal of the Physical Society of Japan, Vol. 12(10) (1957) 1083-1098.*

[4] F. Zhou, S. Kotru, and R. K. Pandey, Pulsed laser-deposited ilmenite-hematite films for application in high-temperature electronics, *Thin Solid Films, Vol. 408 (2002) 33-36.*

[5] P. F. McMonald, A. Parasiris, R. K. Pandey, B. L. Gries, and W. P. Kirk, Paramagnetic resonance and susceptibility of ilmenite, $FeTiO_3$ crystal, *Journal of Applied Physics, Vol. 69 (2) (1991) 1104-1106.*

[6] Y. Ishikawa and S. Sawada, The study on substances having the ilmenite structure, physical properties of synthesized $FeTiO_3$ and $NiTiO_3$ ceramics, *Journal of Physical Society of Japan, Vol. 11(5) (1956) 496-835.*

[7] Y. Ishikawa and S. Akimoto, Magnetic property and crystal chemistry of ilmenite ($FeTiO_3$) and hematite (Fe_2O_3) system, crystal chemistry, *Journal of the Physical Society of Japan, Vol. 13(10) (1958) 1110-1118.*

[8] D. S. Ginley and M. A. Butler, The photoelectrolysis of water using iron titanate anodes, *Journal of Applied Physics, Vol. 48(5) (1977) 2019-2021.*

[9] Y. Chen, Low-temperature oxidation of ilmenite ($FeTiO_3$) induced by high energy ball milling at room temperature, *Journal of Alloys and Compound, Vol. 257 (1997) 156-160.*

[10] Y. Chen, Different oxidation reactions of ilmenite induced by high energy ball milling, *Journal of Alloys and Compound, Vol. 266 (1998) 150-154.*

CHAPTER 6

Photoelectrochemical Characteristics of TiO_2 and TiO_2-Fe_3O_4 Electrodes

6.1. Introduction

The radiant energy on the earth surface from the sun is 420 to 1260 J/m^2 [1]. Recently, electrochemical reactions on semiconductor electrodes have been investigated extensively. The "photo-sensitized electrolytic reaction" on an illuminated semi-conductor electrode is one of the most interesting features of semiconductor electrochemistry[2~5], and the idea of using multiple-band-gap cells in order to capture a greater fraction of the solar spectrum has motivated much work in the area of photovoltaic solar cells [2].

Photocatalysis by semiconductor is the result of the interaction of electrons and holes generated in an activated solid with the surrounding medium [6]. The activation behavior has similarity to that of Si solar cell. As discussed in Chapter 4, multiple-band-gap photocatalytic reaction cell formed in composite TiO_2-10%Fe_3O_4 coating. Moreover, $FeTiO_3$ is a kind of p-type semiconductor [7~9], and TiO_2 is a kind of n-type semiconductor [10, 11], thus solid p-n junction formation in the sprayed coating is possible in thermal spraying processes.

The formation of a plasma sprayed deposit is formed by a stream of molten droplets impacting on the substrate followed by flattening, rapid solidifying and cooling process. The individual molten (or half-molten) droplets spread to thin splat/lamellae, the stacking of which constitutes the deposit (**Fig.6.1**) [12, 13]. It is easy to deposit composite coatings by plasma spraying technique if the feedstock powders are composite materials. The composite substances may react with each other and then produce new compounds in plasma spraying processes; and the interface between two kinds of compounds is very large because the droplets spread to very thin lamellae (micron order). Therefore, the formation of microelectrochemical cell between two individual splats is reasonable. One splat is photo-anode and another is regarded as photo-cathode.

With respect to these suppositions, investigations on the photoelectrochemical characteristics of plasma sprayed TiO_2 and TiO_2-10%Fe_3O_4 electrodes were motivated.

The photocatalytic activity of TiO_2 and TiO_2-10%Fe_3O_4 coatings was evaluated. TiO_2-10%Fe_3O_4 splat was formed and its element distributions were analyzed. These results are presented in this chapter.

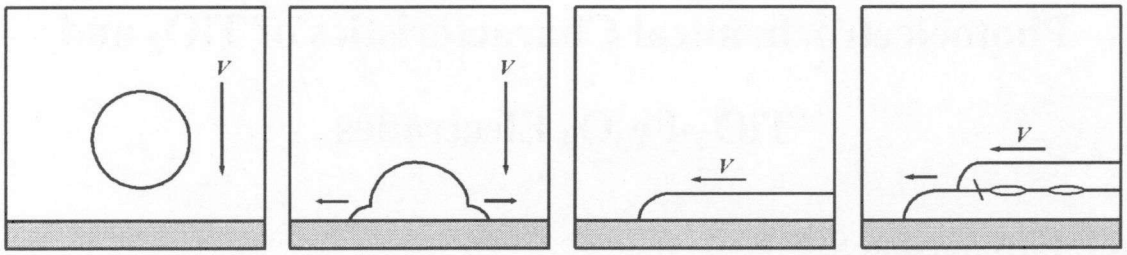

(a) (b) (c) (d)

Fig.6.1. Coating formation processes by thermal spraying. (a) Flying of melted particle, (b) Impacting of droplet, (c) Flattening of droplet, (d) Solidification and stacking of splat.

6.2. Materials and Experimental Procedures

6.2.1 Feedstock Powders and Substrates

The feedstock powders were agglomerated TiO_2 powder and TiO_2-10%Fe_3O_4 composite powder. The substrate for electrode or coating preparation was stainless steel (JIS SUS304). However, to analyze the Fe element distribution in the splat, the substrate for splat formation was copper, or else the Fe element from steel substrate will disturb the EDAX analysis.

6.2.2. Plasma Spraying Equipment

The thermal spraying equipment was a plasma spraying system (Plasmadyne-Mach1 manufactured by Plasmadyne Company). The thermal spraying parameters are given in **Table 6.1**.

Table 6.1 Plasma spraying parameters.

Argon gas pressure (MPa) /flow (slpm)	0.42/58
Helium gas pressure (MPa) /flow (slpm)	0.21/9
Arc current (A)	600
Arc voltage (V)	30
Spraying distance (mm)	70

6.2.3. Splat Preparation Set-up and Procedures

The schematic diagram of the set-up used for splat formation is shown in **Fig.6.2.** To get the individual splat, the diameter of the holes of mask was 1mm. The distance from plasma gun to the substrate was 70mm, which was the same with the spraying distance applied for coating or electrode preparation.

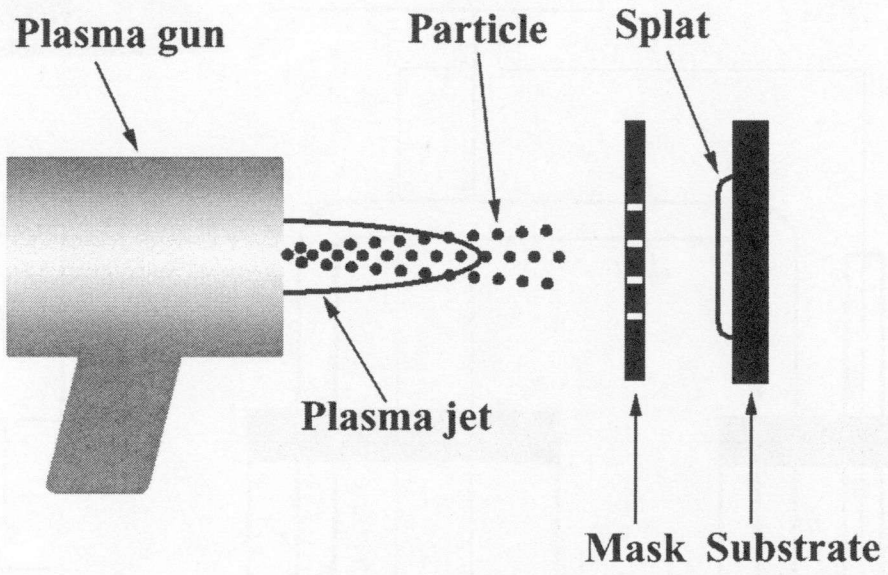

Fig.6.2. Individual splat formation set-up.

6.2.4. Photoelectrochemical Characteristics Measurement

The schematic diagram of photoelectrochemical characteristics evaluation apparatus is shown in **Fig.6.3.** The voltammetry was performed in a three electrodes glass cell at room temperature, in which a commercial saturated calomel electrode (SCE) was used as the reference electrode and a platinum plate (30×30mm) as the counter electrode. The electrolyte was 0.1N NaOH solution and deaerated by purging with Ar gas for 30 minutes before the experiments. The photocurrent against potential at each sprayed electrode (10×10mm) was measured using a scanning potentiostat and recorded by a personal computer through an AD converter (NR-110, KEYENCE company). The sweep speed of the potential was 2mV/s in every experiment except in the transient photocurrent measurement experiment. A 500W xenon lamp was used as light source and the light intensity was measured by a UV radiometer (UVR-2, TOPCON, Tokyo, Japan) with UD-40 detector.

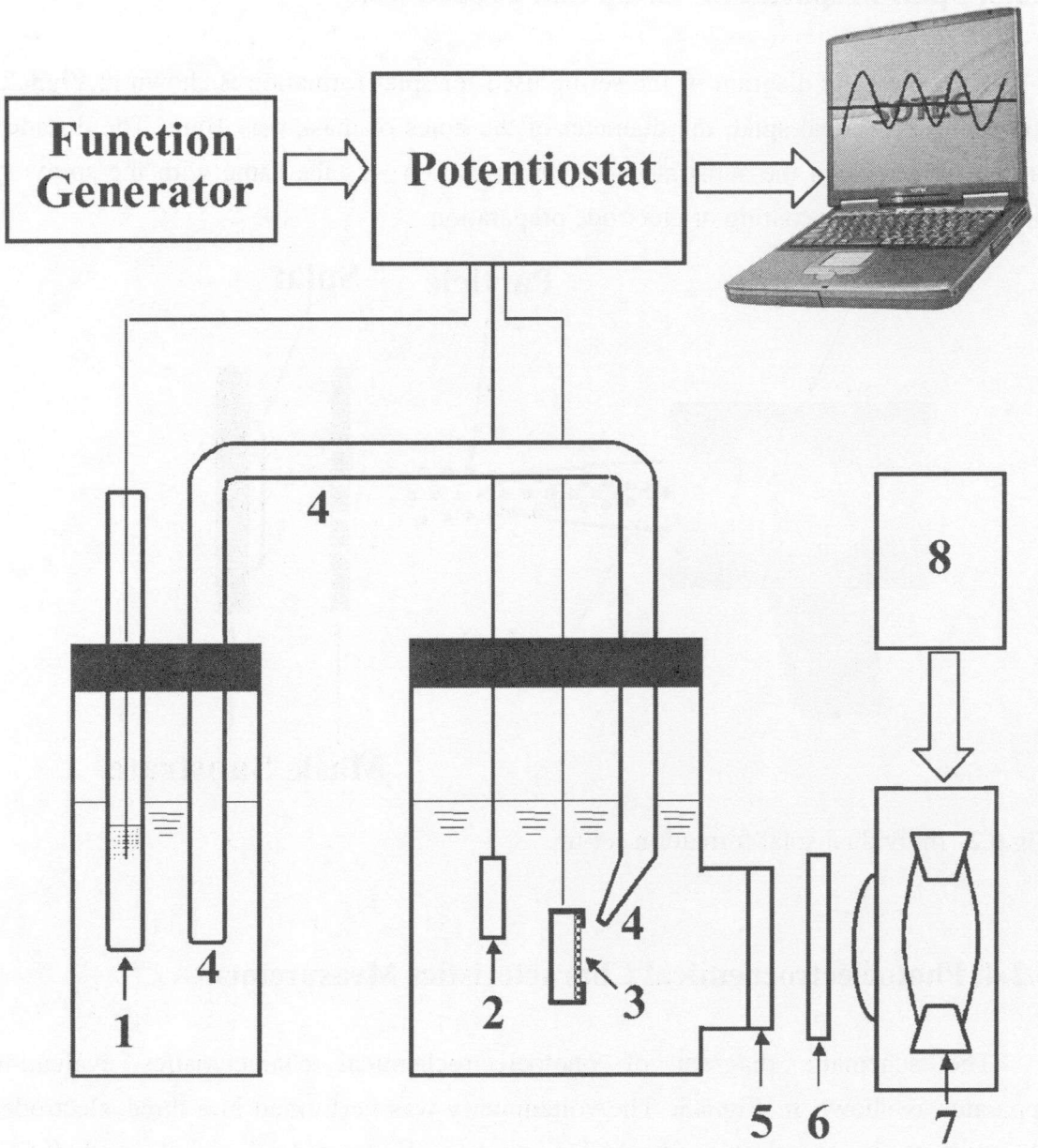

1. Saturated calomel electrode
2. Counter electrode
3. Working electrode
4. NaOH solution
5. Quartz window
6. Optical filter
7. Xe lamp
8. Power supply

Fig.6.3. Photoelectrochemical characteristics measurement set-up.

6.2.5. Photocatalytic Activity Evaluation Method

The photocatalytic activity of the sprayed coatings was evaluated through the degradation of acetaldehyde under 1mW/cm^2 ultraviolet light irradiation. The τ value was calculated by Equation (2.6). The details are given in Chapter 2.

6.2.6. General Characterization

The microstructure and phase characterization of the sprayed coatings and splat were performed by electron probe surface roughness analyzer, energy dispersive analysis of x-ray (ERA-8800FE, Elionix Co. Ltd., Japan) and x-ray diffraction (M03XHF, MAC Science Co. Ltd.).

6.3. Results and Discussion

6.3.1. Structure and Composition of TiO_2 and TiO_2-10%Fe_3O_4 Coatings

The surface morphologies and cross sections of TiO_2 and TiO_2-10%Fe_3O_4 coatings prepared by plasma spraying under the arc current of 600A are shown in **Fig.6.4**. In the figures, "U", "P" and "M" denote un-melted zone, partially melted zone and melted zone, respectively. The TiO_2 powders were not melted fully. The TiO_2 coatings were not very dense, contained many holes. Un-melted or partially melted TiO_2-10%Fe_3O_4 particles in the TiO_2-10%Fe_3O_4 coating were fewer than TiO_2 particles in TiO_2 coating. The reasons are given in Chapter 4 in detail. Because the electric resistance is a factor to affect the photocurrent, the coating thickness (for electrode preparation) was about the same. In this study, the thickness of the sprayed coating used for electrode was approximate to 70μm as confirmed from Fig.6.4(b) and (d).

The EDAX analysis results of TiO_2 and TiO_2-10%Fe_3O_4 coatings sprayed under the arc current of 600A are illustrated in **Fig.6.5**. The Fe/(Ti+Fe) ratio in the sprayed TiO_2-10%Fe_3O_4 coating equaled to 0.12, which was directly comparable to that of the feedstock powder.

The x-ray diffraction patterns of plasma sprayed TiO_2 and TiO_2-10%Fe_3O_4 coatings are shown in **Fig.6.6**. As shown in Fig.6.6(b), the sprayed TiO_2-10%Fe_3O_4 coating consisted of rutile phase, anatase phase and iron titanium oxide. Furthermore, the x-ray diffraction intensity of the anatase TiO_2 was very low, which evidenced the melting state of TiO_2-10%Fe_3O_4 feedstock powder too.

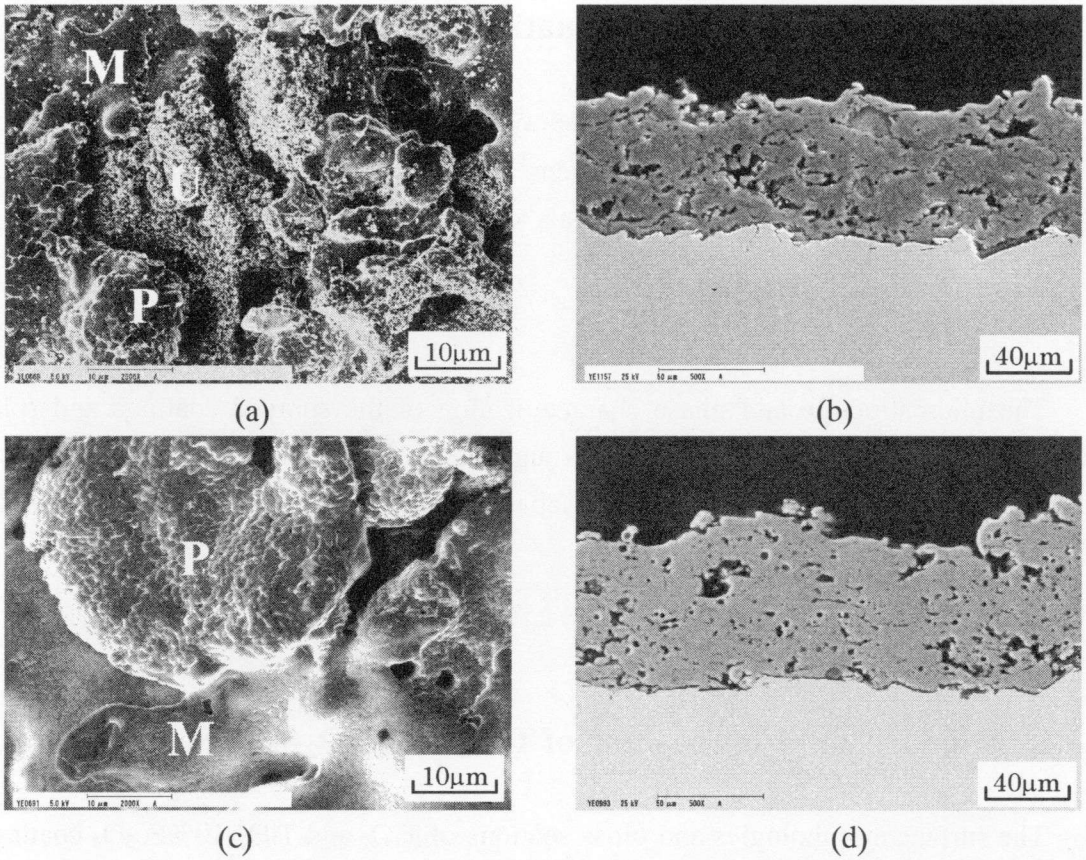

Fig.6.4. SEM views of coatings sprayed under 600A. (a) and (b) morphology and cross section of TiO_2 coating, respectively, (c) and (d) morphology and cross section of TiO_2-10%Fe_3O_4 coating, respectively. (Notes: "U", "P" and "M" denote un-melted zone, partially melted zone and melted zone, respectively.)

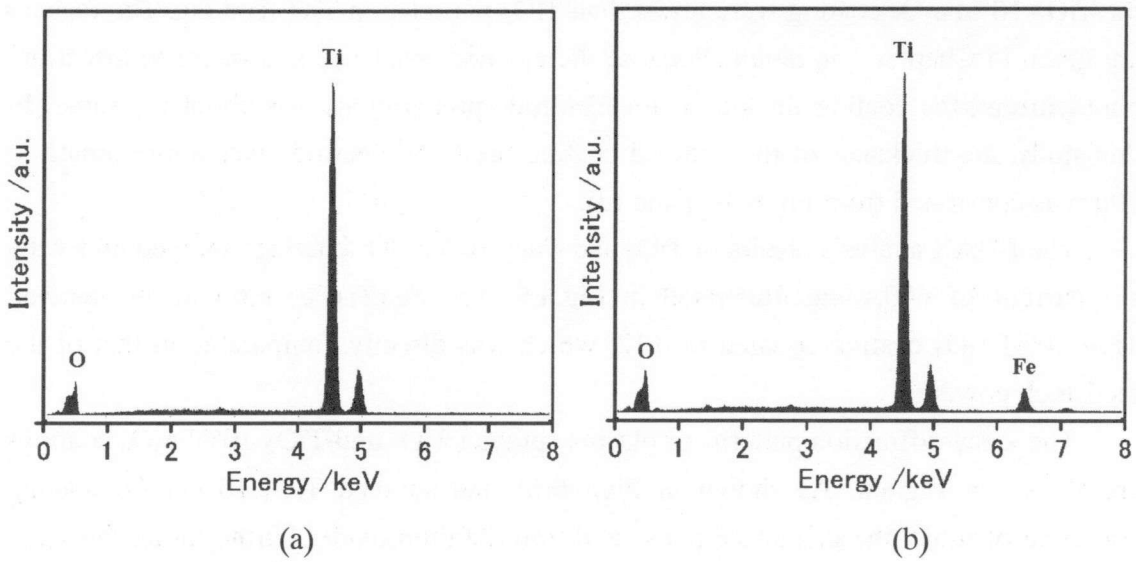

Fig.6.5. EDAX analysis results of TiO_2 (a) and TiO_2-10%Fe_3O_4 (b) coatings plasma sprayed under the arc current of 600A.

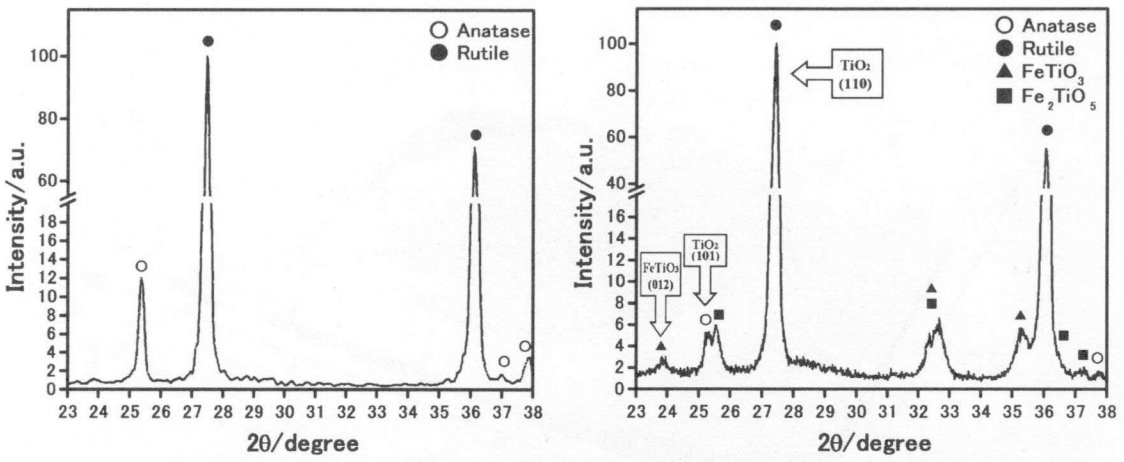

(a) (b)

Fig.6.6. X-ray diffraction patterns of plasma sprayed TiO_2 (a) and TiO_2-10%Fe_3O_4 (b) coatings.

6.3.2. Characterization Results of TiO_2-10%Fe_3O_4 Splat

Figure 6.7 shows the plane view, 3-D view of TiO_2-Fe_3O_4 splat, and Ti, Fe elements distribution of line A illustrated in plane view. The thickness of splat was not over 1μm. The circumference was thicker than the center district, which may result from the high impacting speed of the particle on the substrate. The Ti and Fe elements distributed uniformly as illustrated in Fig.6.7(c). The Fe/(Fe+Ti) ratio in the TiO_2-Fe_3O_4 splat was approximates to 0.12, which is in good agreement with the amount of the feedstock powder and sprayed coating.

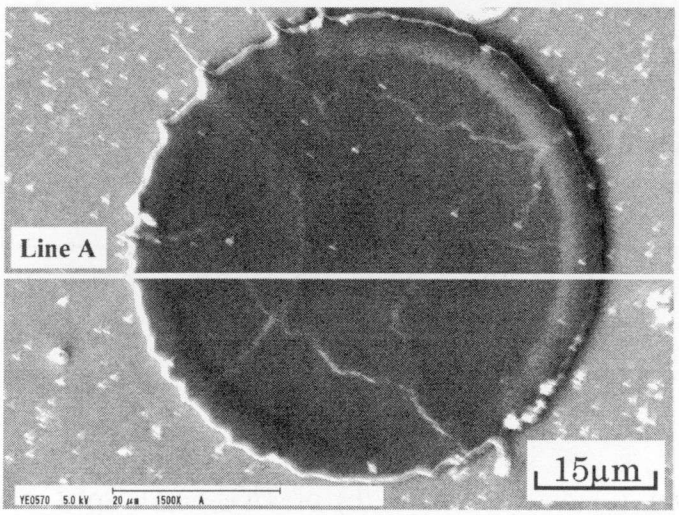

(a)

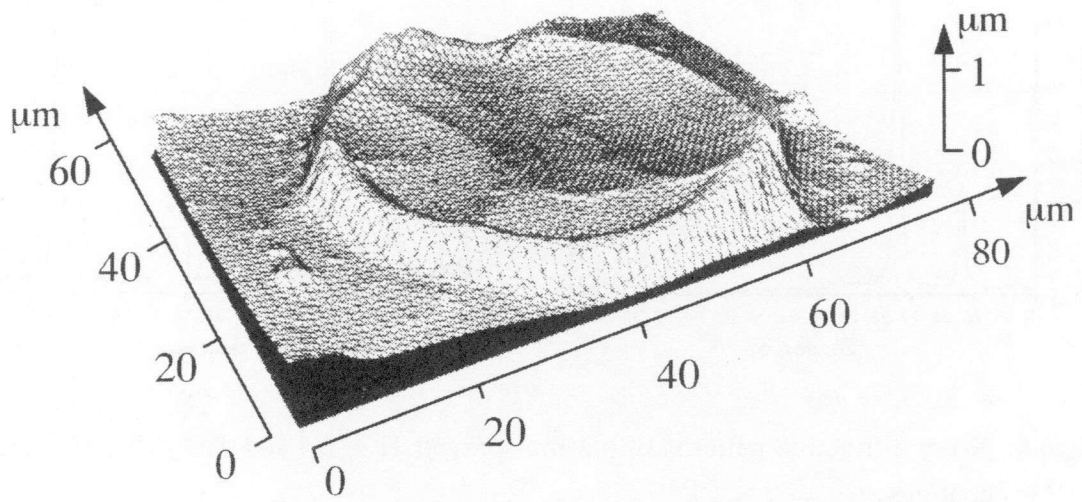

(b)

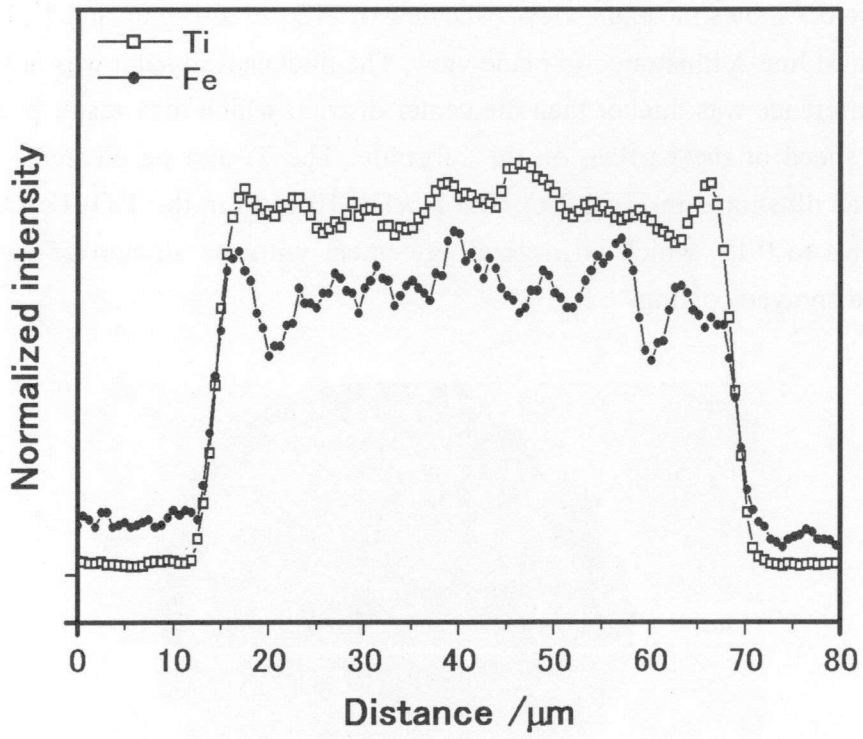

(c)

Fig.6.7. Plane view (a) and 3-D view (b) of TiO_2-Fe_3O_4 splat, and Ti, Fe element distributions (c) of line A illustrated in plane view.

6.3.3. Photocatalytic Activity of TiO_2 and TiO_2-10%Fe_3O_4 Coatings

The photocatalytic decomposition characteristics of acetaldehyde by prepared TiO_2 and TiO_2-10%Fe_3O_4 coatings are illustrated in **Fig.6.8.** The photocatalytic degradation efficiency (reciprocal of τ value) of TiO_2-10%Fe_3O_4 coating was approximately two times than that of TiO_2 coating as shown in **Fig.6.9**. The good photocatalytic activity of TiO_2-10%Fe_3O_4 coating resulted possibly from the good light absorbance and the good electron transfer character of the coating. With respect to electron transfer action, the details are given in Chapter 4. When the TiO_2-10%Fe_3O_4 coating is irradiated, the electron possibly transfers (moves) to conduction band in two steps. First step: the electron is initiated from the valence band to the conduction band of TiO_2, and second step: the electron in the conduction band of TiO_2 injects to the conduction band of $FeTiO_3$. For this two-steps electron transfer mechanism, the lifetime of initiated electron-hole pair becomes longer.

Another reason for the good photocatalytic activity of TiO_2-10%Fe_3O_4 coating is given in Section 6.3.5.

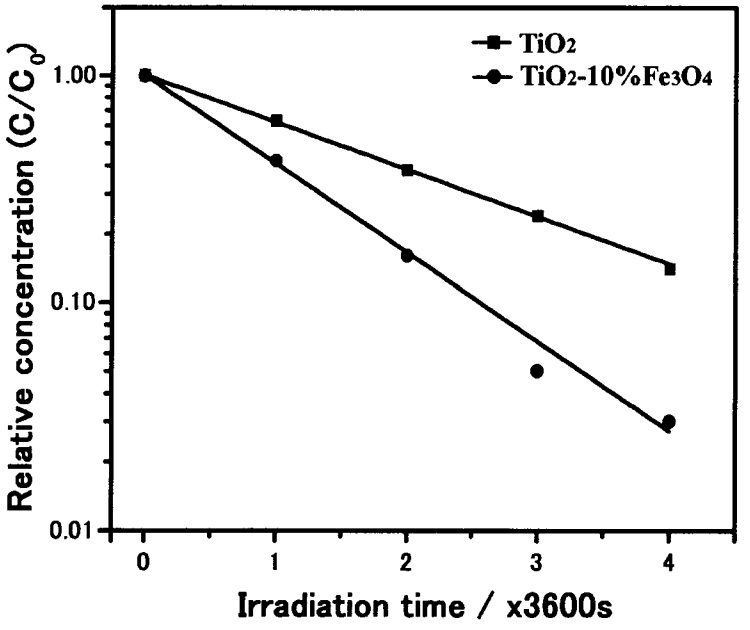

Fig.6.8. Photocatalytic decomposition characteristics of the acetaldehyde by the TiO_2 and TiO_2-10%Fe_3O_4 coatings sprayed under the arc current of 600A and spraying distance of 70mm.

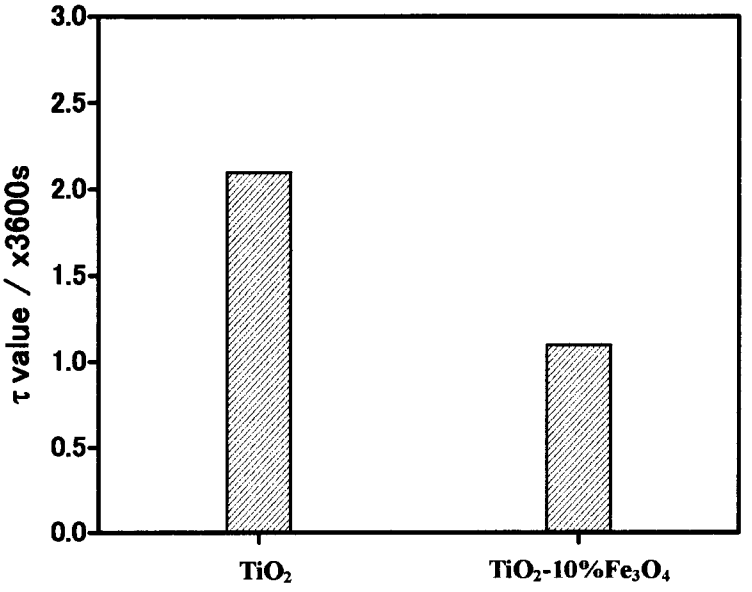

Fig.6.9. τ values of TiO_2 and TiO_2-10%Fe_3O_4 coatings sprayed under the arc current of 600A and spraying distance of 70mm.

6.3.4. Photoelectrochemical Characteristics of TiO_2 and TiO_2-10%Fe_3O_4 Electrodes

The use of n-type wide-bandgap semiconductor (SC) as photo-electrode in photoelectrochemical cells has been widely developed since A. Fujishima and K. Honda reported in 1972 that water could be photo-electrolyzed at an n-TiO_2 electrode illuminated with UV light. It is well established that water photoelectrolysis in a photoelectrochemical cell (PEC) is the result of two processes. Firstly, photos are absorbed by the SC and generate electron-hole pairs. Secondly, those pairs are separated by the electrostatic field, the electrons migrating toward the bulk and the holes toward the surface. The study of the transient photocurrent-time behaviour, frequently observed with semiconductor electrodes in a PEC, has been used by different authors as an interesting tool for the analysis of the mechanisms of charge at the SC/electrolyte interface [14]. **Fig.6.10** shows a typical photocurrent-time profile of TiO_2 electrode with hand-chopped light. An anodic photocurrent spike appeared immediately after the light was turned on, and then decreased continuously with time until a steady state photocurrent reached. When the light was turned off, the photocurrent decreased quickly down to zero. The initial anodic photocurrent spike was due to instantaneous photo-induced electron transitions to the conduction band as discussed by P. Salvador et

al. [14] and C. Liu et al. [15]. This kind of phenomenon was also observed for single crystal TiO_2 and polycrystalline TiO_2 [14–16].

Figure 6.11 illustrates the photocurrent-potential curves with and without light irradiation of the TiO_2 electrode prepared under arc current of 600A. The photocurrent increased obviously from the applied potential of –0.6V to –0.3V, and then increased slightly till to 0.4V, and finally broke. The photo-response characteristic of the sprayed electrode was comparable to that of single crystal TiO_2, but the breakdown voltage was approximately 0.5V (vs. SCE), which is similar to the plasma sprayed electrode prepared by R. Wang [17]. The short-circuit current (Jsc) of TiO_2 electrode was 1.05mA/cm^2 under 30mW/cm^2 light illumination from xenon lamp, and it increased linearly with the light intensity as shown in **Fig.6.12**. It implied that the light absorption coefficient (α) was very small.

Figure 6.13 illustrates the photocurrent-potential curves with and without light irradiation of the TiO_2-10%Fe_3O_4 electrode prepared under arc current of 600A. The photocurrent increased slightly from the applied potential of –0.6V to 0.4V, and then broke over 0.5V. The short-circuit current (Jsc) of TiO_2-10%Fe_3O_4 electrode was 0.07mA/cm^2 under 30mW/cm^2 light illumination from xenon lamp, which was notably lower than that of TiO_2 electrode. However, the bubbles (came from water photolysis) formation speed from TiO_2-10%Fe_3O_4 electrode was obviously higher than that from the latter.

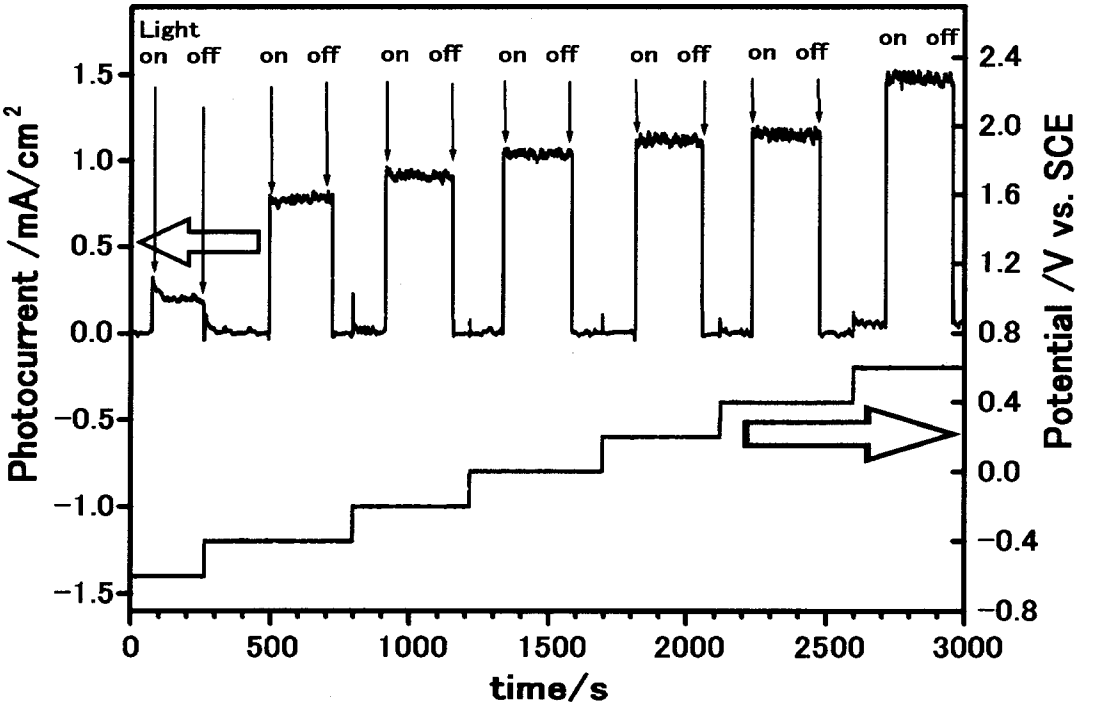

Fig.6.10. Typical photocurrent-time profile of TiO_2 electrode with hand-chopped light.

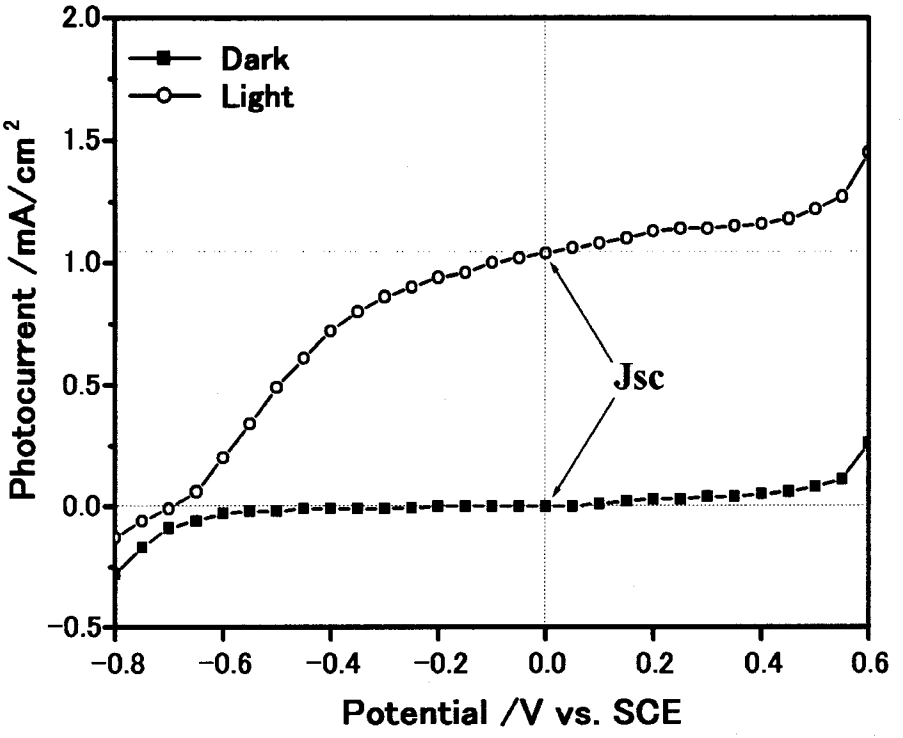

Fig.6.11. Photocurrent-potential curves with and without light irradiation of the TiO_2 electrode prepared under arc current of 600A.

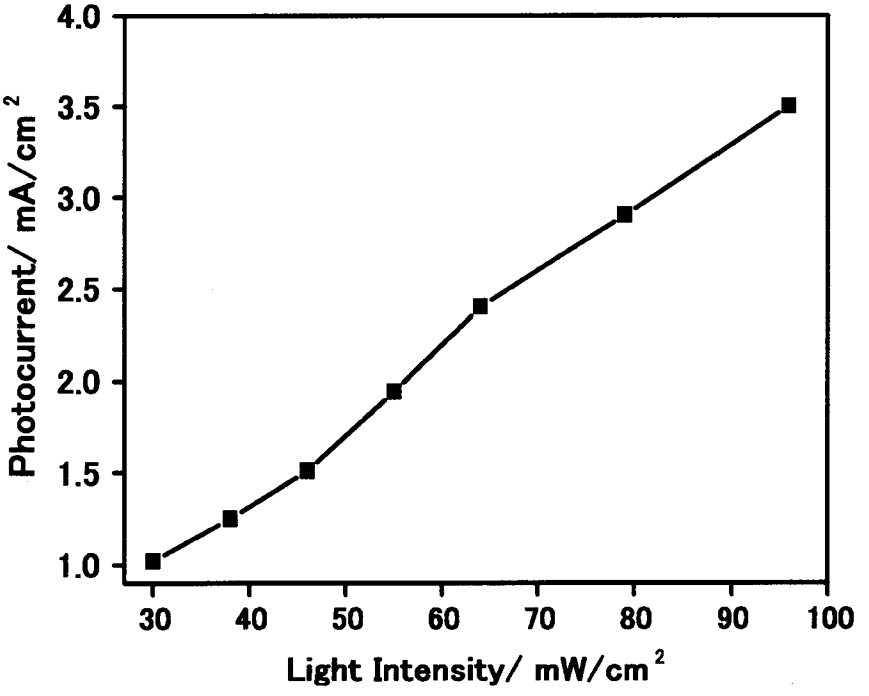

Fig.6.12. Relation between short-circuit photocurrent and light intensity of TiO_2 electrode.

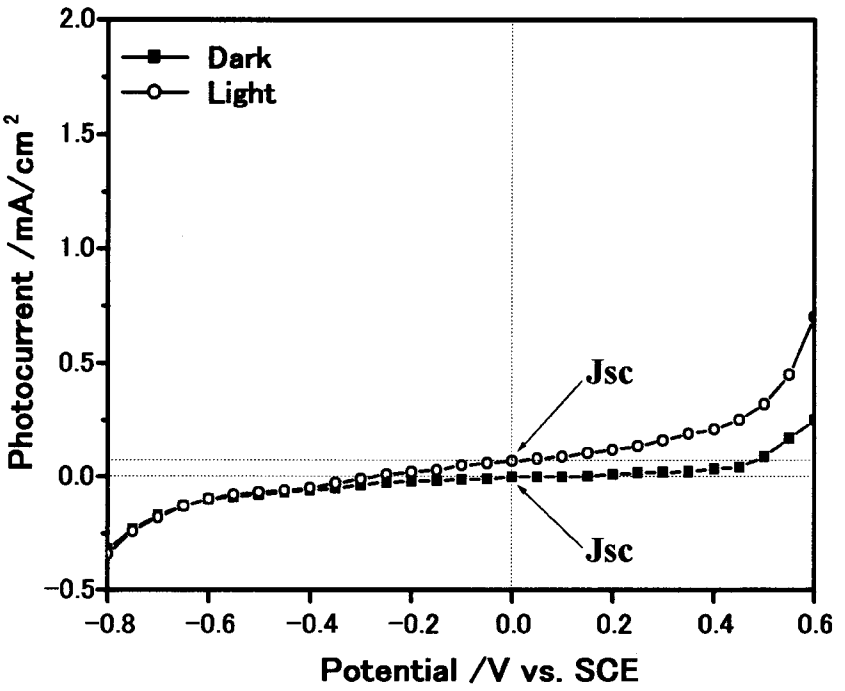

Fig.6.13. Photocurrent-potential curves with and without light irradiation of TiO_2-10% Fe_3O_4 electrode prepared under arc current of 600A.

6.3.5. P-N Junction Formation Model

According to the x-ray diffraction pattern, the n-type TiO_2 semiconductor particle reacted with Fe_2O_3 or Fe_3O_4 particle and concurrently produced p-type $FeTiO_3$ in the TiO_2-10%Fe_3O_4 coating, thus solid p-n junction formation in the sprayed coating is possible in thermal spraying process.

The bubbles (came from water photolysis) formation speed from TiO_2-10%Fe_3O_4 electrode was higher than that from TiO_2 electrode. Furthermore, H_2 and O_2 generation coincided on TiO_2-10%Fe_3O_4 electrode. Moreover, the short-circuit current (Jsc) of TiO_2-10%Fe_3O_4 electrode was notably lower. These facts implied that the $FeTiO_3$/TiO_2 island acted as micro-photoelectrolysis cell in a short circuit configuration in TiO_2-10%Fe_3O_4 coating. Therefore, the existence of solid p-n junction between p-type $FeTiO_3$ and n-type TiO_2 was confirmed.

According to the above mentioned results and the special particle flattening phenomenon in plasma spraying process, a p-n junction formation model in plasma sprayed TiO_2-10%Fe_3O_4 coating is illustrated in **Fig.6.14(a)**. In fact, an agglomerated

TiO_2-10%Fe_3O_4 powder contains many micro TiO_2 particles with average diameter of 0.2μm, therefore, it is reasonable that one small splat flattened from primary TiO_2 particle may generate a micro p-n junction with $FeTiO_3$, and then it is inferred that a TiO_2-10%Fe_3O_4 splat shown in Fig.6.7(a) comprised a lot of micro p-n junctions. **Fig.6.14(b)** shows the schematic diagram of electron-hole separation process in a p-n junction. The micro-TiO_2 and $FeTiO_3$ constituted innumerable micro-cell.

For the formation of micro p-n junction, which may spatially separate the photo generated electrons and holes as like Si solar cell, the photocatalytic activity of TiO_2-10%Fe_3O_4 coating was improved significantly as shown in Fig.6.8. Therefore, it is concluded that plasma spraying is a promising technique to deposit high performance photocatalytic coating for its special advantage.

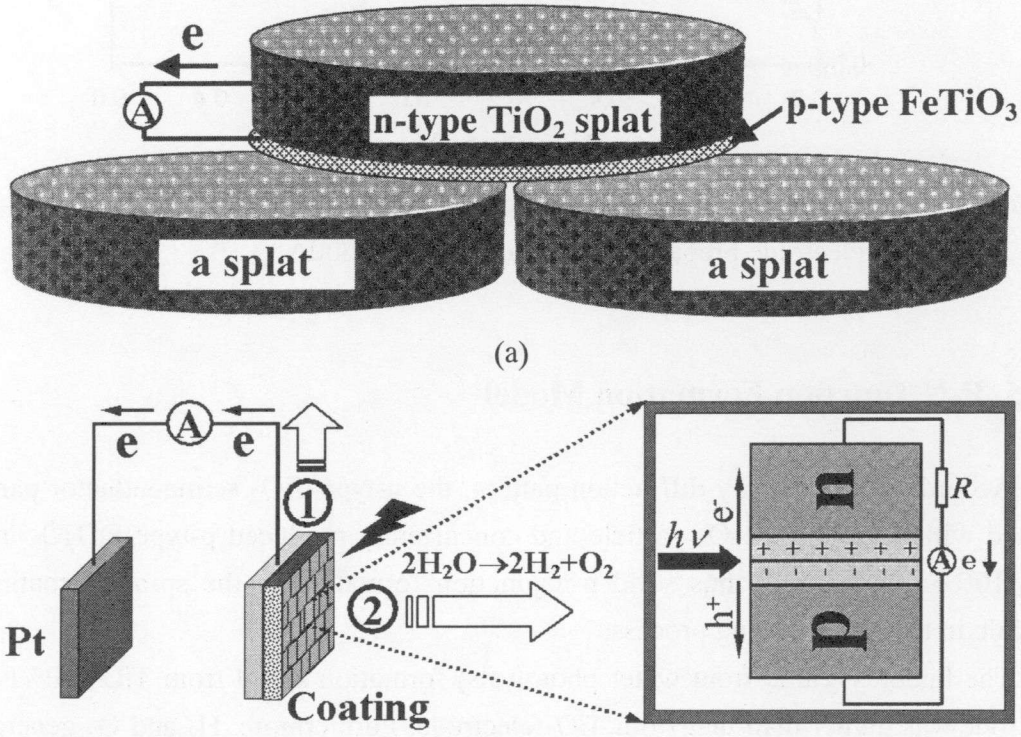

Fig.6.14. A proposed p-n junction formation model in TiO_2-10%Fe_3O_4 coating (a) and schematic diagram of electron-hole separation process in p-n junction (b).

6.4. Conclusions

Photoelectrochemical characteristics of plasma sprayed TiO_2 and TiO_2-10%Fe_3O_4

electrodes were investigated. The photo-response of the sprayed TiO_2 electrode was comparable to that of single crystal TiO_2, but the breakdown voltage was approximate to 0.5V (vs. SCE). The short-circuit current of TiO_2 electrode was 1.05mA/cm^2, which was 15 times than that of TiO_2-10%Fe_3O_4 electrode under 30mW/cm^2 light illumination from xenon lamp. $FeTiO_3$ compound obviously improved the photocatalytic activity of the TiO_2 coating for the formation of p-n junction, which may spatially separate the photo-generated electrons and holes. From these investigations, it is concluded that plasma spraying is a promising technique for manufacturing high performance photocatalytic coating.

References

[1] K. H. Yoon and S. O. Yoon, Photoeffects in polycrystalline TiO_2 electrodes, *Japanese Journal of Applied Physics, Vol. 23(8) (1984) 1137-1140.*

[2] D. A. Tryk, A. Fujishima, and K. Honda, Recent topics in photoelectrochemistry: achievements and future prospects, *Electrochimica Acta, Vol. 45 (2003) 2363-2376.*

[3] A. Mills and S. L. Hunte, An overview of semiconductor photocatalysis, *Journal of Photochemistry and Photobiology A: Chemistry, Vol. 108 (1997) 1-35.*

[4] K. Pirkanniemi and M. Silanpaa, Heterogeneous water phase catalysis as an environmental application: a review, *Chemosphere, Vol. 48 (2002) 1047-1060.*

[5] J. Zhao and X. D. Yang, Photocatalytic oxidation for indoor air purification: a literature review, *Building and Environment, Vol. 38 (2003) 645-654.*

[6] O. M. Alfano, D. Bahnemann, A. E. Cassano, R. Dillert, and R. Goslich, Photocatalysis in water environments using artificial and solar light, *Catalysis Today, Vol. 58 (2000) 199-230.*

[7] Y. Ishikawa and S. Sawada, The study on substances having the ilmenite structure, physical properties of synthesized $FeTiO_3$ and $NiTiO_3$ ceramics, *Journal of Physical Society of Japan, Vol. 11(5) (1956) 496-835.*

[8] Y. Ishikawa and S. Akimoto, Magnetic property and crystal chemistry of ilmenite($FeTiO_3$) and hematite (Fe_2O_3) system, crystal chemistry, *Journal of the Physical Society of Japan, Vol. 13(10) (1958) 1110-1118.*

[9] P. F. McMonald, A. Parasiris, R. K. Pandey, B. L. Gries, and W. P. Kirk, Paramagnetic resonance and susceptibility of ilmenite, $FeTiO_3$ crystal, *Journal of Applied Physics, Vol. 69 (2) (1991) 1104-1106.*

[10] Y. Nakato, H. Akanuma, J. Shimizu, and Y. Magari, Photo-oxidation reaction of water on an n-TiO_2 electrode: Improvement in efficiency through formation of surface micropores by photo-etching in H_2SO_4, *Journal of Electroanalytical Chemistry, Vol. 396(1-2) (1995) 35-39.*

[11] L. Y. Su and Z. H. Lu, Photochromic and photocatalytic behaviors on immobilized TiO_2 particulate films, *Journal of Photochemistry and Photobiology A: Chemistry, Vol. 107 (1997) 245-248.*

[12] C. J. Li and A. Ohmori, Relationships between the microstructure and properties of thermally sprayed deposits, *Journal of Thermal Spray Technology, Vol. 11(3) (2002) 365-374.*

[13] Y. Arata, A. Ohmori, and C. J. Li, Electrochemical method to evaluate the connected porosity in ceramic coatings, *Thin Solid Films, Vol. 156(2) (1988) 315-326.*

[14] P. Salvador, Subbandgap photoresponse of n-TiO_2 electrodes: transient photocurrent-time behavior, *Surface Science, Vol. 192 (1987) 36-46.*

[15] C. Liu, Y. Chen, and W. Li, Direct observation of elementary steps in charge transfer mediated by surface states on TiO_2 electrode under illumination, *Surface Science, Vol. 163 (1985) 383-390.*

[16] R. H. Wilson, Observation and analysis of surface states on TiO_2 electrodes aqueous electrolytes, *Journal of the Electrochemical Society, Vol. 127 (1980) 228-233.*

[17] R. Wang and C. H. Henager Jr., Arc-plasma-sprayed rutile anodes for photoelectrolysis of water, *Journal of the Electrochemical Society, Vol. 126(1) (1979) 83-85.*

CHAPTER 7

Summary

In this dissertation, TiO_2 and composite TiO_2 coatings were deposited on stainless steel by plasma spraying technique. The microstructure, phase composition, photo absorbance and photocatalytic activity of sprayed coatings were investigated systematically. The photoelectrochemical characteristics of TiO_2 and TiO_2-10%Fe_3O_4 electrodes were studied in detail. Two-steps electron transfer model and p-n junction formation model were proposed. The content of each chapter is summarized as follows:

In **Chapter 1**, fundamental and general aspects of heterogeneous photocatalysis were briefly introduced after the emphasis of the importance of sustainable development. An overview of TiO_2 photocatalyst and the recent topics in photoelectrochemistry were described. The necessity for coating photocatalyst and the advantage of plasma spraying technique were given.

In **Chapter 2**, TiO_2 coatings were prepared by plasma spraying technique using agglomerated anatase TiO_2 powder. The content of anatase TiO_2 in the sprayed coatings was approximate to 7-15%. The anatase to rutile phase transformation temperature of agglomerated anatase TiO_2 powder was about 1173K. TiO_2 coating sprayed under the arc current of 400A had good photocatalytic activity for the relative high content of anatase phase in it. However, the relative deposition speed of powder, which was approximate to 5μm/pass, was very low. For the high temperature of plasma jet, it is not easy to fabricate high performance photocatalytic coatings by plasma spray using the pure anatase TiO_2 powder applying the technique of inhibiting anatase phase transformation.

In **Chapter 3**, phase composition, microstructure and photocatalytic activity of plasma sprayed TiO_2-10%Fe_3O_4, TiO_2-10%Al_2O_3, and TiO_2-10%Y_2O_3 composite coatings were characterized and discussed in detail. The addition of Fe_3O_4 to TiO_2 improved the anatase-rutile transformation. The anatase content of TiO_2 in the sprayed coating was affected by the melting degree of TiO_2 particle in thermal spraying process. Although the content of anatase TiO_2 was very low in the sprayed TiO_2-10%Fe_3O_4 coating, the photocatalytic activity was better than that of TiO_2 coating under the same spraying conditions, which implied the photocatalytic activity was not only controlled by anatase content of TiO_2. The relative deposition speed of TiO_2-10%Fe_3O_4 powder was 2.6 times comparing with that of TiO_2 powder under the arc current of 400A and

spraying distance of 70mm. However, the addition of Al_2O_3 and Y_2O_3 particle to TiO_2 particle had not favorable effect on the photocatalytic activity of TiO_2 coating. Therefore, the influence of additive on the photocatalytic activity of TiO_2 is greatly controlled by not only the kind of additive, but also by the synthetic process.

In **Chapter 4**, the influence of Fe_3O_4 content on the properties of TiO_2 coating was investigated. The results showed that the TiO_2-Fe_3O_4 coatings consisted of anatase TiO_2, rutile TiO_2, and pseudobrookite Fe_2TiO_5 phase which appeared when the content of Fe_3O_4 additive was equal to or over 10%. With relative low amount addition of Fe_3O_4, ilmenite $FeTiO_3$ phase existed in the sprayed coatings. The content of anatase TiO_2 in the sprayed coatings decreased with the increasing of Fe_3O_4 content. The photocatalytic activity was improved with an increase of $FeTiO_3$ content in the coating, which was explained by the good photo absorbance capacity and by two-steps electron transfer model. Moreover, initiated electrons could separate with holes easily because Fe^{2+} can be regarded as a trap of initiated electrons. However, the presence of large amount of Fe_2TiO_5 compound substantially reduced the photocatalytic efficiency of the sprayed TiO_2-Fe_3O_4 coatings for the unfavorable electron-hole transfer process.

In **Chapter 5**, the composition and photocatalytic activity of plasma sprayed $FeTiO_3$, TiO_2-30%$FeTiO_3$ and TiO_2-50%$FeTiO_3$ coatings were investigated. The influence of $FeTiO_3$ compound on the photocatalytic activity of TiO_2 coating was clarified. The TiO_2-30%$FeTiO_3$ coating sprayed under the arc current of 400A had good photocatalytic activity because the coating did not contain the unfavorable Fe_2TiO_5 phase. However, the relative deposition speed of TiO_2-30%$FeTiO_3$ powder under arc current of 400A, which was approximate to 4μm/pass, was very low. Although pure $FeTiO_3$ compound nearly did not show photocatalytic performance, the existence of $FeTiO_3$ phase would improve the photocatalytic activity of anatase TiO_2 if $FeTiO_3$ contacts coherently with TiO_2.

In **Chapter 6**, photoelectrochemical characteristics of plasma sprayed TiO_2 and TiO_2-10%Fe_3O_4 electrodes were examined. The photo-response of the sprayed TiO_2 electrode was comparable to that of single crystal TiO_2, but the breakdown voltage was approximate to 0.5V (vs. SCE). The short-circuit current of TiO_2 electrode was 1.05mA/cm^2, which was 15 times than that of TiO_2-10%Fe_3O_4 electrode under 30mW/cm^2 light illumination from xenon lamp. $FeTiO_3$ compound obviously improved the photocatalytic activity of the TiO_2 coating for the formation of p-n junction, which may spatially separate the photo-generated electrons and holes. From these investigations, it is concluded that plasma spraying is a promising technique for manufacturing high performance photocatalytic coating.

In **Chapter 7**, it gives a summary of whole dissertation.

Publication Lists

• Main Papers

[1] F. -X. Ye, A. Ohmori and C. -J. Li, Formation of p-n junction by plasma spraying technique to enhance the photocatalytic activity of TiO_2, ***Journal of Materials Science Letters,(2003) (In press).***

[2] F. -X. Ye, A. Ohmori and C. -J. Li, New approach to enhance the photocatalytic activity of plasma sprayed TiO_2 coating using p-n junctions, ***Surface and Coatings Technology, (2003) (In press).***

[3] F. -X. Ye and A. Ohmori, The influence of $FeTiO_3$ formation on the photocatalytic property of plasma sprayed TiO_2 coatings, ***Journal of High Temperature Society, Vol. 29(4) (2003) 160-163.***

[4] F. -X. Ye and A. Ohmori, Fabrication of advanced photocatalytic TiO_2 coatings by thermal spraying technique, ***Thermal Spraying Technique, Vol. 23(1) (2003) 45-51 (In Japanese).***

[5] F. -X. Ye and A. Ohmori, The photocatalytic activity and photo-absorption of plasma sprayed TiO_2-Fe_3O_4 binary oxide coatings, ***Surface and Coatings Technology, Vol.160 (2002) 62-67.***

[6] F. -X. Ye and A. Ohmori, Phase composition and photocatalytic activity of TiO_2-Fe_3O_4 coatings prepared by plasma spraying technique, ***Transactions of JWRI, Vol. 32(1) (2003) 167-174.***

[7] F. -X. Ye and A. Ohmori, The microstructure and photoelectrochemical characteristics of TiO_2-ZnO electrodes prepared by plasma spraying technique, ***Transactions of JWRI, Vol. 31(2) (2002) 201-205.***

[8] F. -X. Ye and A. Ohmori, Photocatalytic activity and photo-absorption of plasma sprayed TiO_2-10%Fe_3O_4 coatings, ***Transactions of JWRI, Vol. 30(2) (2001) 73-78.***

• International Conferences

[1] F. -X. Ye and A. Ohmori, Photoresponse and donor concentration of plasma sprayed TiO_2 and TiO_2-ZnO electrodes, ***Proceedings of the International Thermal Spray Conference 2004, 10-12 May 2004, Osaka, Japan, (In press).***

[2] **F. -X. Ye**, A. Ohmori and C.-J. Li, Investigation on the photocatalytic efficiencies of plasma sprayed TiO_2-Fe_3O_4 coatings, ***Proceedings of the International Thermal Spray Conference 2003***, *5-8 May 2003, Orlando, Florida, USA, 169-174.*

[3] A. Ohmori, **F. -X. Ye** and C. -J. Li, The effects of the additives on photocatalytic performance of plasma sprayed titanium dioxide coatings, ***Proceedings of the International Thermal Spray Conference & Exposition 2002***, *4-6 March 2002, Essen, Germany, 165-169.*